Engineering Journal

Second Quarter 2019 | Volume 56, No. 2

Smarter. Stronger. Steel.

63 Torsion of Rectangular Connection Elements
Bo Dowswell

89 Guidance on Shear Rupture, Ductility and Element Capacity in Welded Connections
Patrick J. Fortney, Larry S. Muir and William A. Thornton

109 Probabilistic Assessment of Seismic Force Demands in Biaxially Loaded Columns in Chevron-Configured Special Concentrically Braced Frames
Henry V. Burton, Nilofar Doorandish and Thomas Sabol

Steel Structures Research Update

123 Steel Diaphragm Innovation Initiative
Judy Liu

131 Errata

Engineering Journal

American Institute of Steel Construction

Dedicated to the development and improvement of steel construction, through the interchange of ideas, experiences and data.

Engineering Journal (ISSN 0013-8029) is published quarterly. Subscriptions: Members: one subscription, $40 per year, included in dues; Additional Member Subscriptions: $40 per year. Non-Members U.S.: $160 per year. Foreign (Canada and Mexico): Members $80 per year. Non-Members $160 per year. Published by the American Institute of Steel Construction at 130 E Randolph Street, Suite 2000, Chicago, IL 60601.

Periodicals postage paid at Chicago, IL and additional mailing offices. **Postmaster:** Send address changes to *Engineering Journal* in care of the American Institute of Steel Construction, 130 E Randolph Street, Suite 2000, Chicago, IL 60601.

Subscriptions: subscriptions@aisc.org, 312.670.2400

Archives: Search at **www.aisc.org/ej**. Article downloads are free for current members and are avaialable for a nominal fee for non-members.

TORSION OF RECTANGULAR CONNECTION ELEMENTS

BO DOWSWELL

ABSTRACT

Traditionally, the torsional design of rectangular members has been based on elastic calculations. For member design, this approach is justified because beams subjected to torsion are usually controlled by torsional rotation serviceability limits. However, designs that are based on a first yield criterion underestimate the strength of connection elements. To evaluate the true torsional behavior of connection elements, various factors affecting the torsional strength of short rectangular members are investigated, showing that the torsional strength of connection elements can be predicted with rational analysis models using an ultimate strength approach.

The torsional strength of connection elements can be attributed to the resistance due to uniform torsion, warping torsion, and the Wagner effect. A method is proposed for calculating the strength of rectangular connection elements subjected to any possible combination of loads, including torsion. The design method results in a significant increase in torsional strength compared to traditional analysis methods. The method can be used to analyze extended single-plate connections subjected loads in any direction, including axial forces and combined vertical and horizontal shear forces. Three design examples show the proper application of the design method.

Keywords: torsion, torsional strength, torsional rotation, warping, rectangular connection elements, ultimate strength.

INTRODUCTION

Traditionally, the torsional design of rectangular members has been based on elastic calculations. For member design, this approach is justified because beams subjected to torsion are usually controlled by torsional rotation serviceability limits. However, designs that are based on a first-yield criterion underestimate the strength of connection elements.

For extended single-plate connections, the elastic uniform (Saint Venant) torsion strength was used by Sherman and Gorbanpoor (2002) to develop a proposed design equation for the limit state of torsion. More recently, Thornton and Fortney (2011) derived an equation to calculate the torsional strength of extended single-plate connections using the plastic uniform torsion strength. Dowswell (2015) proposed an interaction equation for the plastic strength of rectangular connection elements subjected to various loads, including torsion.

Although the theoretical plastic uniform torsion strength is 50% greater than the elastic strength (Dowswell, 2015), an evaluation of the existing research on extended single-plate shear connections revealed strengths much higher than the plastic uniform torsion strength. Additionally, experiments on single-plate connections subjected only to torsion (no shear or moment), showed that the connection torsional strength greatly exceeds the uniform torsion strength (Bennets et al., 1981).

To evaluate the true torsional behavior of connection elements, various factors affecting the torsional strength of short rectangular members are investigated in this paper. The purpose of this paper is to show that the torsional strength of connection elements can be predicted with rational analysis models using an ultimate strength approach. A design method based on these models, including the interaction of torsion with other loads, is proposed. The results from practical connections are evaluated and compared to existing analysis methods, and three design examples show the practical implementation of the proposed design method.

UNIFORM TORSION

For uniform torsion, also known as Saint Venant torsion, the applied torque is resisted by shear stresses distributed over the cross section. The uniform torsional moment is

$$T_u = GJ\theta' \tag{1}$$

For uniform members with constant torque along the length, $\theta' = \theta/L$. The torsional constant for a rectangular member is

$$J = k_u d t^3 \tag{2}$$

where $k_u = ⅓ - 0.2t/d$ for $d/t < 10$ and $k_u = ⅓$ for $d/t \geq 10$ (Seaburg and Carter, 1997). The first-yield torsional moment is

$$T_{uy} = \frac{\tau_y J}{t} \tag{3}$$

Bo Dowswell, P.E., Ph.D., Principal, ARC International, LLC, Birmingham, AL. Email: bo@arcstructural.com

Paper No. 2017–06R

For $d/t \geq 10$, which satisfies the geometry for most connection elements,

$$T_{uy} = \frac{\tau_y d t^2}{3} \quad (4)$$

For uniform members with constant torque along the length, the elastic rotation is

$$\theta_u = \frac{T_u L}{GJ} \quad (5)$$

The yield rotation is

$$\theta_{uy} = \frac{\tau_y L}{Gt} \quad (6)$$

The plastic uniform torsion strength is

$$T_{up} = \frac{\tau_y d t^2}{2} \quad (7)$$

where

F_y = specified minimum yield strength, ksi
G = shear modulus of elasticity = 11,200 ksi
J = torsional constant, in.^{4}
L = member length, in.
T_u = uniform torsional moment, kip-in.
d = member depth, in.
t = member thickness, in.
z = distance along the member length, in.
τ_y = shear yield stress = $0.6F_y$, ksi
θ = angle of rotation, rad
θ' = angle of rotation per unit length, first derivative of θ with respect to z, rad

By comparing Equation 4 to Equation 7, it can be seen that $T_{up} = 1.5T_{uy}$. The torsional stiffness is linear up to the yield moment, T_y, and then the curve becomes nonlinear up to a maximum value of $T = T_{up} = 1.5T_{uy}$, as shown in Figure 1 (Dowswell, 2015).

WARPING

Except for circular cross sections, warping is present in all members subjected to torsion. Warping is classified as either primary or secondary. For primary warping, torsion is resisted by stresses across the element depth, and secondary warping is where torsion is resisted by stresses across the element thickness. For most members, any resistance developed through secondary warping is insignificant compared to uniform torsion and primary warping resistances.

For typical rectangular members, warping is negligible compared to uniform torsion. Therefore, the common practice of neglecting any warping contribution for rectangular members is justified. However, warping can provide significant torsional resistance to connection elements where the length is relatively short compared to the cross-sectional dimensions. This behavior was shown by Reissner and Stein (1951), who solved the differential equation of a rectangular cantilever plate subjected to a concentrated torsional moment at the free end, and by Baba and Kajita (1982), who developed inelastic finite element models of rectangular cantilever members subjected to a free-end concentrated torsion.

Elastic Strength

The elastic warping behavior can be analyzed using AISC Design Guide 9, *Torsional Analysis of Structural Steel Members* (Seaburg and Carter, 1997). The warping torsional moment is

$$T_w = -EC_w\theta''' \quad (8)$$

The warping constant for a rectangular member is

$$C_w = k_w d^3 t^3 \quad (9)$$

For narrow rectangles with $d/t \geq 10$ (Gjelsvik, 1981)

$$k_w = \frac{1}{144} \quad (10)$$

For rectangular members with $d/t < 10$ (Balaz and Kolekova, 2002)

$$k_w = \frac{1}{144}\left[1 - 4.88\left(\frac{t}{d}\right)^2 + 4.97\left(\frac{t}{d}\right)^3 - 1.07\left(\frac{t}{d}\right)^5\right] \quad (11)$$

Figure 2 shows warping stress distributions for elastic warping, inelastic warping and plastic warping. The maximum value for the elastic warping normal stress distribution

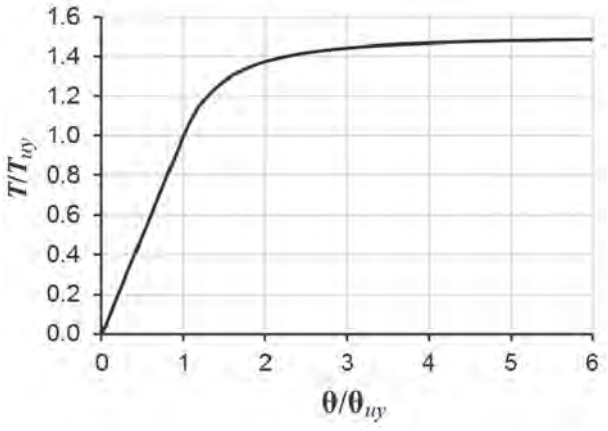

Fig. 1. Normalized torsion versus normalized angle of twist (Dowswell, 2015).

as shown in Figure 2(a), which occurs at the corners, is

$$\sigma_{wc} = EW_{nc}\theta'' \tag{12}$$

The normalized warping function at the corner of the cross section is

$$W_{nc} = \frac{dt}{4} \tag{13}$$

where

C_w = warping constant, in.^{6}
E = modulus of elasticity, ksi
W_{nc} = normalized warping function at the corner of the cross section, in.^{2}
θ'' = second derivative of θ with respect to z, rad
θ''' = third derivative of θ with respect to z, rad

Figure 3 shows the deformed shape of a single-plate connection subjected to twisting (Sherman and Ghorbanpoor, 2002; Moore and Owens, 1992; Abou-Zidan, 2014; Suleiman, 2013). The double-curvature along the length indicates that warping is fixed at both ends of the plate.

Case 2 in AISC Design Guide 9, Appendix B, provides charts for determining θ, θ', θ'' and θ''' for members subjected to concentrated end torques with warping fixed at each end. The values can also be calculated with the equations in Moore and Mueller (2002). The maximum warping stresses are at the member ends ($z = 0$ and $z = L$), where the equation for θ'' reduces to

$$\theta'' = \frac{T}{GJa}\tanh\left(\frac{L}{2a}\right) \tag{14}$$

where

$$a = \sqrt{\frac{EC_w}{GJ}} \tag{15}$$

T = torsional moment, kip-in.

Isolated Flange Method

Gjelsvik (1981) showed that the elastic torsional moment is statically equivalent to a couple formed of two equal and opposite out-of-plane forces, F, acting on each half of the cross section at $h = 2d/3$, as shown in Figure 4(a). Gjelsvik's equivalent couple can be expanded to simplify warping calculations for connection elements, where only the shaded portion of the cross section on each half of the member depth is effective in resisting force, F. The equivalent cross-section $t \times \alpha d$ is modeled as a flexural member of length L with the fixed-slider boundary conditions shown in Figure 4(b). The required moment at each end of the member is

$$M_{re} = \frac{FL}{2} \tag{16}$$

This isolated-flange analysis method is common in the torsional analysis of I-shaped members, where the flanges are isolated and treated as flexural members to calculate the warping strength.

For elastic stresses, $\alpha = 1/4$ and the out-of-plane force, F, is

$$F = \frac{3T_w}{2d} \tag{17}$$

The weak-axis yield moment of the equivalent beam, M_{ye}, is

$$M_{ye} = \frac{F_y \alpha d t^2}{6} \tag{18}$$

Setting Equation 16 equal to Equation 18 and solving for F results in the out-of-plane force required to initiate first yield, F_{wy}.

$$F_{wy} = \frac{F_y \alpha d t^2}{3L} = \frac{F_y d t^2}{12L} \tag{19}$$

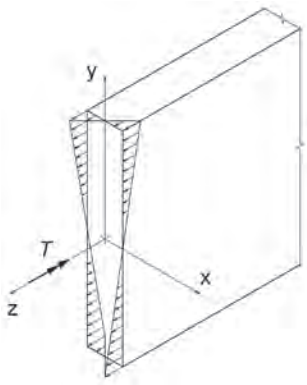

(a) elastic

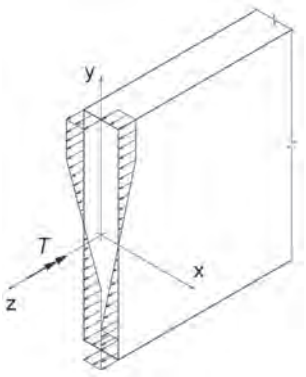

(b) inelastic

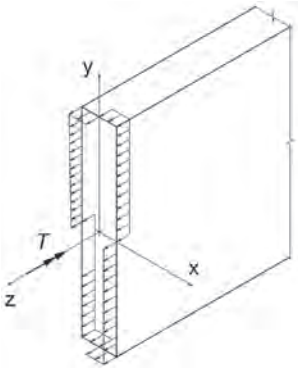

(c) plastic

Fig. 2. Warping stresses.

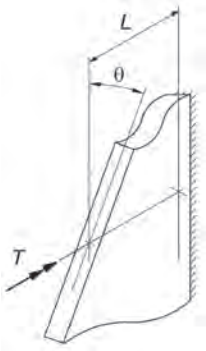

Fig. 3. Torsional deformation of a connection element.

Setting Equation 17 equal to Equation 19 and solving for T_w results in the warping torsion required to initiate first yield.

$$T_{wy} = \frac{F_y d^2 t^2}{18L} \tag{20}$$

The rotation can be estimated from the free-end deflection of the equivalent beam, δ, shown in Figure 4(b). The end deflection is

$$\delta = \frac{FL^3}{12EI_e} \tag{21}$$

The weak-axis moment of inertia of the equivalent beam is

$$I_e = \frac{\alpha d t^3}{12} = \frac{dt^3}{48} \tag{22}$$

Substituting Equations 17 and 22 into Equation 21 results in

$$\delta = \frac{6T_w L^3}{Ed^2 t^3} \tag{23}$$

Using the geometry in Figure 5, the rotation is

$$\theta_w = \frac{2\delta}{d} = \frac{12T_w}{E}\left(\frac{L}{dt}\right)^3 = \frac{T_w L^3}{12EC_w} \tag{24}$$

Substituting Equations 19 and 22 into Equation 21 results in the yield deflection

$$\delta_y = \frac{F_y L^2}{3Et} \tag{25}$$

The yield rotation is

$$\theta_{wy} = \frac{2\delta_y}{d} = \frac{2F_y L^2}{3Edt} \tag{26}$$

Finite element models of rectangular members subjected to torsion (May and Al-Shaarbaf, 1989; Baba and Kajita, 1982; Bathe and Chaudhary, 1982) exhibited an inelastic

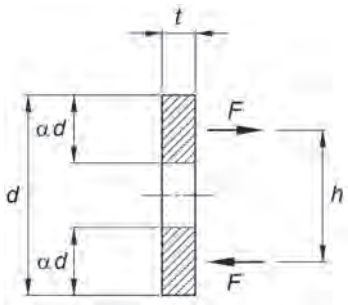

(a) cross section

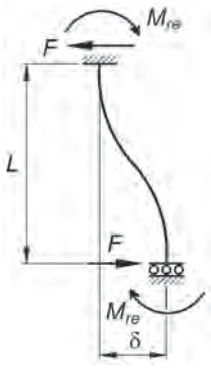

(b) top view

Fig. 4. Isolated flange method for warping analysis.

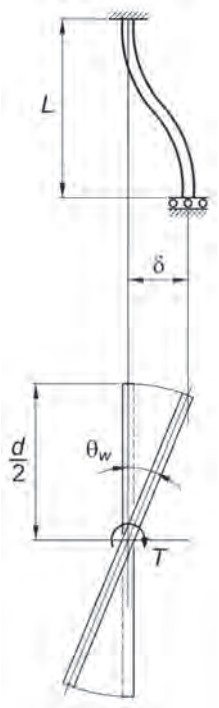

Fig. 5. Isolated flange method for warping rotation.

warping response similar to the uniform torsion curve in Figure 1, with the inelastic warping torsion contributing significantly to the total torsional resistance. For calculating the inelastic strength, F is assumed to act at the center of the effective depth, αd. The out-of-plane forces are

$$F = \frac{T_w}{h} = \frac{T_w}{d(1-\alpha)} \tag{27}$$

The weak-axis plastic flexural strength of the equivalent beam is

$$M_{pe} = \frac{F_y \alpha d t^2}{4} \tag{28}$$

Setting Equation 16 equal to Equation 28 and solving for F results in the out-of-plane force required for the plastic strength.

$$F_{wy} = \frac{F_y \alpha d t^2}{2L} \tag{29}$$

Setting Equation 27 equal to Equation 29 and solving for T_w results in the inelastic warping resistance.

$$T_{wp} = \frac{F_y d^2 t^2}{2L} \alpha(1-\alpha) \tag{30}$$

At $\alpha = ½$, the plastic warping strength, shown in Figure 2(c), is

$$T_{wp} = \frac{F_y d^2 t^2}{8L} \tag{31}$$

Comparing Equation 31 to Equation 20 shows that the plastic warping strength is 2.25 times the first-yield moment. However, the condition used to derive Equation 31 cannot be reached due to out-of-plane translation compatibility requirements at the member mid-depth. At $\alpha = 0.2113$, the plastic strength is reached only at the top and bottom fibers of the cross section, resulting in an inelastic warping strength of

$$T_{wi} = \frac{F_y d^2 t^2}{12L} \tag{32}$$

where

F = horizontal couple force, kips
I = moment of inertia, in.^{4}
T_w = warping torsional moment, kip-in.
αd = effective depth of the equivalent cross section, in.
δ = deflection of equivalent beam, in.
δ_y = yield deflection of equivalent beam, in.

THE WAGNER EFFECT

Also neglected in the design of torsion members is the Wagner effect (Wagner, 1936), which is a nonlinear, second-order torque that increases the torsional strength and stiffness (Kjar, 1967; Gregory, 1960). The Wagner torque is negligible for many connection geometries at practical serviceability rotations. However, a discussion is merited because the Wagner torsion contributes to the stable inelastic torsion-rotation curves exhibited by extended single-plate connection tests and finite element models. Also, the Wagner effect may explain why short connection elements, such as conventional single-plate connections, are only rarely limited by torsional rotations.

Elastic Strength

The Wagner solution for rectangular members was documented by Timoshenko (1956) and later by Cook and Young (1985) and Trahair (2003). Rotation of the member causes a longitudinal elongation of the fibers that are farthest from the center of rotation. Figure 6 shows that the tensile stresses caused by the elongation exerts a resisting torque about the

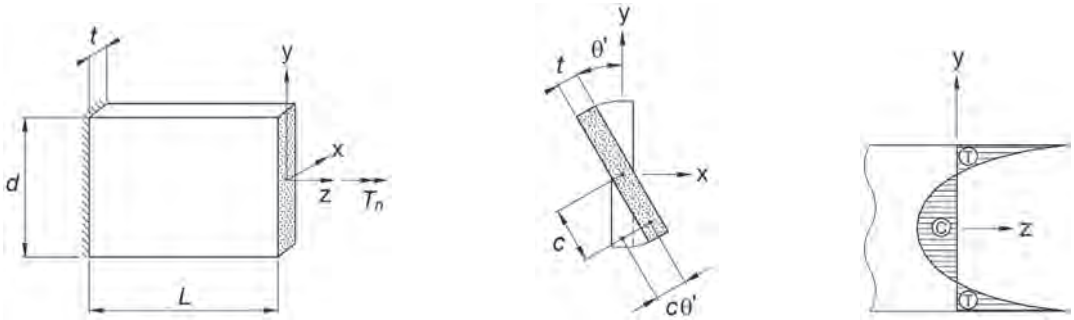

(a) torsionally loaded member *(b) cross section* *(c) longitudinal stresses*

Fig. 6. Mechanics of the Wagner effect.

axis of twist that increases with θ. The Wagner torsion is (Trahair, 2003)

$$T_n = \frac{EI_n}{2}(\theta')^3 \tag{33}$$

The Wagner constant is

$$I_n = \frac{d^5 t}{180} \tag{34}$$

Geometrically nonlinear elastic finite element models showed the accuracy of Equations 33 and 34 (Trahair, 2003). The axial stress developed by the Wagner effect, as shown in Figure 6(c), is (Cook and Young, 1985)

$$\sigma_n = \frac{E(\theta')^2}{2}\left(c^2 - \frac{d^2}{12}\right) \tag{35}$$

The maximum stress is located at the top and bottom edges of the member, where $c = d/2$

$$\sigma_{nt} = \frac{Ed^2(\theta')^2}{12} \tag{36}$$

If warping is neglected, the torsional resistance is the sum of the Wagner torsion and the uniform torsion (Cook and Young, 1985), resulting in

$$\begin{aligned} T_e &= T_u + T_n \\ &= \frac{Gdt^3\theta'}{3} + \frac{Ed^5 t(\theta')^3}{360} \\ &= \beta T_u \end{aligned} \tag{37}$$

and β is the normalized increase in torsional resistance due to the Wagner effect

$$\beta = 1 + \frac{Ed^4(\theta')^2}{120Gt^2} \tag{38}$$

For uniform members with constant torque along the length, $\theta' = \theta/L$ and the normalized increase in torsional resistance due to the Wagner effect is

$$\beta = 1 + \frac{Ed^4}{120G}\left(\frac{\theta}{tL}\right)^2 \tag{39}$$

where

I_n = Wagner constant, in.^{6}

T_n = Wagner torsional moment, kip-in.

c = distance to outermost fiber, in.

Evaluation of Equation 39 indicates that the torsional resistance is dependent on the rotation angle and can increase significantly with member depth. The Wagner torsion decreases with length and thickness.

Due to the short length of conventional single-plate shear connections, the Wagner effect can be significant. Figure 7(a) plots the torsion-rotation curve for a ⅜-in. × 18-in. plate, showing the uniform torsion, Wagner torsion, and the total torsional resistance. The plate is 3 in. long, which is the typical distance between the bolt line and the weld line for a conventional single-plate shear connection. The Wagner torsion is negligible for θ < 0.5° but is significant at 1° and provides a 220% increase in torsional resistance at θ = 2°. However, at θ = 2°, the maximum tensile stress is 106 ksi. For F_y = 50 ksi, first yield due to normal stress occurs at θ = 1.37°, where the increase in torsional resistance is 100%. For four different plate geometries, β is plotted in Figure 7(b) as a function of θ, where the substantial effect of decreasing the plate depth is clear.

Because extended single-plate shear connections are longer, and usually thicker, than conventional single-plate shear connections, the Wagner effect is often negligible for extended configurations. Figure 8(a) is a plot of the torsion-rotation curve for a ¾-in. × 18-in. plate, showing the uniform torsion, Wagner torsion and the total torsional resistance. The plate is 10 in. long, representing a common distance between the bolt line and the weld line for an extended single-plate shear connection. The Wagner torsion is negligible for the practical range of serviceability rotations, providing only 11% of the total torsion at θ = 3°. For four different plate geometries, β is plotted in Figure 8(b) as a function of θ, where the Wagner effect is shown to be significant only for plates with high depth-to-thickness ratios.

COMBINING TORSIONAL EFFECTS

The elastic torsional resistance is the sum of the uniform torsion, the warping torsion, and the Wagner torsion. However, because each torsional component contributes to the total resistance based on its relative stiffness, only one of the three components is likely to contribute its full first-yield torsional moment. In the elastic range, uniform and warping torsion can be combined using a stiffness analysis according to AISC Design Guide 9. This approach is preferred for member design, where beams are usually controlled by torsional rotation serviceability limits. However, designs that are based on a first-yield criterion underestimate the strength of connection elements.

Rotation

According to Trahair et al. (2008), the angle of rotation calculated for both uniform torsion and warping torsion can be calculated independently and combined using Equation 40 to estimate the actual angle of rotation.

$$\theta = \frac{\theta_u \theta_w}{\theta_u + \theta_w} \tag{40}$$

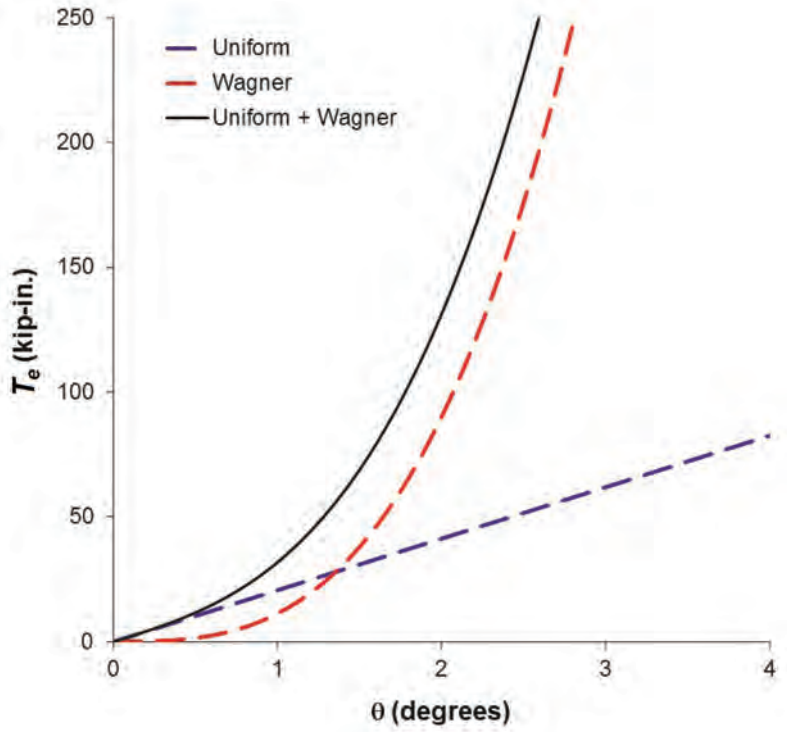

(a) T_e versus θ for a ⅜×18×3-in.-long plate

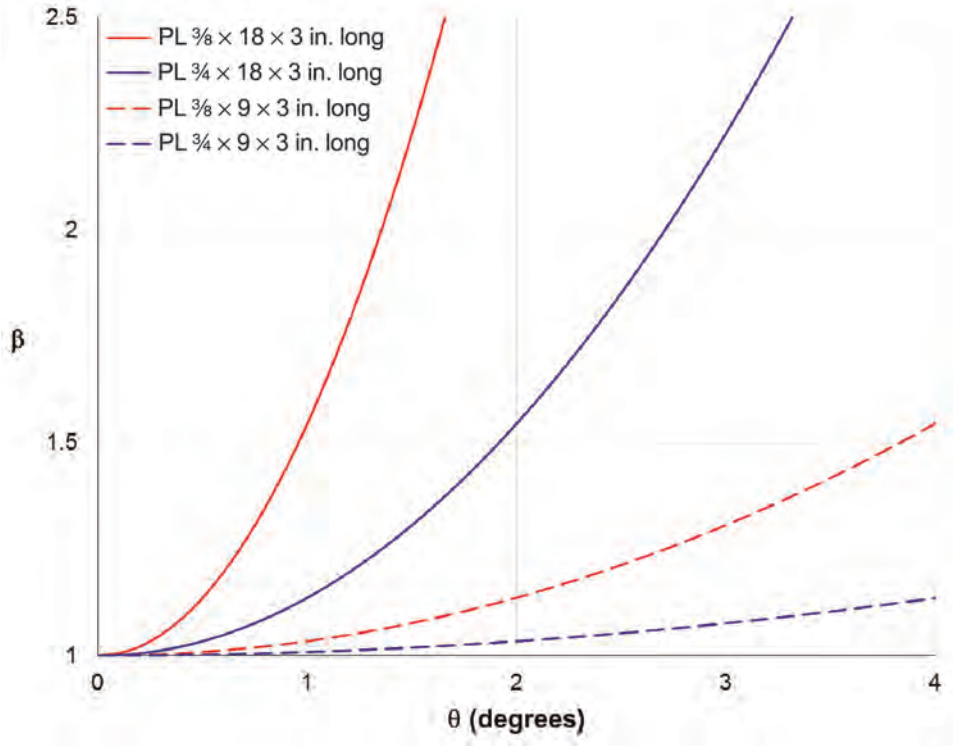

(b) β versus θ

Fig. 7. The Wagner effect for conventional single-plate shear connections.

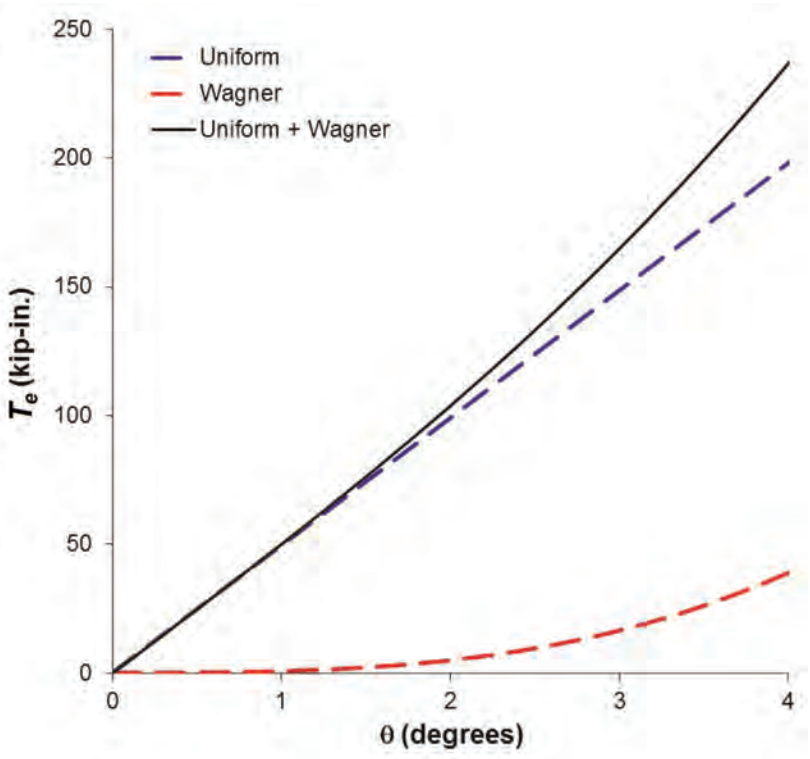

(a) T_e *versus* θ *for a ¾×18×10-in.-long plate*

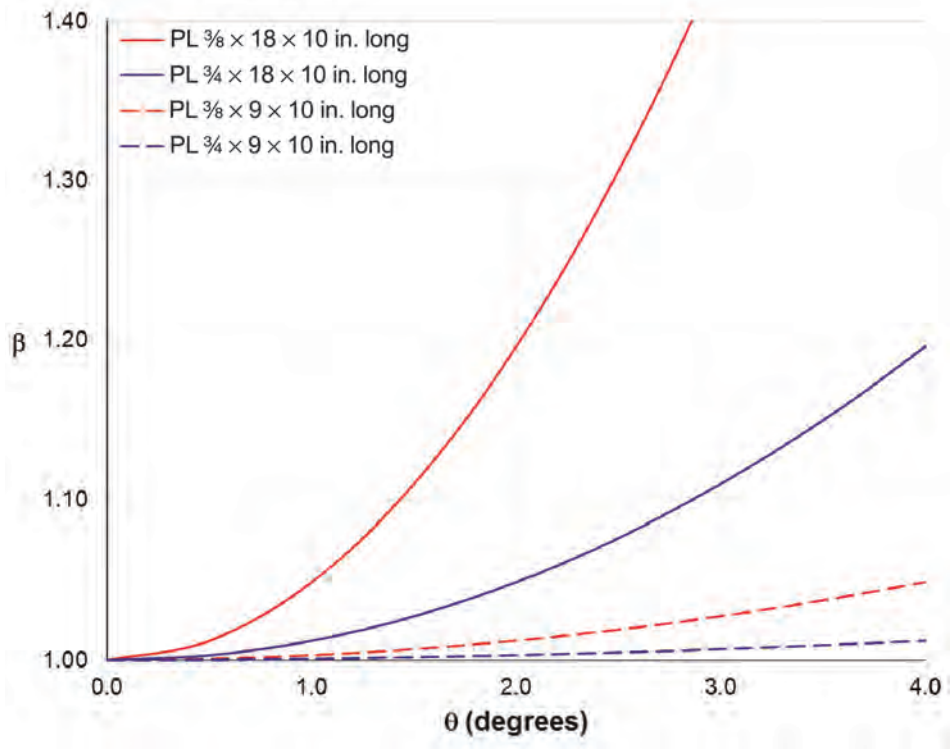

(b) β *versus* θ

Fig. 8. The Wagner effect for extended single-plate shear connections.

For members in the inelastic range, the angle of rotation can be estimated with Equation 41 (Pi and Trahair, 1994).

$$\theta_i = \frac{\theta}{1 - \frac{T_r}{2T_p}} \tag{41}$$

where

T_p = plastic torsional moment, kip-in.

T_r = required torsional moment, kip-in.

θ_u = angle of rotation for uniform torsion, rad

θ_w = angle of rotation for warping, rad

Plastic Strength

Because the Wagner effect requires large rotations for significant torsional resistance and the behavior under inelastic conditions is unclear, the Wagner torsion will be neglected. Dinno and Merchant (1965) and Pi and Trahair (1995) proposed a plastic torsion analysis where the plastic uniform torsion and the plastic warping torsion are evaluated independently and then added together to determine the total torsional resistance. This method assumes no interaction between uniform and warping torsion, which agrees well with experimental results on small-scale I-shaped members documented by Dinno and Merchant. Using the interaction suggested by Dinno and Merchant, the plastic torsional strength is

$$T_p = T_{up} + T_{wp} = T_{up}\left(1 + \frac{d}{2.4L}\right) \tag{42}$$

where

T_{up} = plastic uniform torsional moment, kip-in.

T_{wp} = plastic warping torsional moment, kip-in.

Figure 9 shows the predicted inelastic torsion versus rotation curves for a ¾×18×10-in.-long ASTM A572 Grade 50 plate. To show the effect of warping, both the uniform torsion curve and the uniform plus warping curves are plotted. The dashed lines show the elastic response and the solid lines show the inelastic curves. For the uniform torsion curve, the first-yield torsion is 101 kip-in. at $\theta = 2.05°$, and 96% of the plastic strength is developed at $\theta = 6.14°$. When warping is included, yielding is caused by warping normal stresses at a torsion of 72.7 kip-in. at $\theta = 0.447°$. However, the inelastic warping response shows a dramatic increase in stiffness and inelastic strength compared to the uniform torsion curve.

COMBINING TORSION WITH OTHER LOADS

Members subjected to both flexure and torsion must consider second-order effects and the strength reduction due to load interaction. After the required flexural and second-order torsional moments are determined, the available strength is calculated by combining the load ratios in an interaction equation.

Plastic Strength

Dowswell (2015) proposed Equation 43 for the interaction of flexure, shear, axial and torsion; however, the torsional interaction term was developed for uniform torsion and does not include the effects of warping and Wagner torsion. Because

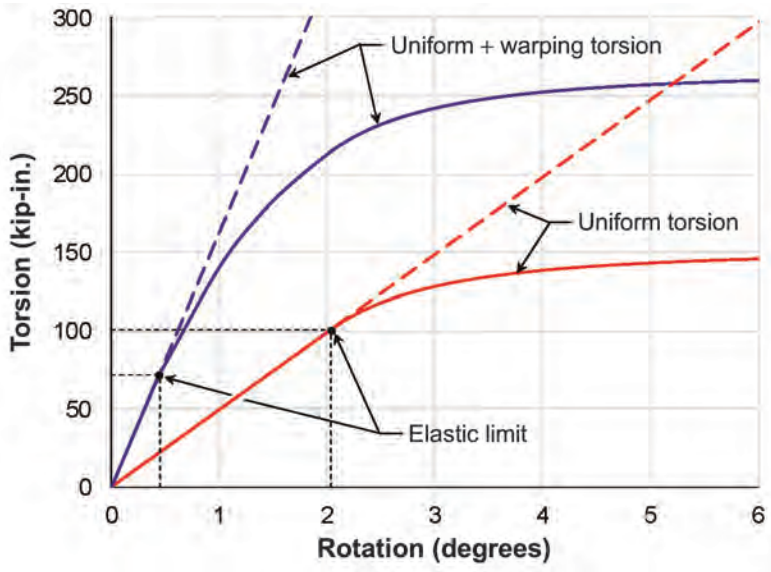

Fig. 9. Torsion-rotation curves for a ¾×18×10-in.-long ASTM A572 Grade 50 plate.

both warping and Wagner torsion develop longitudinal normal stresses, the resulting stress distributions are similar to the axial and flexural stresses. However, separating the torsional components and combining them with the flexural and axial load ratios would lead to unnecessary complexity in the interaction equation. Furthermore, due to the lack of research in this area, the accuracy of such an equation could not be verified. For design purposes, it is believed that T_p, as calculated with Equation 42, can be used in the torsion ratio of Equation 43.

$$\left(\frac{P_r}{P_y}\right)^2+\left(\frac{T_r}{T_p}\right)^2+\left(\frac{V_r}{V_p}\right)^4+\left[\left(\frac{M_{rx}}{M_{px}}\right)^{1.7}+\left(\frac{M_{ry}}{M_{py}}\right)^{1.7}\right]^{0.59}=1.0 \tag{43}$$

where

M_{px} = plastic bending moment about the x-axis, kip-in.
M_{py} = plastic bending moment about the y-axis, kip-in.
M_{rx} = required x-axis flexural strength, kip-in.
M_{ry} = required y-axis flexural strength, kip-in.
P_r = required axial strength, kips
P_y = axial yield load, kips
V_p = plastic shear strength, kips
V_r = required shear strength, kips

Second-Order Effects

For open sections subjected to both torsion and strong-axis flexure, the second-order torsional effects are dependent on the critical lateral-torsional buckling moment. Second-order torsional moments and rotations can be calculated by amplifying the results of a first-order analysis (Ashkinadze, 2008; Lindner and Glitsch, 2005; Boissonnade et al., 2002; Trahair and Teh, 2000; Pi and Trahair, 1994; Pastor, 1977). The amplification factor for rectangular members is (Zahn, 1984)

$$B=\frac{1}{1-\left(\frac{M_{rx}}{M_{cr}}\right)^2} \tag{44}$$

The second-order torsional rotation is

$$\theta_2=B\theta_1 \tag{45}$$

The second-order torsional moment is

$$T_2=BT_1 \tag{46}$$

The critical moment used in Equation 44 is

$$M_{cr}=F_{cr}S_x \tag{47}$$

The critical stress is calculated with AISC *Specification* (AISC, 2016) Equation F11–4

$$F_{cr}=\frac{1.9Et^2C_b}{Ld} \tag{48}$$

where

C_b = lateral-torsional buckling modification factor
F_{cr} = critical stress, ksi
M_{cr} = elastic critical buckling moment for strong-axis flexure, kip-in.
S_x = elastic section modulus about the x-axis, in.^{3}
T_1 = first-order torsional moment, kip-in.
θ_1 = first-order torsional rotation, rad

SINGLE-PLATE SHEAR CONNECTIONS

Single-plate shear connections, where the beam is field-bolted to a connecting plate as shown in Figure 10, have an

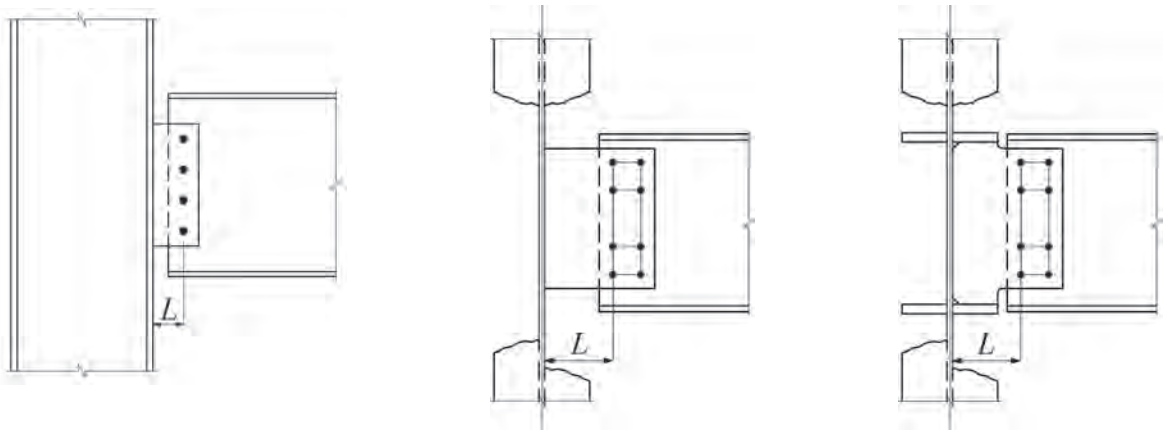

(a) conventional *(b) extended with no stiffener* *(c) extended with stiffener*

Fig. 10. Single-plate connections.

out-of-plane eccentricity between the beam and the plate. Under shear loading, this eccentricity causes a torsional moment, which has been previously discussed by Muir and Hewitt (2009) and Thornton and Fortney (2011).

Conventional Configuration

Of the many experimental research projects studying the behavior of conventional single-plate connections [Figure 10(a)], only the results of Moore and Owens (1992) showed significant torsional rotations. In these, and the remaining tests, the out-of-plane eccentricity had a negligible effect on the serviceability and strength and was not considered by the researchers as a significant design parameter. As discussed in previous sections of this paper, the conventional single-plate geometry maximizes the torsional resistance provided by warping and the Wagner effect.

Extended Configuration

Nonstiffened and stiffened extended single-plate shear connections are shown in Figures 10(b) and 10(c), respectively. Twisting of extended single-plate connections subjected to shear loading has been reported in experimental specimens (Sherman and Ghorbanpoor, 2002) and finite element models (Hijaj and Mahamid, 2017; Abou-Zidan, 2014; Suleiman, 2013). The experimental measurements of Goodrich (2005) and Sherman and Ghorbanpoor (2002) showed an increase in torsional strength and rotational stiffness when the plate is welded to a stiffener. The finite element models of Rahman et al. (2007) and Mahamid et al. (2007) showed similar results.

For nonstiffened connections, the design procedure in the AISC *Steel Construction Manual* (AISC, 2017) was developed by Muir and Hewitt (2009). The equations implicitly limit excessive torsional rotations by combining the shear and flexural strengths using an elliptical interaction to approximate von Mises theory. If the torsional loads are explicitly included in the calculations, the load ratios can be combined using plastic interaction according to Equation 49, which is simplified from Equation 43.

$$\frac{M_{rx}}{M_{nx}}+\left(\frac{T_2}{T_p}\right)^2+\left(\frac{R_r}{V_p}\right)^4=1.0 \tag{49}$$

The total plastic torsional strength, T_p, is calculated with Equations 7, 31 and 42. The second-order torsional moment is calculated with Equations 44 and 46, and the first-order torsional moment is

$$T_1=R_r e \tag{50}$$

The eccentricity is

$$e=\frac{t+t_w}{2} \tag{51}$$

The strong-axis flexural moment, M_{rx}, is dependent on the location of the inflection point. At flexible supports, it is conservative to assume the connection behaves as a frictionless pin, resulting in

$$M_{rx}=R_r L \tag{52}$$

The plastic shear strength is

$$V_p=0.6F_y td \tag{53}$$

where

M_{nx} = strong-axis flexural strength, kip-in.
R_r = required beam end shear reaction, kips
T_2 = second-order torsional moment, kip-in.
e = horizontal eccentricity for a single-plate connection, in.
t = plate thickness, in.
t_w = beam web thickness, in.

The strong-axis flexural strength, M_{nx}, can be calculated according to AISC *Specification* Section F11, with $C_b = 1.84$ when the beam is braced near the end and $C_b = 1.26$ when the beam is unbraced near the end (Dowswell, 2004). These C_b factors are also used in Equation 48 to calculate the critical stress for the second-order torsion amplifier.

The plastic strength according to the equations in this section are compared to the available experimental and finite element results in Table 1. Only nonstiffened specimens with no beam bracing near the connection were considered. The four specimens listed failed by excessive twisting of the plate. R_c is the shear strength calculated with the actual dimensions and yield strengths, R_e is the approximate experimental shear load where the load-deflection curve became nonlinear, and R_u is the maximum experimental shear load.

The last column of the table lists the test-to-calculated ultimate strength ratio, R_u/R_c, which has an average of 1.28 for the four specimens. Therefore, the plastic interaction equation is conservative, possibly because the Wagner effect and the effects of strain hardening were neglected. Because the calculations were based on the plastic strength, nonlinear behavior was expected at loads significantly below R_c; however, for two of the specimens, R_e/R_c is greater than 1.00.

Lateral Bracing

Thornton and Fortney (2011) derived a method to predict the torsional resistance of extended single-plate shear connections with a slab or deck attached to the beam top flange. For torsional resistance, the method utilizes both the uniform torsion strength of the plate and the torsional resistance provided by the slab/deck flexural strength. A design method has not been established for the case where the beam top flange is restrained against lateral translation, but not rotation. The equations presented in this section rely only on the lateral resistance of the beam bracing.

Table 1. Nonstiffened Single-Plate Connections											
Reference	Spec. No.	t (in.)	d (in.)	t_w (in.)	L (in.)	F_y (ksi)	R_c (kips)	R_e (kips)	R_u (kips)	R_e/R_c	R_u/R_c
Sherman and Ghorbanpoor (2002)	2U	0.371	15.00	0.495	6.30	42.6	71.4	65	82.9	0.910	1.16
	4U	0.495	15.00	0.495	10.0	43.5	77.7	82	98.7	1.06	1.27
	6UB	0.495	18.00	0.650	10.0	43.5	96.0	119	136	1.24	1.42
Abou-Zidan (2014)	15	0.394	9.05	0.382	6.38	50.8	43.7	36	55.1	0.82	1.26

R_c = calculated shear strength, kips
R_e = the approximate experimental shear load where the load-deflection curve became nonlinear, kips
R_u = the maximum experimental shear load, kips

When lateral bracing is present at both the top and bottom flanges [Figure 11(a)], the eccentric torsion can be resisted completely by the braces. Finite element models by Abou-Zidan (2014) and Suleiman (2013) showed that top-flange lateral bracing near the beam end significantly increases the torsional resistance of extended single-plate shear connections. For cases where only top-flange bracing is present, a portion of the eccentric torsion can be resisted with a couple between the brace and the centroid of the plate [Figure 11(b)].

$$T_b = Fh \tag{54}$$

Assuming the plate deforms in double-curvature, as shown in Figure 4(b), the required weak-axis moment at each end of the plate is

$$M_{ry} = \frac{FL}{2} \tag{55}$$

The resisting moment of the plate is

$$M_{py} = F_y \frac{dt^2}{4} \tag{56}$$

Setting $M_{ry} = M_{py}$, solving for F, and substituting into Equation 54 results in a torsional resistance of

$$T_b = F_y \frac{hdt^2}{2L} \tag{57}$$

T_b can be combined with the uniform torsion strength to get the total torsional resistance.

$$T_p = T_{up} + T_b = T_{up}\left(1 + \frac{5h}{3L}\right) \tag{58}$$

where

T_b = torsional resistance provided by a top flange lateral brace, kip-in.

h = distance between couple forces, F, in.

Although no interaction is assumed between the two torsional components, Equation 58 is believed to be adequate for design purposes. The available information on flexure-torsion interaction of rectangular members was summarized by Dowswell (2015); however, the interaction of torsion with other loads is not well understood. For example, the theory

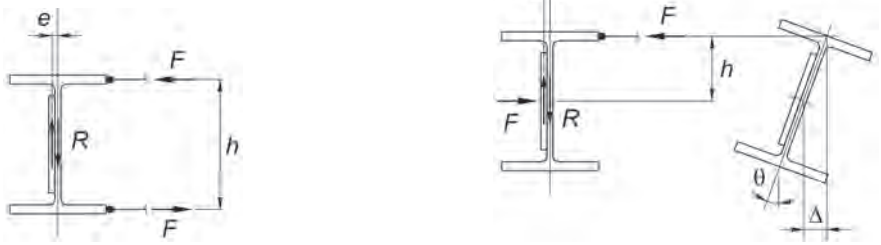

(a) lateral bracing at top and bottom flanges *(b) lateral bracing at top flange*

Fig. 11. Torsional rotation at braced beam ends.

Table 2. Nonstiffened Single-Plate Connections with Top-Flange Lateral Bracing											
Spec. No.	Failure Mode	t (in.)	d (in.)	t_w (in.)	L (in.)	F_y (ksi)	R_c (kips)	R_e (kips)	R_u (kips)	R_e/R_c	R_u/R_c
11	Yielding	0.236	9.05	0.382	6.38	50.8	28.5	39	61.8	1.37	2.17
13	Twisting	0.394	9.05	0.382	6.38	50.8	54.6	56	94.4	1.03	1.73

R_c = calculated shear strength, kips
R_e = the approximate experimental shear load where the load-deflection curve became nonlinear, kips
R_u = the maximum experimental shear load, kips

and experiments of Neal (1950) and Witrick (1952) showed that the torsional stiffness remains at its elastic value after the member has yielded in flexure. For single-plate connections, contrasting results were obtained by Suleiman (2013), where nonlinear torsional behavior initiated at loads well below the corresponding yield loads based on the vertical shear-deformation curves (Figure 12). Additionally, the research summarized by Dowswell (2015) showed that Equation 49 is conservative for flexure-torsion interaction. Furthermore, any reduction in load due to interaction is likely to be offset by neglecting the Wagner torsion and warping torsion.

Only one of the finite element models by Abou-Zidan (2014) failed due to excessive twisting. For another model, failure was caused by yielding of the plate between the weld line and the bolt line. For both of these specimens, T_p was calculated with Equation 58 and the torsion ratio was combined with the shear and flexure ratios according to Equation 49. The results are listed in Table 2, where it is shown that the equations are conservative. The last column of the table lists the test-to-calculated ultimate strength ratio, R_u/R_c, which is close to two for both specimens. With an average R_e/R_c ratio of 1.20, the proposed equations provide reasonable estimates of the load causing the onset of nonlinear behavior for both models.

Practical Results

This section shows the results of including torsion in the analysis of single plate connections. The discussions include connections with various configurations supporting a W18×35 beam, which has a web thickness, t_w, of 0.300 in. In all cases, the plate material is ASTM A572 Gr. 50 and the depth, d, is 15 in.

The first results are for a conventional single-plate shear connection, as shown in Figure 10(a), with a plate thickness of t = ⅜ in. and L = 3 in. The Wagner strength, calculated with Equation 33 at a rotation of 0.03 rad., is 22.9 kip-in. Adding this to the plastic torsional strength calculated with Equation 42 results in a plastic torsional resistance of 120 kip-in. The elastic uniform torsional resistance, T_{uy}, is 21.1 kip-in., which is only 18% of the plastic torsional resistance at 0.03 rad. Using Equation 49 to combine the flexural, torsional and shear loads results in a nominal shear strength of 149 kips. For a plate with 15⁄16-in.-diameter holes, the AISC *Manual* design procedure results in a nominal shear strength of 146 kips, which is controlled by the shear rupture limit state. Because plate yielding is a key component in the rotational ductility of these connections, the torsional stresses may actually enhance the performance. These results show why the common practice of neglecting torsion in the design of conventional single-plate shear connections is warranted.

The next results are for extended single-plate shear connections, as shown in Figure 10(b), with t = ⅝ in. and L = 9 in. Several bracing conditions were considered: Case 1, unbraced beam; Case 2, beam with top-flange lateral bracing near the connection; and Case 3, beam with torsional bracing near the connection. The AISC *Manual* design procedure results in a nominal shear strength of 161 kips;

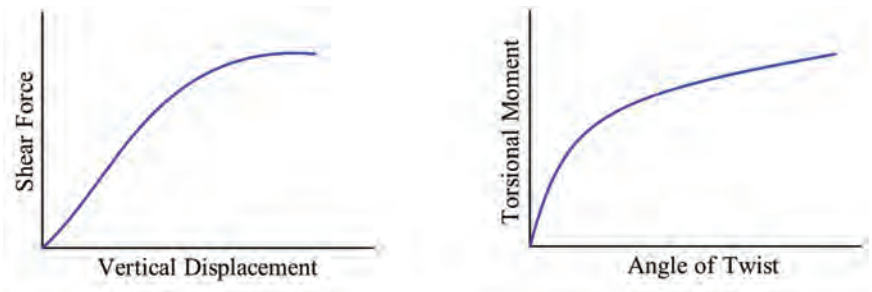

Fig. 12. Shear-displacement and torsion-rotation curves (Suleiman, 2013).

however, the results are valid only for beams with bracing located near the connection. In all cases, the Wagner torsion is neglected and load interaction is calculated according to Equation 49. The elastic uniform torsional resistance is 93.8 kip-in.

Case 1: Because beam bracing is not provided near the connection, the AISC *Manual* design procedure is not applicable. Also, this configuration can significantly reduce the lateral-torsional buckling strength of the beam. The plastic torsional strength calculated with Equation 42 is 202 kip-in., which is more than double the elastic uniform torsional resistance. The second-order amplification factor and the buckling strength of the plate were calculated with $C_b = 1.26$. The calculations resulted in a shear strength of 151 kips, which is 6% less than the strength calculated with the AISC *Manual* design procedure.

Case 2: For this case, the plastic torsional strength can be calculated using either Equation 42 or Equation 58. The plastic torsional strength calculated with Equation 42 is the same as for Case 1. The plastic torsional strength calculated with Equation 58 is 285 kip-in., which is three times the elastic uniform torsional resistance. The second-order amplification factor and the buckling strength of the plate were calculated with $C_b = 1.84$. The calculations resulted in shear strengths of 153 kips and 161 kips when using Equation 42 and Equation 58, respectively. In both cases, the result is within 5% of the strength calculated with the AISC *Manual* design procedure.

Case 3: For this case, the torsion is resisted by the beam bracing system and $T_2 = 0$, resulting in a shear strength of 170 kips. This is 6% greater than the strength calculated with the AISC *Manual* design procedure.

PROPOSED DESIGN METHOD

The design process can be simplified by limiting the second-order amplification factor to 1.10 and solving for the minimum thickness required to reach the plastic flexural strength. Substituting $B = 1.10$ and $M_{rx} = \phi M_{px}$ into Equation 44, combining with Equations 47 and 48, and solving for t results in Equation 59.

$$t_{min} = 1.54\sqrt{\frac{LdF_y}{C_b E}} \tag{59}$$

where

C_b = 1.84 when the connection element is braced at both ends

= 1.26 when the connection element is braced only at one end

This minimum plate thickness also ensures that AISC *Specification* Section F11 will always result in $M_{nx} = M_{px}$ for $C_b \geq 1.07$. For $t \geq t_{min}$, the required second-order torsional moment is

$$T_r = 1.1T_1 \tag{60}$$

Based on the design recommendations of Dowswell (2016), Equation 43 can be used for design by modifying the exponent applied to the axial load ratio and substituting the available strengths for plastic strengths.

$$\left(\frac{P_r}{P_c}\right)^k + \left(\frac{T_r}{T_c}\right)^2 + \left(\frac{V_r}{V_c}\right)^4 + \left[\left(\frac{M_{rx}}{M_{cx}}\right)^{1.7} + \left(\frac{M_{ry}}{M_{cy}}\right)^{1.7}\right]^{0.59} = 1.0 \tag{61}$$

where

M_{cx} = available flexural strength about the x-axis, kip-in.
= ϕM_{px} (LRFD) or M_{px}/Ω (ASD)

M_{cy} = available flexural strength about the y-axis, kip-in.
= ϕM_{py} (LRFD) or M_{py}/Ω (ASD)

P_c = available axial strength calculated according to AISC *Specification* Section J4.1(a) or Section J4.4 for tension and compression elements, respectively, kips
= ϕP_n (LRFD) or P_n/Ω (ASD)

T_c = available torsional strength, kips
= ϕT_p (LRFD) or T_p/Ω (ASD)

V_c = available shear strength calculated according to AISC *Specification* Section J4.2(a), kips
= ϕV_n (LRFD) or V_n/Ω (ASD)

k = 1 for compression loads
= 2 for tensile loads

For connection elements that are braced only at one end and free at the other end, the nominal plastic torsional strength, T_p, is calculated with Equation 42. For extended single-plate shear connections with beam top flange lateral bracing near the connection, T_p can be calculated with Equation 58. For extended single-plate shear connections with beam lateral and torsional bracing near the connection, the torsional load at the plate can be neglected ($T_r = 0$).

DESIGN EXAMPLES

Example 1

Given

In this example, a W21×111 beam is connected to a column web with an extended single-plate connection, as shown in Figure 13. The beam is not braced, but the effect of the connection on the lateral-torsional buckling strength has been considered in the beam design. The connection is subjected to an axial tension force, P, a vertical shear force, R, and a horizontal out-of-plane force, F. The plate is ¾-in. × 15-in. ASTM A572 Grade 50.

The vertical and horizontal forces are:

LRFD	ASD
P_u = 30 kips R_u = 60 kips F_u = 6 kips	P_a = 20 kips R_a = 40 kips F_a = 4 kips

Solution

A572 Gr. 50: F_y = 50 ksi
W18×50: t_w = 0.550 in.
Plate: t = ¾ in. d = 15 in. L = 10 in.
C_b = 1.26
k = 2

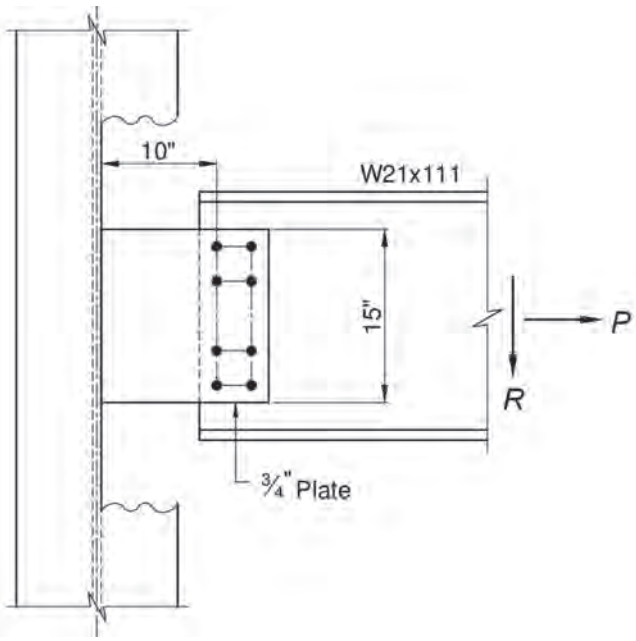

Fig. 13. Beam connection for Example 1.

The required minimum plate thickness calculated with Equation 59 is:

$$t_{min} = 1.54\sqrt{\frac{LdF_y}{C_bE}} \tag{59}$$

$$= 1.54\sqrt{\frac{(10 \text{ in.})(15 \text{ in.})(50 \text{ ksi})}{(1.26)(29{,}000 \text{ ksi})}}$$

$$= 0.698 \text{ in.} < 0.750 \text{ in.} \quad \textbf{o.k.}$$

Combining Equations 50, 51 and 60, the required torsional moment, T_r, is:

LRFD	ASD
$T_u = 1.1R_u\left(\frac{t+t_w}{2}\right)$	$T_a = 1.1R_a\left(\frac{t+t_w}{2}\right)$
$= (1.1)(60 \text{ kips})\left(\frac{0.550 \text{ in.} + 0.750 \text{ in.}}{2}\right)$	$= (1.1)(40 \text{ kips})\left(\frac{0.550 \text{ in.} + 0.750 \text{ in.}}{2}\right)$
$= 42.9$ kip-in.	$= 28.6$ kip-in.

The required shear force, V_r, is:

LRFD	ASD
$V_u = \sqrt{R_u^2 + F_u^2}$	$V_a = \sqrt{R_a^2 + F_a^2}$
$= \sqrt{(60 \text{ kips})^2 + (6 \text{ kips})^2}$	$= \sqrt{(40 \text{ kips})^2 + (4 \text{ kips})^2}$
$= 60.3$ kips	$= 40.2$ kips

The required strong-axis flexural strength, M_{rx}, is:

LRFD	ASD
$M_{ux} = (60 \text{ kips})(10 \text{ in.})$	$M_{ax} = (40 \text{ kips})(10 \text{ in.})$
$= 600$ kip-in.	$= 400$ kip-in.

The required weak-axis flexural strength, M_{ry}, is:

LRFD	ASD
$M_{uy} = (6 \text{ kips})(10 \text{ in.})$	$M_{ay} = (4 \text{ kips})(10 \text{ in.})$
$= 60.0$ kip-in.	$= 40.0$ kip-in.

The nominal axial tensile strength is:

$$P_n = (50 \text{ ksi})(0.750 \text{ in.})(15 \text{ in.})$$
$$= 563 \text{ kips}$$

The available axial tensile strength is:

LRFD	ASD
$\phi P_n = (0.90)(563 \text{ kips})$	$P_n/\Omega = 563 \text{ kips}/1.67$
$= 507$ kips	$= 337$ kips

Combining Equations 7 and 42, the nominal torsional strength is:

$$T_p = \frac{(0.6)(50\text{ ksi})(0.750\text{ in.})^2(15\text{ in.})}{2}\left[1+\frac{15\text{ in.}}{(2.4)(10\text{ in.})}\right]$$
$$= 185\text{ kip-in.}$$

The available torsional strength is:

LRFD	ASD
$\phi T_p = (0.90)(185\text{ kip-in.})$ $= 167\text{ kip-in.}$	$T_p/\Omega = 185\text{ kip-in.}/1.67$ $= 111\text{ kips}$

The nominal shear strength is:

$$V_n = (0.6)(50\text{ ksi})(0.750\text{ in.})(15\text{ in.})$$
$$= 338\text{ kips}$$

The available shear strength is:

LRFD	ASD
$\phi V_n = (1.00)(338\text{ kips})$ $= 338\text{ kips}$	$V_n/\Omega = 338\text{ kips}/1.50$ $= 225\text{ kips}$

The nominal strong-axis flexural strength is:

$$M_{nx} = (50\text{ ksi})\left[\frac{(0.750\text{ in.})(15\text{ in.})^2}{4}\right]$$
$$= 2{,}110\text{ kip-in.}$$

The available strong-axis flexural strength is:

LRFD	ASD
$\phi M_{nx} = (0.90)(2{,}110\text{ kip-in.})$ $= 1{,}900\text{ kip-in.}$	$M_{nx}/\Omega = 2{,}110\text{ kip-in.}/1.67$ $= 1{,}260\text{ kip-in.}$

The nominal weak-axis flexural strength is:

$$M_{ny} = (50\text{ ksi})\left[\frac{(15\text{ in.})(0.750\text{ in.})^2}{4}\right]$$
$$= 105\text{ kip-in.}$$

The available weak-axis flexural strength is:

LRFD	ASD
$\phi M_{ny} = (0.90)(105\text{ kip-in.})$ $= 94.5\text{ kip-in.}$	$M_{ny}/\Omega = 105\text{ kip-in.}/1.67$ $= 62.9\text{ kip-in.}$

For LRFD, interaction according to Equation 61 is:

$$\left(\frac{30\text{ kips}}{507\text{ kips}}\right)^2+\left(\frac{42.9\text{ kip-in.}}{167\text{ kip-in.}}\right)^2+\left(\frac{60.3\text{ kips}}{338\text{ kips}}\right)^4+\left[\left(\frac{600\text{ kip-in.}}{1{,}900\text{ kip-in.}}\right)^{1.7}+\left(\frac{60.0\text{ kip-in.}}{94.5\text{ kip-in.}}\right)^{1.7}\right]^{0.59} \tag{61}$$

$$=0.812<1.0 \quad \textbf{o.k.}$$

For ASD, interaction according to Equation 61 is:

$$\left(\frac{20\text{ kips}}{337\text{ kips}}\right)^2+\left(\frac{28.6\text{ kip-in.}}{111\text{ kip-in.}}\right)^2+\left(\frac{40.2\text{ kips}}{225\text{ kips}}\right)^4+\left[\left(\frac{400\text{ kip-in.}}{1{,}260\text{ kip-in.}}\right)^{1.7}+\left(\frac{40.0\text{ kip-in.}}{62.9\text{ kip-in.}}\right)^{1.7}\right]^{0.59} \tag{61}$$

$$=0.815<1.0 \quad \textbf{o.k.}$$

Example 2

Given

During erection of the W21 beam in Example 1, a field correction requires the beam to be moved ½ in. horizontally, perpendicular to the beam axis. If a ½-in. filler plate is installed between the ¾-in. plate and the beam web, is the plate strength adequate?

Solution

The eccentricity increases to:

$$e=\frac{0.550\text{ in.}+0.750\text{ in.}}{2}+0.500\text{ in.}$$

$$=1.15\text{ in.}$$

The required torsional moment, T_r, increases to:

LRFD	ASD
$T_u=(1.1)(60\text{ kips})(1.15\text{ in.})$ $=75.9\text{ kip-in.}$	$T_a=(1.1)(40\text{ kips})(1.15\text{ in.})$ $=50.6\text{ kip-in.}$

For LRFD, interaction according to Equation 61 is:

$$\left(\frac{30\text{ kips}}{507\text{ kips}}\right)^2+\left(\frac{75.9\text{ kip-in.}}{167\text{ kip-in.}}\right)^2+\left(\frac{60.3\text{ kips}}{338\text{ kips}}\right)^4+\left[\left(\frac{600\text{ kip-in.}}{1{,}900\text{ kip-in.}}\right)^{1.7}+\left(\frac{60.0\text{ kip-in.}}{94.5\text{ kip-in.}}\right)^{1.7}\right]^{0.59} \tag{61}$$

$$=0.953<1.0 \quad \textbf{o.k.}$$

For ASD, interaction according to Equation 61 is:

$$\left(\frac{20\text{ kips}}{337\text{ kips}}\right)^2+\left(\frac{50.6\text{ kip-in.}}{111\text{ kip-in.}}\right)^2+\left(\frac{40.2\text{ kips}}{225\text{ kips}}\right)^4+\left[\left(\frac{400\text{ kip-in.}}{1{,}260\text{ kip-in.}}\right)^{1.7}+\left(\frac{40.0\text{ kip-in.}}{62.9\text{ kip-in.}}\right)^{1.7}\right]^{0.59} \tag{61}$$

$$=0.956<1.0 \quad \textbf{o.k.}$$

Example 3

Given

In this example, a gusset plate connects a WT horizontal brace to a roof beam and a truss top chord. Figure 14 shows the connection rotated into the roof plane. Both the brace and the roof beam are in the roof plane, which is sloped at 20° from horizontal, and the chord web is in the horizontal plane. Because the chord is rotated 20° relative to the gusset plate, the gusset-to-chord interface has been detailed with a skewed end plate welded to the gusset plate. The end plate is 1-in. × 18-in. ASTM A572 Grade 50. The brace component parallel to the truss chord, P_L, is transferred into the chord, and the component perpendicular to the chord, P_T, is transferred into the roof beam. Because the bracing work point is located at the chord centroid, the chord was designed assuming concentric axial loading; therefore, P_L must be transferred to the work point at the chord centroid. For static equilibrium of the connection, the 1-in. end plate is subjected to both flexure and torsion. Only the end plate at the gusset-to-chord interface will be designed in this example.

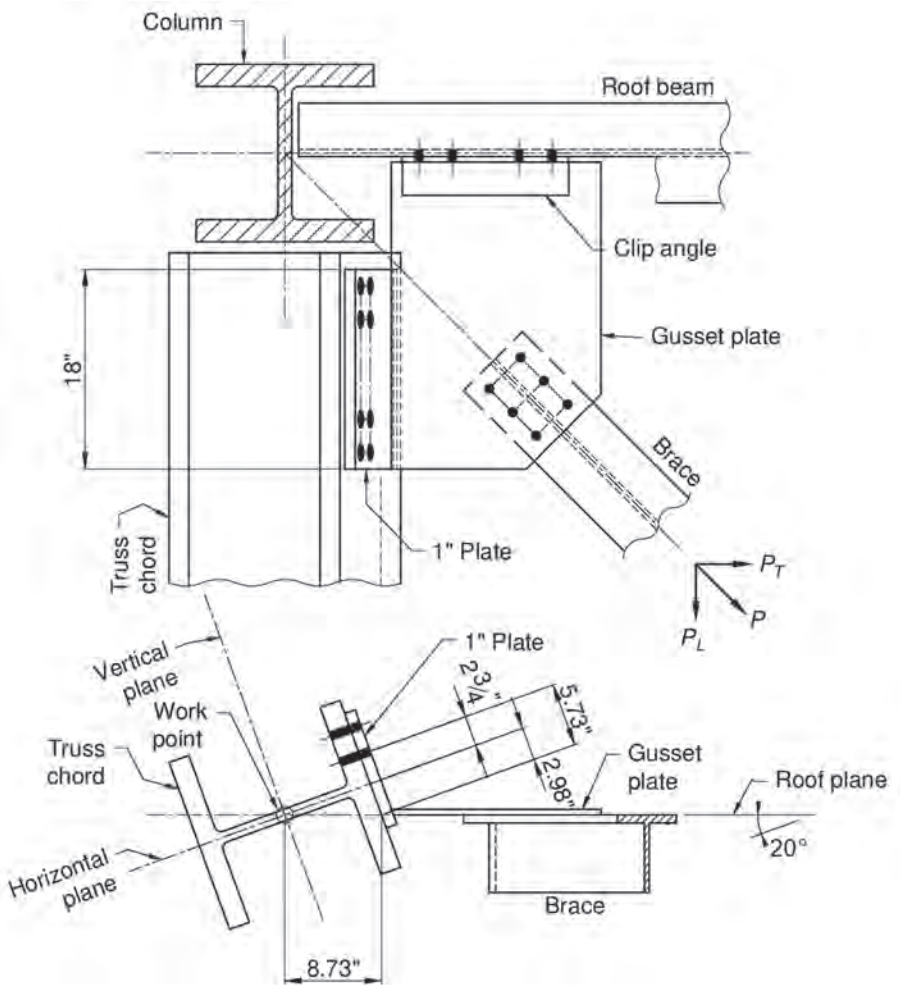

Fig. 14. Horizontal brace connection for Example 3.

Solution

The brace component parallel to the truss chord axis is:

LRFD	ASD
$P_{uL} = 50.0$ kips	$P_{aL} = 33.3$ kips

A572 Gr. 50: $F_y = 50$ ksi
Plate: $t = 1$ in. $d = 15$ in. $L = 5.73$ in.
$C_b = 1.84$

The required minimum plate thickness calculated with Equation 59 is:

$$t_{min} = 1.54\sqrt{\frac{LdF_y}{C_bE}} \tag{59}$$

$$= 1.54\sqrt{\frac{(5.73 \text{ in.})(15 \text{ in.})(50 \text{ ksi})}{(1.84)(29{,}000 \text{ ksi})}}$$

$$= 0.284 \text{ in.} < 1 \text{ in.} \quad \textbf{o.k.}$$

The moment in the roof plane is P_L multiplied by the eccentricity in the roof plane, which is the distance from the work point to the faying surface between the chord flange and the 1-in. end plate.

LRFD	ASD
$M_{ui} = (50 \text{ kips})(8.73 \text{ in.})$ $= 437$ kip-in.	$M_{ai} = (33.3 \text{ kips})(8.73 \text{ in.})$ $= 291$ kip-in.

The required strong-axis flexural strength of the end plate, M_{rx}, is:

LRFD	ASD
$M_{ux} = (437 \text{ kip-in.})\sin(20°)$ $= 149$ kip-in.	$M_{ax} = (291 \text{ kip-in.})\sin(20°)$ $= 99.5$ kip-in.

The first-order torsional moment in the end plate is:

LRFD	ASD
$T_{u1} = (437 \text{ kip-in.})\cos(20°)$ $= 411$ kip-in.	$T_{a1} = (291 \text{ kip-in.})\cos(20°)$ $= 273$ kip-in.

The required second-order torsional strength of the end plate, T_r, is:

LRFD	ASD
$T_u = (1.1)(411 \text{ kip-in.})$ $= 452$ kip-in.	$T_a = (1.1)(273 \text{ kip-in.})$ $= 300$ kip-in.

The required shear strength of the end plate, V_r, is:

LRFD	ASD
$V_u = P_{uL} = 50.0$ kips	$V_a = P_{aL} = 33.3$ kips

These loads are shown on the free-body diagram in Figure 15.

Combining Equations 7 and 42, the nominal torsional strength is:

$$T_p = \frac{(0.6)(50 \text{ ksi})(1 \text{ in.})^2 (18 \text{ in.})}{2}\left[1 + \frac{18 \text{ in.}}{(2.4)(5.73 \text{ in.})}\right]$$

$$= 623 \text{ kip-in.}$$

The available torsional strength is:

LRFD	ASD
$\phi T_p = (0.90)(623 \text{ kip-in.})$ $= 561 \text{ kip-in.}$	$T_p/\Omega = 623 \text{ kip-in.}/1.67$ $= 373 \text{ kips}$

The nominal shear strength is:

$$V_n = (0.6)(50 \text{ ksi})(1 \text{ in.})(18 \text{ in.})$$

$$= 540 \text{ kips}$$

The available shear strength is:

LRFD	ASD
$\phi V_n = (1.00)(540 \text{ kips})$ $= 540 \text{ kips}$	$V_n/\Omega = 540 \text{ kips}/1.50$ $= 360 \text{ kips}$

The nominal strong-axis flexural strength is:

$$M_{nx} = (50 \text{ ksi})\left[\frac{(1 \text{ in.})(18 \text{ in.})^2}{4}\right]$$

$$= 4{,}050 \text{ kip-in.}$$

The available strong-axis flexural strength is:

LRFD	ASD
$\phi M_{nx} = (0.90)(4{,}050 \text{ kip-in.})$ $= 3{,}650 \text{ kip-in.}$	$M_{nx}/\Omega = 4{,}050 \text{ kip-in.}/1.67$ $= 2{,}430 \text{ kip-in.}$

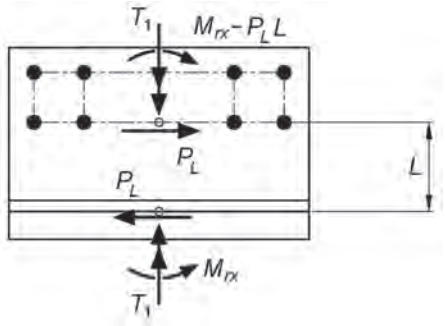

Fig. 15. Free-body diagram of 1-in. end plate.

For LRFD, interaction according to Equation 61 is:

$$\left(\frac{452 \text{ kip-in.}}{561 \text{ kip-in.}}\right)^2+\left(\frac{50.0 \text{ kips}}{540 \text{ kips}}\right)^4+\frac{149 \text{ kip-in.}}{3{,}650 \text{ kip-in.}} \tag{61}$$
$$= 0.690 < 1.0 \quad \textbf{o.k.}$$

For ASD, interaction according to Equation 61 is:

$$\left(\frac{300 \text{ kip-in.}}{373 \text{ kip-in.}}\right)^2+\left(\frac{33.3 \text{ kips}}{360 \text{ kips}}\right)^4+\frac{99.5 \text{ kip-in.}}{2{,}430 \text{ kip-in.}} \tag{61}$$
$$= 0.688 < 1.0 \quad \textbf{o.k.}$$

CONCLUSIONS

The torsional strength of connection elements can be attributed to the resistance due to uniform torsion, warping torsion, and the Wagner effect. For long members subjected to reasonable torsional rotations, the contribution of both the warping and Wagner torsions are negligible. However, for short members and connection elements, their effect can be significant. If only the elastic uniform (Saint Venant) torsion is considered, the resistance can be significantly underestimated.

For many connection elements, this investigation showed that the torsional strength can be defined as the sum of the plastic uniform torsion strength and the plastic warping strength. For long connection elements, such as extended single-plate connections, the Wagner torsional resistance is negligible at reasonable service rotation limits. However, the Wagner resistance is significant for short connection elements such as conventional single-plate connections, allowing torsional effects to be neglected for these connections.

A method has been proposed for the ultimate strength design of rectangular connection elements subjected to any possible combination of loads, including torsion. The design method results in a significant increase in torsional strength compared to traditional analysis methods. Several design examples showed the proper application of the proposed design method.

For nonstiffened extended single-plate connections, the design procedure in the AISC *Manual* (AISC, 2017) implicitly limits excessive torsional rotations. For connections subjected only to shear loads, the proposed design method results in strengths similar to the AISC *Manual* procedure by explicitly considering torsional effects. The proposed method can also be used to analyze extended single-plate connections subjected to axial forces and out-of-plane forces.

SYMBOLS

B	Amplification factor for second-order torsional effects
C_b	Lateral-torsional buckling modification factor
C_w	Warping constant, in.^{6}
E	Modulus of elasticity, ksi
F	Horizontal couple force, kips
F_{cr}	Critical stress, ksi
F_y	Specified minimum yield strength, ksi
F_{wy}	Horizontal couple force required to initiate first yield, kips
G	Shear modulus of elasticity = 11,200 ksi
I_e	Moment of inertia for the equivalent beam, in.^{4}
I_n	Wagner constant, in.^{6}
J	Torsional constant, in.^{4}
L	Member length, in.
M_{cr}	Elastic critical buckling moment for strong-axis flexure, kip-in.
M_{cx}	Available flexural strength about the x-axis, kip-in.
M_{cy}	Available flexural strength about the y-axis, kip-in.
M_{nx}	Strong-axis flexural strength, kip-in.
M_p	Plastic flexural strength, kip-in.
M_{pe}	Plastic flexural strength of the equivalent beam, kip-in.
M_{px}	Plastic flexural strength about the x-axis, kip-in.

M_{py} Plastic flexural strength about the y-axis, kip-in.

M_{re} Required moment for the equivalent beam, kip-in.

M_{rx} Required x-axis flexural strength, kip-in.

M_{ry} Required y-axis flexural strength, kip-in.

M_{ye} Yield moment of the equivalent beam, kip-in.

P_c Available axial strength, kips

P_r Required axial strength, kips

P_y Axial yield load, kips

R_r Required beam end shear reaction, kips

R_c Calculated shear strength, kips

R_e Approximate experimental shear load where the load-deflection curve became nonlinear, kips

R_u Maximum experimental shear load, kips

S_x Elastic section modulus about the x-axis, in.^{3}

T_1 First-order torsional moment, kip-in.

T_2 Second-order torsional moment, kip-in.

T_b Torsional resistance provided by a top flange lateral brace, kip-in.

T_c Available torsional strength, kips

T_e Sum of the Wagner torsional moment and the uniform torsional moment, kip-in.

T_n Wagner torsional moment, kip-in.

T_p Plastic torsional moment, kip-in.

T_r Required torsional moment, kip-in.

T_u Uniform torsional moment, kip-in.

T_{up} Plastic uniform torsional moment, kip-in.

T_{uy} First-yield uniform torsional moment, kip-in.

T_w Warping torsional moment, kip-in.

T_{wi} Inelastic warping torsional moment, kip-in.

T_{wp} Plastic warping torsional moment, kip-in.

T_{wy} First-yield warping torsional moment, kip-in.

V_c Available shear strength, kips

V_p Plastic shear strength, kips

V_r Required shear strength, kips

W_{nc} Normalized warping function at the corner of the cross section, in.^{2}

a Constant as defined by Equation 15, in.

c Distance to outermost fiber, in.

d Member depth, in.

e Horizontal eccentricity for a single-plate connection, in.

h Distance between couple forces, F, in.

k Exponent applied to the axial load ratio

t Member thickness, plate thickness, in.

t_w Beam web thickness, in.

z Distance along the member length, in.

αd Effective depth of the equivalent cross section, in.

β Normalized increase in torsional resistance due to the Wagner effect

δ Deflection of equivalent beam

δ_y Yield deflection of equivalent beam

τ_y Shear yield stress = $0.6F_y$, ksi

θ Angle of rotation, rad

θ_i Inelastic angle of rotation, rad

θ_u Angle of rotation for uniform torsion, rad

θ_{uy} First-yield angle of rotation for uniform torsion, rad

θ_w Angle of rotation for warping, rad

θ_{wy} First-yield angle of rotation for warping, rad

θ_1 First-order torsional rotation, rad

θ_2 Second-order torsional rotation, rad

θ' Angle of rotation per unit length, first derivative of θ with respect to z, rad/in.

θ'' Second derivative of θ with respect to z, rad/in.^{2}

θ''' Third derivative of θ with respect to z, rad/in.^{3}

σ_n Axial stress developed by the Wagner effect, ksi

σ_{nt} Maximum axial stress developed by the Wagner effect, ksi

σ_{wc} Maximum warping normal stress, ksi

REFERENCES

Abou-Zidan, A. (2014), *Finite Element Study on Unstiffened Extended Single Plate Shear Connections*, Master's Thesis, Dalhousie University, Halifax, Nova Scotia.

AISC (2016), *Specification for Structural Steel Buildings*, ANSI/AISC 360–16, American Institute of Steel Construction, Chicago, IL.

AISC (2017), *Steel Construction Manual*, 15th Ed., American Institute of Steel Construction, Chicago, IL.

Ashkinadze, K. (2008), "Proposals for Limit States Torsional Strength Design of Wide-Flange Steel Members," *Canadian Journal of Civil Engineering*, Vol. 35, pp. 200–209.

Baba, S. and Kajita, T. (1982), "Plastic Analysis of Torsion of a Prismatic Beam," *International Journal for Numerical Methods in Engineering*, Vol. 18, pp. 927–944.

Balaz, I. and Kolekova, Y. (2002), "Warping," *Stability and Ductility of Steel Structures*, Proceedings of the Otto Halasz Memorial Session, Editor: Ivanyi, M., Akademiai Kiado, Budapest.

Bathe, K.J. and Chaudhary, A. (1982), "On the Displacement Formulation of Torsion of Shafts with Rectangular Cross-Sections," *International Journal for Numerical Methods in Engineering*, Vol. 18, pp. 1565–1580.

Bennetts, I.D., Thomas, I.R. and Grundy, P. (1981), "Torsional Stiffness of Shear Connections," *Proceedings of the Metal Structures Congress,* National Committee on Metal Structures of the Institution of Engineers, Australia, Newcastle, May 11–14, pp. 102–106.

Boissonnade, N., Muzeau, J.P. and Villette, M. (2002), "Amplification Effects for Lateral Torsional Buckling," *Stability and Ductility of Steel Structures*, pp. 73–80.

Cook, R.D. and Young, W.C. (1985), *Advanced Mechanics of Materials*, Macmillan Publishing Company, London, England.

Dinno, K.S. and Merchant, W. (July 1965), "A Procedure for Calculation the Plastic Collapse of I-Sections Under Bending and Torsion," *The Structural Engineer*, Vol. 43, No. 7, pp. 219–221.

Dowswell, B. (2004), "Lateral-Torsional Buckling of Wide Flange Cantilever Beams," *Engineering Journal*, AISC, Vol. 41, No. 2, pp. 85–91.

Dowswell, B. (2015), "Plastic Strength of Connection Elements," *Engineering Journal*, AISC, Vol 52, No. 1, pp. 47–65.

Dowswell, B. (2016), "Stability of Rectangular Connection Elements," *Engineering Journal*, AISC, Vol. 53, No. 4, pp. 171–202.

Gjelsvik, A. (1981), *The Theory of Thin Walled Bars*, John Wiley and Sons.

Goodrich, W. (2005), *Behavior of Extended Shear Tabs in Stiffened Beam-to-Column Web Connections*, Master's Thesis, Vanderbilt University.

Gregory, M. (1960), "The Bending and Shortening Effect of Pure Torque," *Australian Journal of Applied Science*, Vol. 11, pp. 209–216.

Hijaj, M.A. and Mahamid, M. (2017), "Behavior of Skewed Extended Shear Tab Connections Part I: Connection to Supporting Web," *Journal of Constructional Steel Research*, Vol. 128, pp. 305–320.

Kjar, A.R. (1967), "The Axis of Distortion," *International Journal of Mechanical Science*, Vol. 9, pp. 873–883.

Lindner, J. and Glitsch, T. (2005), "Simplified Design of Crane Girders with Open Cross Sections Subjected to Biaxial Bending and Torsion," *Advances in Steel Structures*, Vol. 1, pp. 95–104.

Mahamid, M., Rahman, A. and Ghorbanpoor, A. (2007), "The Analysis of Extended Shear Tab Connections Part II: Stiffened Connections," *Engineering Journal*, AISC, Vol. 44, No. 2, pp. 133–145.

May, I.M. and Al-Shaarbaf, I.A.S. (1989), "Elasto-Plastic Analysis of Torsion Using a Three-Dimensional Finite Element Model," *Computers and Structures*, Vol. 33, No. 3, pp. 667–678.

Moore, W.E. and Mueller, K.M. (2002), "Technical Note: Torsional Analysis of Steel Sections," *Engineering Journal*, AISC, Vol. 39, No. 4, pp. 182–188.

Moore, D.B., and Owens, G.W. (February 1992), "Verification of Design Methods for Finplate Connections," *The Structural Engineer,* Vol. 70, No. 3/4.

Muir, L.S. and Hewitt, C.M. (2009), "Design of Unstiffened Extended Single-Plate Shear Connections," *Engineering Journal*, AISC, Vol. 46, No. 2, pp. 67–79.

Neal, B.G. (January 1950), "The Lateral Instability of Yielded Mild Steel Beams of Rectangular Cross-Section," *Philosophical Transactions of the Royal Society of London*, Vol. 242, No. 846, pp. 197–242.

Pastor, T.P. (1977), *Behavior of Beams Loaded both Flexurally and Torsionally*, Master's Thesis, The University of Connecticut, Mansfield, CT.

Pi, Y.L. and Trahair, N.S. (December 1994), "Inelastic Bending and Torsion of Steel I-Beams," *Journal of Structural Engineering*, ASCE, Vol. 120, No. 12, pp. 3397–3417.

Pi, Y.L. and Trahair, N.S. (October 1995), "Plastic-Collapse Analysis of Torsion," *Journal of Structural Engineering*, ASCE, Vol. 121, No. 10, pp. 1389–1395.

Rahman, A., Mahamid, M., Amro, A. and Ghorbanpoor, A. (2007), "The Analysis of Extended Shear Tab Connections Part I: The Unstiffened Connections," *Engineering Journal*, AISC, Vol. 44, No. 2, pp. 117–132.

Reissner, E. and Stein, M. (1951), *Torsion and Transverse Bending of Cantilever Plates*, NACA Technical Note 2369, National Advisory Committee for Aeronautics, June.

Seaburg, P.A. and Carter, C.J. (1997), *Torsional Analysis of Structural Steel Members*, Design Guide 9, AISC, Chicago, IL.

Sherman, D.R. and Ghorbanpoor, A. (2002), *Design of Extended Shear Tabs,* Final Report, American Institute of Steel Construction, Chicago, IL.

Suleiman, M.F. (2013), *Non-Linear Finite Element Analysis of Extended Shear Tab Connections*, Ph.D. Dissertation, University of Cincinnati, Cincinnati, OH.

Timoshenko, S. (1956), *Strength of Materials*, D. Van Nostrand Company.

Thornton, W.A. and Fortney, P.J. (2011), "On the Need for Stiffeners for and the Effect of Lap Eccentricity on Extended Single-Plate Connections," *Engineering Journal*, AISC, Vol. 48, No. 2, pp. 117–125.

Trahair, N.S. (2003), *Non-Linear Elastic Non-Uniform Torsion*, Research Report No. R828, Center for Advanced Structural Engineering, University of Sydney, Sydney, Australia, June.

Trahair, N.S., Bradford, M.A., Nethercot, D.A. and Gardner, L. (2008), *The Behavior and Design of Steel Structures to EC3*, 4th Ed., Taylor and Francis.

Trahair, N.S. and Teh, L.H. (2000), *Second Order Moments in Torsion Members*, Research Report No. R800, Centre for Advanced Structural Engineering, University of Sydney, Sydney, Australia.

Wagner, H. (1936), *Torsion and Buckling of Open Sections*, NACA Technical Memorandum No. 807, National Advisory Committee for Aeronautics.

Wittrick, W.H. (1952), "Lateral Instability of Rectangular Beams of Strain-Hardening Material Under Uniform Bending," *Journal of the Aeronautical Sciences*, Vol. 19, No. 12, December, pp. 835–843.

Zahn, J.J. (1984), "Loss of Torsional Stiffness Caused by Beam Loading," *Journal of Structural Engineering*, ASCE, Vol. 110, No. 1, January, pp. 47–54.

Guidance on Shear Rupture, Ductility and Element Capacity in Welded Connections

PATRICK J. FORTNEY, LARRY S. MUIR and WILLIAM A. THORNTON

ABSTRACT

Several considerations need to be made while in the process of designing welds and welded connections. For the most part, the AISC *Specification for Structural Steel Buildings*, in combination with corresponding parts of the AISC *Steel Construction Manual*, provides fairly good guidance on what is required to design *Specification*-compliant welds. However, there seems to be some confusion and controversy in regard to a few of these considerations. Specifically: (1) When is the load path from the weld to the connecting element(s) unclear? (2) When should the ductility factor be applied to a weld? (3) When should a weld be sized to develop the strength of a connecting plate? This paper is written in an effort to provide guidance in regard to these three considerations. Background into the development of the equations used to make these checks along with some discussion on the intent of application is provided and supported with some anecdotal examples. It is the objective of the authors to shed some light on these issues and hopefully clear any confusion and/or controversy, as well as to encourage more consistency throughout the steel construction industry with regard to these three considerations.

Keywords: welded connections, shear rupture, ductility, element capacity.

INTRODUCTION

In the authors' opinion, three of the most misunderstood and misapplied limit state checks in welded connection design are (1) application of matching fillet weld strength to base material strength when the load path within the base metal under the load is not readily known (AISC, 2017a, p. 9-5), (2) when to apply the ductility factor (1.25) when sizing a weld, and (3) when a weld should develop the strength of the connecting material. The objective of this paper is to shed some light on the development of the equations used to make these three types of checks, provide discussion in regard to the various applications of these checks, and present example problems demonstrating those applications.

Data related to every possible condition that might be encountered in practice simply are not available. In some instances, the authors are recommending practices based on their own knowledge, experience and judgment. Many of the recommendations are conservative, though considered reasonable by the authors. Sources of conservatism are noted. Though the authors often approached the topics discussed with divergent views, this paper represents a consensus of the authors.

Patrick J. Fortney, Ph.D., P.E., S.E., P.Eng., Associate Professor, University of Cincinnati, Cincinnati, OH. Email: patrick.fortney@uc.edu (corresponding)

Larry S. Muir, P.E., Consultant, Muir Consulting, Atlanta, GA. Email: larrymuir@larrymuir.com

William A. Thornton, Ph.D., P.E., NAE, Consultant, Cives Engineering Corporation, Alpharetta, GA. Email: bthornton@cives.com

Paper No. 2017–27R

PART 1: MATCHING WELD AND BASE MATERIAL STRENGTHS

Derivation

Part 9 of the AISC *Steel Construction Manual*, hereafter referred to as the AISC *Manual*, provides a brief discussion of how to address base material rupture strength at welds entitled, "Connecting Element Rupture Strength at Welds." The equations given in the AISC *Manual* for one- and two-sided fillet welds (Equations 9-2 and 9-3) are repeated here for convenience (see Equations 1 and 2, respectively).

$$t_{min} = \frac{3.09D}{F_u} \tag{1}$$

$$t_{min} = \frac{6.19D}{F_u} \tag{2}$$

In Equations 1 and 2, D is the weld size in sixteenths of an inch and F_u is the specified minimum tensile strength of the base material adjacent to the weld.

The derivations of Equations 1 and 2 are fairly straightforward. As already stated, the intent is to match the weld strength to the base material strength. In other words, ensure that the shear rupture strength of the base material is at least equal to the rupture strength of the weld.

Figure 1 shows a one-sided weld condition. As shown in Figure 1, the shear rupture plane in the weld is assumed to be along the throat of the weld as shown with solid shading.

To ensure that the base material is at least thick enough to develop the rupture strength of the weld, a minimum thickness will be required for the rupture area of the base material shown in Figure 1 with cross hatching. We simply write equations to describe the shear rupture strengths of the two areas and set the two to equal each other. For the weld strength, the area is written in terms of the weld leg size in sixteenths of an inch (commonly known as *D*). Also, as can be seen in the derivation, the specified minimum tensile strength of the weld material, F_{EXX}, is assumed to be 70 ksi.

Note that the length of the weld, *l*, as shown in Figure 1 is not important because the derivation will show that the limit state checks given in Equations 1 and 2 are unit length checks.

The nominal shear rupture strength of the weld, based on the nominal stress, $F_{nw} = 0.60F_{exx}$, from AISC *Specification* Table J2.5 (AISC, 2016c), is given by Equation 3.

$$R_{nw} = 0.60F_{EXX}\cos 45°\left(\frac{D}{16}\right)l$$

If $F_{EXX} = 70$ ksi

$$R_{nw} = (0.60)(70)\cos 45°\left(\frac{D}{16}\right)l$$

$$R_{nw} = 1.856Dl \tag{3}$$

The shear rupture strength of the base material, from AISC *Specification* Section J4, is given in Equation 4 in terms of a minimum plate thickness.

$$R_{np} = 0.60F_u l t_{\min} \tag{4}$$

Setting Equation 3 and 4 equal to each other then rearranging to solve for the minimum plate thickness, t_{min}, gives Equation 1.

$$R_{nw} = R_{np}$$
$$1.856Dl = 0.60F_u l t_{min}$$
$$t_{min} = \frac{1.856Dl}{0.60F_u l}$$

$$t_{min} = \frac{3.09D}{F_u}$$

Suppose the base material shown in Figure 1 has connecting elements on both faces, as shown in Figure 2. In this case, the shear rupture area of the base material does not change. However, the weld rupture area doubles. In this case, the weld shear rupture strength is as given in Equation 5.

$$R_{nw} = (2)0.60F_{EXX}\cos 45°\left(\frac{D}{16}\right)l$$

If $F_{EXX} = 70$ ksi

$$R_{nw} = (2)(0.60)(70)\cos 45°\left(\frac{D}{16}\right)l$$

$$R_{nw} = 3.712Dl \tag{5}$$

Setting Equations 4 and 5 equal to each other and then rearranging to solve for the minimum plate thickness, t_{min}, gives Equation 2.

$$R_{nw} = R_{np}$$
$$3.712Dl = 0.60F_u l t_{min}$$
$$t_{min} = \frac{3.712Dl}{0.60F_u l}$$

$$t_{min} = \frac{6.19D}{F_u}$$

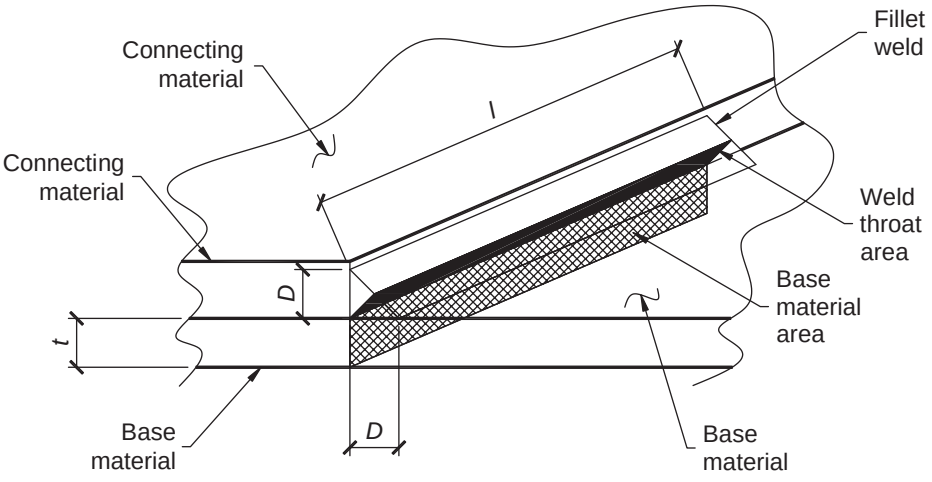

Fig. 1. Weld and base material shear rupture area in a one-sided weld condition.

Discussion

In effect, Equations 1 and 2 ensure that the base material will not rupture in shear adjacent to the weld when the weld size used to calculate t_{min} is provided in the connection. But it is critical to understand how the weld size, D, is calculated in the derivation of Equations 1 and 2. If we examine Equation 3, we find that its derivation is the same as that for the fillet weld equations, Equations 8-2a and 8-2b, provided in AISC *Manual* Part 8. If we multiply Equation 3 by the LRFD ϕ factor (0.75) or divide by the ASD Ω factor (2.00), we get those two well-known equations. Equations 8-2a and 8-2b of the AISC *Manual* are repeated here for convenience. See Equations 6 and 7. Equation 5 is simply Equation 3 multiplied by 2, which is analogous to having two weld lines.

$$R_{nw} = 1.856Dl$$

$$\phi R_{nw} = (0.75)(1.856)Dl$$

$$\phi R_{nw} = 1.392Dl \quad (6)$$

$$R_{nw} = 1.856Dl$$

$$\frac{R_{nw}}{\Omega} = \frac{1.856Dl}{2.00}$$

$$\frac{R_{nw}}{\Omega} = 0.928Dl \quad (7)$$

Equations 1 and 2 can be thought of as a shear rupture check for the base material. However, this is only accurate when the provided fillet weld size is exactly the size calculated from Equations 6 or 7—in other words, when the fillet weld is sized based on strength. If the provided fillet weld size is larger than that calculated using Equations 6 or 7, then Equations 1 and 2 will predict a required plate thickness larger than what is required by a factor of D_{prov}/D_{req}.

In simple terms, Equations 1 and 2 will result in a base material thickness that is able to develop the strength of the weld and is independent of the load required to be transferred by the weld.

Not Readily Known…

When is the shear rupture area not "readily known?" One way to look at this is that the demand on the base material is not readily known. When this is the case, Equations 1 and 2 provide a conservative approach to ensure that the base material adjacent to the weld, at every point along the length of the weld, is thick enough to develop the strength of the weld actually provided independent of the actual required load for which the weld was sized.

Another condition is when a weld group is loaded eccentrically and the weld size is determined using, for instance, the instantaneous center of rotation method. Figure 3 shows a W16×57 beam connected to a W14×90 column with a shop-welded/field-bolted, double-angle connection. The fibers of the web of the beam, adjacent to the weld, are subjected to a combination of shear and tensile stresses induced by the rotational demands inherent with the eccentric nature of the loading on the weld group. Therefore, the stresses in the beam web, adjacent to the weld, are not readily known, and the shear rupture check of the base metal provided by AISC *Specification* Section J4.2 cannot be applied directly.

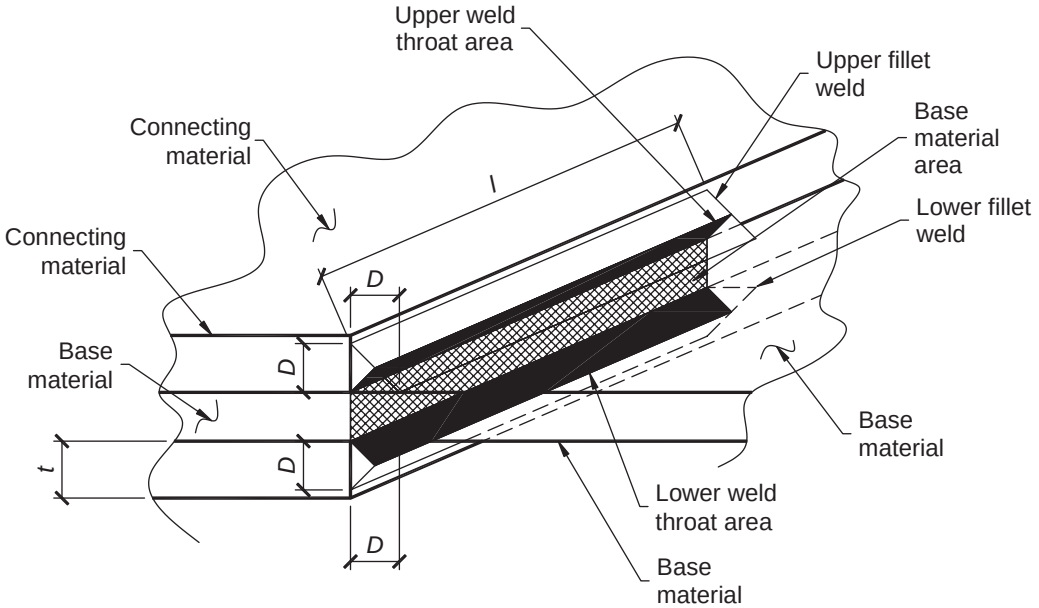

Fig. 2. Weld and base material rupture area in a two-sided weld condition.

Again, in this case, Equations 1 and 2 can be used as a conservative approach to ensure that the base material adjacent to the weld, at every point along the length of the weld, is sufficient to develop the strength of the provided weld.

Byproduct Use of Equations 1 and 2

It is not unprecedented that Equations 1 and 2 have been used to check base material thickness in connections where shear rupture in the base material adjacent to the weld is not an applicable limit state. Figure 5 (discussed later) shows such a condition. Figure 4(a) shows an extended single-plate simple shear connection transferring load to the web of a wide flange column. There are various design example problems in AISC documents where Equations 1 or 2 are used to check the thickness of the column web; even though shear rupture in the column web is not an applicable limit state, the column is continuous past the extent of the plate connection. In the absence of an industry consensus approach to this problem, even though Equations 1 and 2 do not represent a viable limit state, they nevertheless give a conservative result.

There is a phenomenon that will occur as a result of this load transfer. Certainly, the column web will experience some shear stress but, more than likely, in combination with compression and tension stresses as the load, R, accumulates over the length (depth), l, of the plate. Figure 4(b) is a sketch of this possible phenomenon. In Figure 4(b), the load transferred from the plate to the column web may be some combination of the load hanging from the column web above the plate and pushing on the column web below the plate.

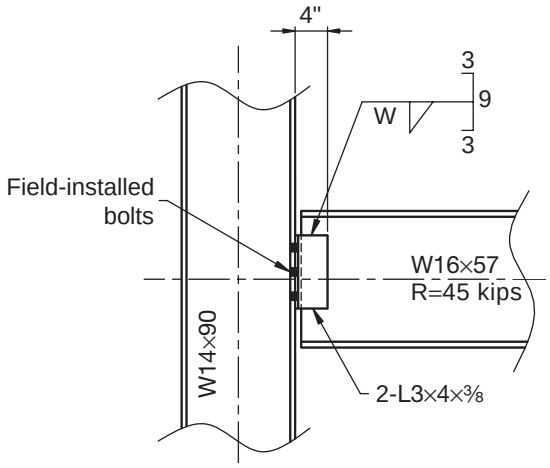

Fig. 3. Shop-welded/field-bolted, double-angle simple shear connection.

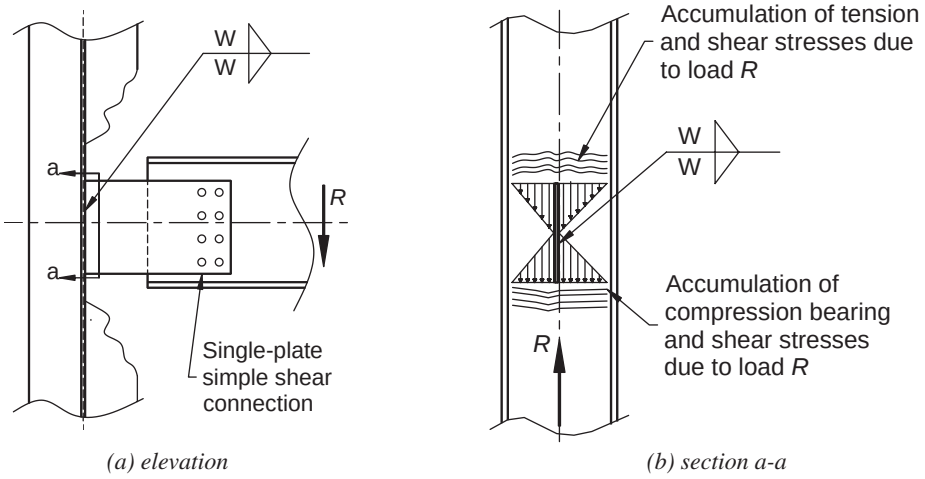

(a) elevation *(b) section a-a*

Fig. 4. Extended single-plate simple shear connection to column web.

How these stresses are actually distributed in the column web would be a function of the slenderness of the column web and the amount of stress present in the web as a result of loads applied from other sources.

Currently, the AISC *Specification* (AISC, 2016c) and the AISC *Manual* (AISC, 2017a) do not address this possible limit state. It is also important to recognize that, as far as the authors are aware, there are no case studies that have identified this as a problem. Regardless, there must be some phenomenon [similar to that shown in Figure 5(b)], occurring in the column web under this type of loading. Some designers, in an effort to address this in some manner, have used Equations 1 and 2 as a check on the web. Although, knowing the formulation of Equations 1 and 2, it is clear that Equations 1 and 2 do not address the phenomenon illustrated in Figure 4(b).

When a plate connection, like that shown in Figure 4, frames to only one side of the column web, Equation 1 has been used to check the column web thickness. When a plate connection frames to both sides of the column web, Equation 2 has been used. If a connection designer chooses to check the thickness of the base material for conditions like or similar to that shown in Figure 4, that is their preference; it certainly is conservative. However, they should consider that it is probably an opiate for the problem.

It should also be recognized that single-plate shear connections often employ a weld size equal to or greater than ⅝ of the plate thickness. Much of the weld size is intended to allow the plate to yield prior to weld fracture. Because steel does not generally fail in the through-thickness direction, the rupture strength of the web, if checked at all, should only be checked relative to the shear reaction. A check based on the weld size is too conservative.

Recommendations

Concentrically Loaded Longitudinal Welds or Weld Groups

1. When shear rupture of the base material adjacent to the weld is an applicable limit state, AISC *Specification* Section J4.2 should always be used.
2. If a longitudinal weld can be sized using Equations 6 and 7 (AISC *Manual* Equations 8-2a and 8-2b) and shear rupture of the base material adjacent to the weld is an applicable limit state, AISC *Specification* Section J4.2 should always be used.
3. Equations 1 and 2 (AISC *Manual* Equations 9-2 and 9-3) can always be used when shear rupture of the base material adjacent to the weld is an applicable limit state. Remember that it is directly a shear rupture check of the base material adjacent to the weld. However, it must be recognized that it is a conservative approach that may result in thicker base material than what is actually required for the load being considered when the provided weld size is larger than that of the weld size required to transfer the load (e.g., D_{prov}/D_{req}).

Eccentrically Loaded Welds or Weld Groups

1. Welds of this nature are not wholly loaded along the longitudinal axis of the welds. For these welds or weld groups, the welds cannot be sized using Equations 6 or 7 (AISC *Manual* Equations 8-2a and 8-2b). Furthermore, the actual stresses in the base material adjacent to the weld are not readily known. As such, when rupture of the base material is an applicable limit state, Equations 1 and 2 (AISC *Manual* Equations 9-2 and 9-3) should be used. It should be recognized that this is a conservative approach, but the authors are not aware of a better alternative.
2. AISC *Specification* Section J4.2 applies but is not readily usable for eccentrically loaded welds.

Byproduct Use of Equations 1 and 2

1. It is somewhat common to use Equations 1 and 2 (AISC *Manual* Equations 9-2 and 9-3) to check base material thickness when shear rupture of the base material adjacent to the weld is not applicable but no other known limit state check is available (like or similar to that shown in Figure 4).
2. Equations 1 and 2 can be used, as noted earlier, but these equations simply were not derived for such a purpose. The designer should recognize that such checks do not really address the issue.

PART 2: THE DUCTILITY FACTOR; INTERFACE WELDS

Background

The ductility factor for welds (some refer to this as the Richard factor), first showed up in AISC documents in the 1992 *Manual of Steel Construction*, Volume II: Connections (AISC, 1992). The ductility consideration arose during the development of the uniform force method (UFM), now commonly used for distributing forces in vertical brace connections framing to beam-column joints. One of the assumptions in the development of the UFM is that interface forces are distributed uniformly along the interfaces regardless of interface length, proximity of connected members, or other variables such as frame action (distortion).

Figure 5 shows a vertical brace connection used in a wind (or low seismic) application. Note the close proximity of the end of the brace relative to the beam-gusset interface.

Although the interface forces are assumed to be distributed uniformly, as shown in Figure 5(b), a stress (or force) concentration in the vicinity of the end of the brace may be present (as such, causing a nonuniform distribution of stress along the welded interface). It is for considerations such as this that the ductility factor was developed and implemented. It is worth noting that the work performed by Williams (1986) and Richard (1986) used in developing the ductility factor considered only braces that frame to beam-column joints.

The ductility factor was born from the work presented in Williams' (1986) dissertation [a summary of that work can be found in Richard (1986)]. Of the work presented in the Williams dissertation, 45 finite element (FE) specimens, similar to the configuration shown in Figure 6, were considered to be loaded to their "ultimate" load, and maximum stresses along the gusset-member interfaces were recorded. Figure 6 shows a copy of the plot provided in the Williams dissertation that plots the ratio of the maximum interface stress to the average interface stress for the 45 concentric connections considered. Table 1 presents the tabulated values illustrated in Figure 6.

The ductility factor equal to 1.40 used in the 1992 AISC *Manual* was determined by evaluating the maximum stress ratio measured by the Williams' finite element analysis. As can be seen in Table 1, run (specimen) 26 has the largest reported value and is equal to 1.39. AISC simply rounded the number to 1.40.

Hewitt and Thornton (2004) subsequently performed statistical analysis on the data provided by Williams (see Tables 1 and 2) and recommended a reduced ratio equal to 1.25 based on a 90% confidence level (see Table 2). Note that, typically, this type of data and sample is evaluated on a 95% confidence level. As can be seen in Table 2, even at this confidence level, the upper bound is 1.26. Thus, even at a 95% confidence level, a ductility factor equal to 1.25 seems reasonable and is the value currently used for sizing welds.

How is the 1.25 factor used to accommodate ductility? Figure 7(a) shows the concentrated loads one might find to act on a welded interface. These interface loads are typically assumed to be uniformly distributed along the interface; the interface moment, M, is assumed to have a plastic stress distribution. The current method for determining whether or not the ductility factor should be used is to evaluate whether or not the peak stress/force, f_{peak}, is larger than 1.25 times the average stress/force, $1.25f_{avg}$, along the interface (the 1.25 coefficient is the value from the upper bound of the

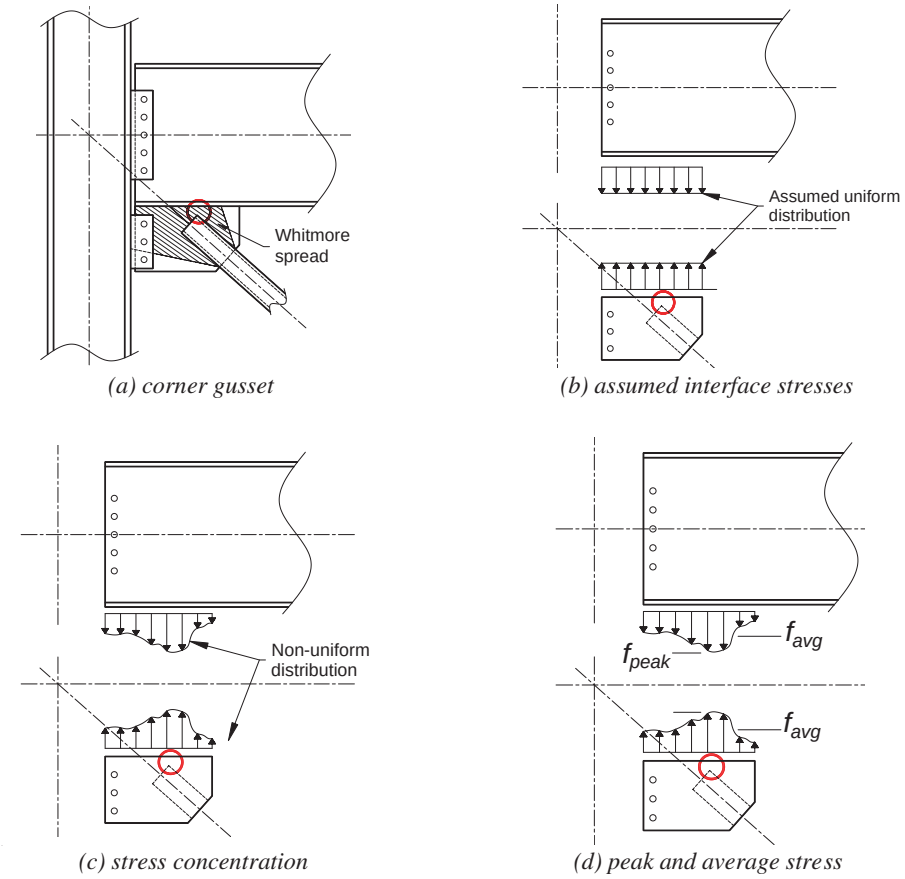

(a) corner gusset *(b) assumed interface stresses*

(c) stress concentration *(d) peak and average stress*

Fig. 5. Corner brace gusset connection.

Table 1. Interface Stress Ratios Reported (Williams, 1986; Richard, 1986)									
Run	Stress Ratio	Run	Stress Ratio	Run	Stress Ratio	Run	Stress Ratio	Run	Stress Ratio
1	1.22	10	1.22	19	1.16	28	1.20	37	1.16
2	1.20	11	1.31	20	1.22	29	1.32	38	1.26
3	1.19	12	1.19	21	1.19	30	1.18	39	1.20
4	1.30	13	1.22	22	1.29	31	1.17	40	1.26
5	1.29	14	1.24	23	1.32	32	1.18	41	1.30
6	1.28	15	1.26	24	1.18	33	1.19	42	1.19
7	1.19	16	1.32	25	1.33	34	1.27	43	1.22
8	1.20	17	1.14	26	1.39	35	1.18	44	1.22
9	1.29	18	1.26	27	1.37	36	1.12	45	1.30

Table 2. Statistical Analysis of Interface Stress Ratios Given in Table 1									
		Confidence Level (90.0%)		Confidence Level (95.0%)		Confidence Interval (90.0%)		Confidence Interval (95.0%)	
Mean	Standard Deviation	Lower	Upper	Lower	Upper	Lower	Upper	Lower	Upper
1.24	0.063	–0.0158	0.0158	–0.0189	0.0189	1.22	1.25	1.22	1.26

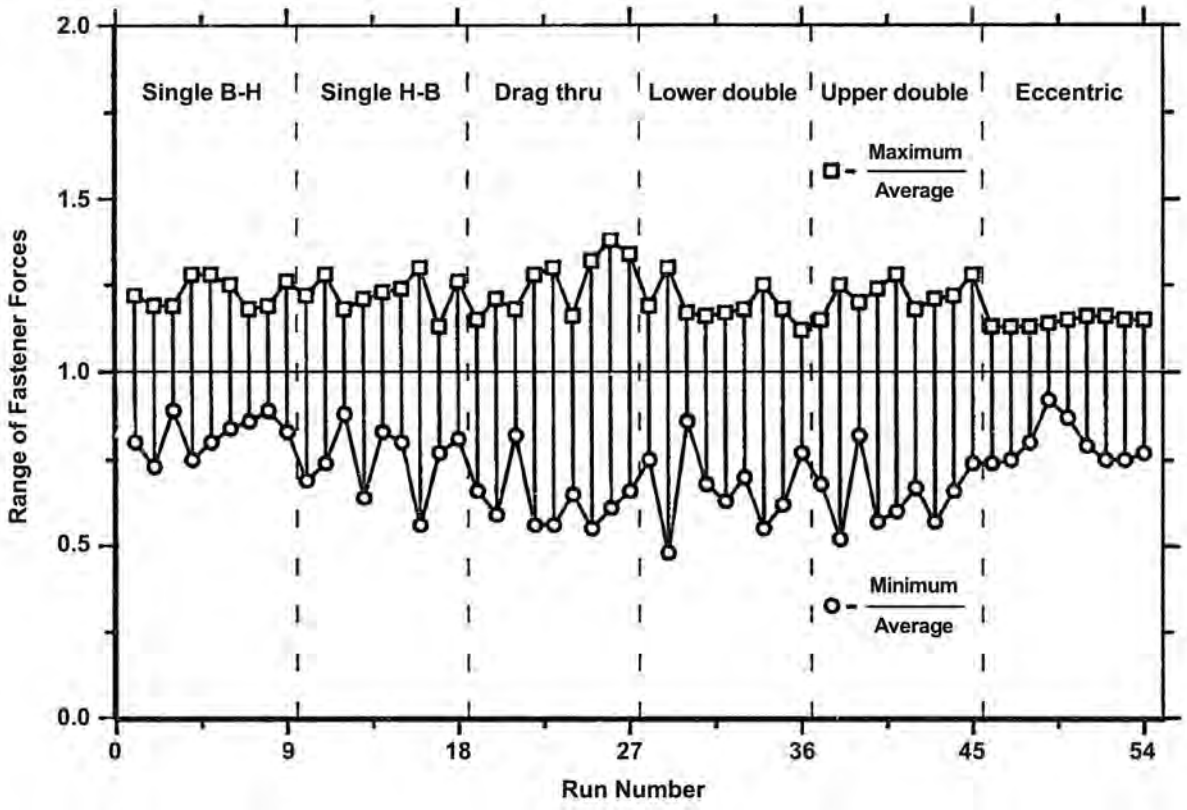

Fig. 6. Reproduction of Williams' Figure 48 (maximum/average stress ratios).

90% confidence interval shown in Table 2). Refer to AISC *Manual* Part 13 and Hewitt and Thornton (2004). To calculate f_{peak} and f_{avg}, refer to Figure 7(b), where f_{peak} is the resultant stress/force acting on the left half of the interface (where m and a act in the same direction) as shown in Equation 8.

$$f_{peak} = \sqrt{v^2 + (a+m)^2} \tag{8}$$

The minimum stress/force, f_{min}, along the interface is on the right half of the interface where m and a act in opposite directions and is given in Equation 9.

$$f_{min} = \sqrt{v^2 + (a-m)^2} \tag{9}$$

The average stress/force is the average of f_{peak} and f_{min} as shown in Equation 10.

$$f_{avg} = \frac{f_{peak} + f_{min}}{2} \tag{10}$$

Figure 8 provides an illustration of the resultant forces obtained for the distribution shown in Figure 7(b). In the comparison of f_{peak} and $1.25f_{avg}$, one can infer that where f_{peak} is smaller than $1.25f_{avg}$ that the assumed uniform distribution is a reasonable assumption.

Discussion

For corner gussets, the ductility factor is always used on the welded interface. The reason for this is primarily due to the effect of frame distortion on interface demands. So, regardless of proximity or connection geometry, a ductility factor is applied due to the consideration of frame distortion. However, application of the ductility factor is not necessarily required for welded interfaces used in other types of connections and deserves consideration of the types of loads, or combination thereof, acting on the interface, connection geometry, and the type of connecting element used. The following is a discussion of welded interfaces in other types of connections and the variation of combined loads and connection geometry.

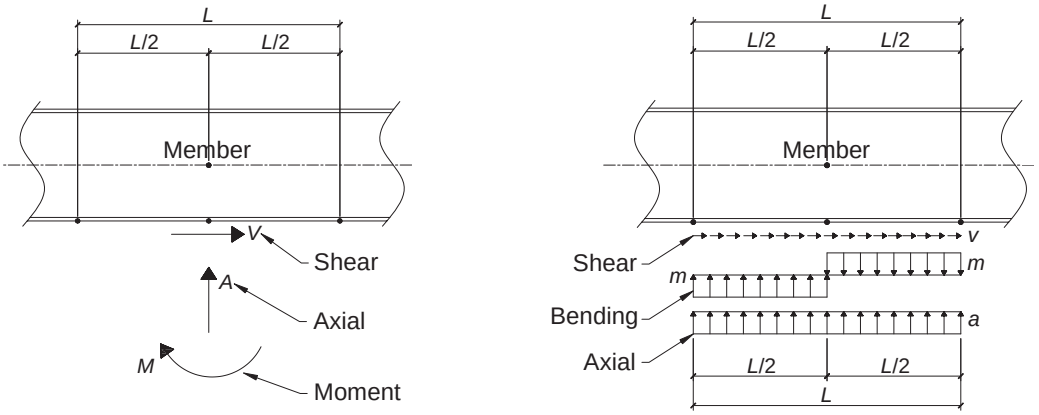

(a) concentrated interface forces *(b) distributed interface forces*

Fig. 7. Generalized interface forces distribution.

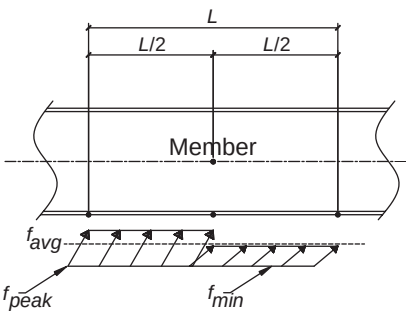

Fig. 8. Resultant interface loads, f_{peak}, f_{min}, *and* f_{avg}.

Shear Only

In this case, there is no moment or axial (normal) forces acting on the interface. As such, the ductility factor is **not** applicable.

Axial Loads

For Equations 8 and 9, the terms v and m are zero, and these equations reduce to those shown in Equations 11 and 12.

$$f_{peak} = \sqrt{v^2 + (a+m)^2}$$
$$f_{peak} = \sqrt{0^2 + (0+m)^2}$$
$$f_{peak} = m \tag{11}$$

$$f_{min} = \sqrt{v^2 + (a-m)^2}$$
$$f_{min} = \sqrt{0^2 + (a-0)^2}$$
$$f_{min} = a \tag{12}$$

Taking the average of Equations 11 and 12 gives that shown in Equation 13.

$$f_{avg} = \frac{f_{peak} + f_{\min}}{2}$$
$$f_{avg} = \frac{a+a}{2}$$
$$f_{avg} = a \tag{13}$$

Thus, for an interface subjected to pure axial force, $1.25f_{avg}$ will always be larger than f_{peak}, suggesting that the ductility factor should always be applied to axial-only cases. However, we need to consider how the ductility factor was originally developed (as discussed previously) and the type of connection that is actually being considered. The discussion given in reference to Figure 5 suggested that proximity was an issue, and it probably is for the connection shown in Figure 5. Referring to Figure 5(a), it can be seen that the Whitmore spread does not engage the entire beam-gusset interface, suggesting that a stress concentration is likely to exist on the interface in the vicinity of the end of the brace-to-gusset connection.

Consider the hanger connection shown in Figure 9(a). The authors have seen the ductility factor applied to such a connection. One argument is that the end of the hanging member is in very close proximity to the welded interface, and as such, a ductility factor should be applied. However, if one is to look at the load transfer from the hanging member to the gusset, it can be reasonably argued that the axial force in the hanger is transferred along the hanger-to-plate welds along a sufficient length and that the connecting material is of nearly the same width as that of the hanging member. Therefore, a uniform distribution is reasonable to assume, and the weld ductility factor need not be applied for this condition. Considering a Whitmore spread of even, say, 10°, as shown in Figure 10, illustrates this claim. Note that, typically, a Whitmore spread is assumed to be effective at as much as

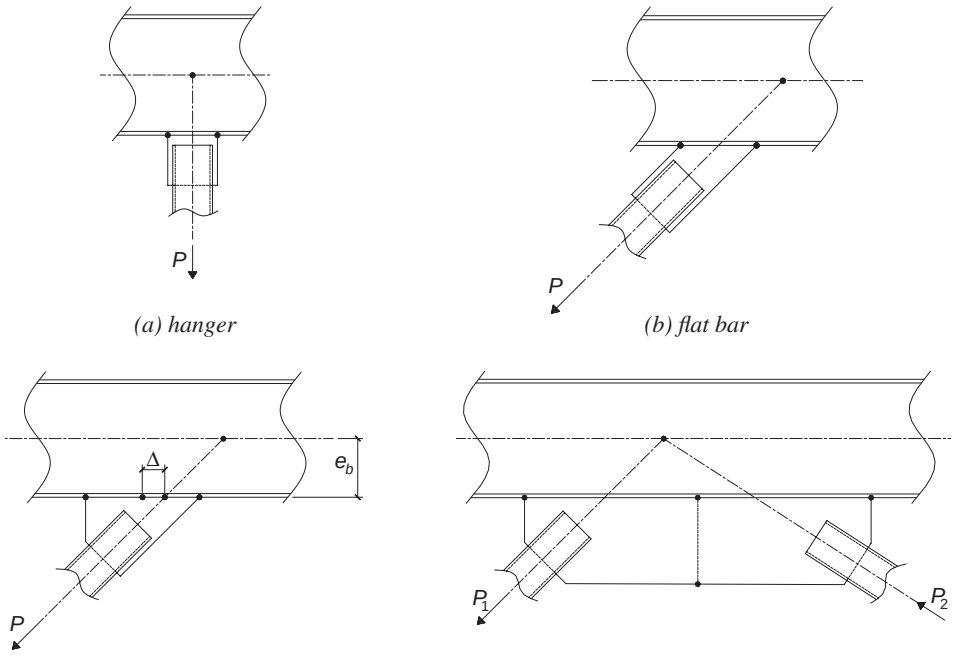

(a) hanger *(b) flat bar*

(c) shaped plate *(d) chevron (a.k.a. mid-span)*

Fig. 9. Various plate interface connections.

30°. The spread of the load in a uniform manner along the line of action of the hanger is analogous to an application of Saint Venant's principle.

Suppose, however, that the interface length shown in Figure 10 has to be increased, as shown in Figures 11(a) and 11(b), in order to accommodate a heavier load. For this case, the Whitmore spread, even considered to be effective at 45°, does not suggest that a uniform distribution will occur. The entire welded interface is not engaged in a manner. For this condition, it is recommended to assume that only the weld within the Whitmore spread projected on the interface is effective when designing the weld. For this approach, the ductility factor would not be applied.

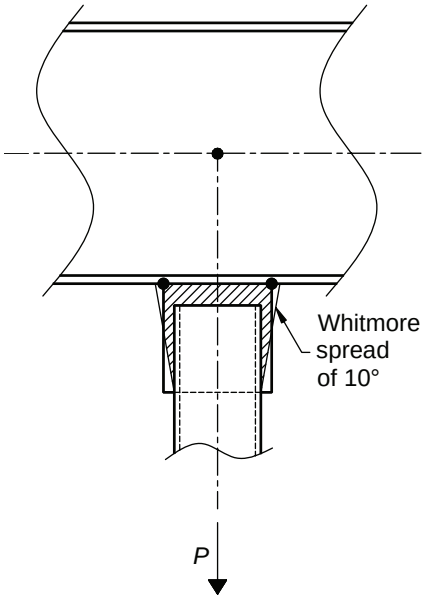

Fig. 10. Axial hanger connection with flat bar plate.

If the designer chooses to use the entire interface length, including the portion outside of the Whitmore length, this is a rational approach to analysis which accounts for the non-uniform stress distribution.

Combined Shear and Axial

Under this loading, the m term in Equations 8 and 9 is zero, giving equations for f_{peak} and f_{min} as shown in Equations 14 and 15.

$$f_{peak} = \sqrt{v^2 + (a+m)^2}$$
$$f_{peak} = \sqrt{v^2 + (a+0)^2}$$
$$f_{peak} = \sqrt{v^2 + a^2} \quad (14)$$

$$f_{min} = \sqrt{v^2 + (a-m)^2}$$
$$f_{min} = \sqrt{v^2 + (a-0)^2}$$
$$f_{min} = \sqrt{v^2 + a^2} \quad (15)$$

Taking the average of Equations 14 and 15 gives that shown in Equation 16.

$$f_{avg} = \frac{f_{peak} + f_{min}}{2}$$
$$f_{avg} = \frac{\sqrt{v^2 + a^2} + \sqrt{v^2 + a^2}}{2}$$
$$f_{avg} = \sqrt{v^2 + a^2} \quad (16)$$

Because f_{peak} and f_{avg} are the same, $1.25f_{avg}$ will always be larger than f_{peak}, suggesting that a ductility factor should always be applied for this type of loading.

Consider the flat bar used for the brace connection shown

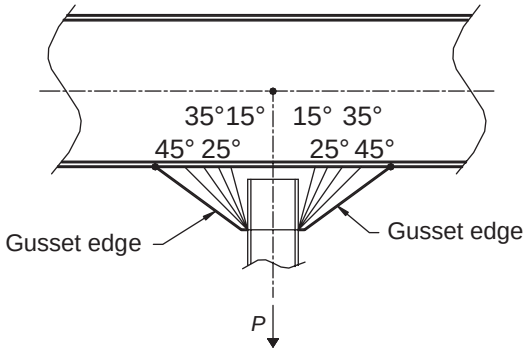

(a) relatively close proximity

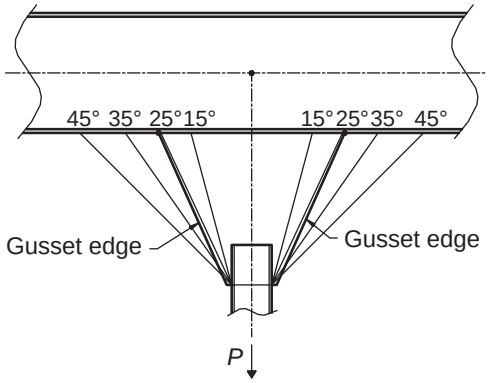

(b) relatively far proximity

Fig. 11. Fanned hanger connections—axially loaded interface welds.

in Figure 9(b). The force distribution at the welded interface is as shown in Figure 12(a). Figure 12(b) shows that if one were to assume a 30° Whitmore spread, it is clear that the load transfer, from the start of the connection, spreads through the gusset such that the entire length of the welded interface is well engaged. Therefore, application of the weld ductility factor is not required here.

Suppose that the plate used for the connection shown in Figure 12 is shaped to increase the interface length in order to satisfy a larger load. This configuration, as shown in Figure 13(a), is a commonly used detail. Figure 13(a) shows such a connection. Figure 13(b) shows a 30° Whitmore spread. As can be seen, the spread does not engage the entire welded interface. For this case, as shown in Figure 13, it would be appropriate to use a ductility factor. A simpler alternative might be to assume only the weld within the Whitmore length is effective without applying the ductility factor.

Combined Shear and Bending

Under this loading, the a term in Equations 8 and 9 is zero, giving equations for f_{peak} and f_{min} as shown in Equations 17 and 18.

$$f_{peak} = \sqrt{v^2 + (a+m)^2}$$
$$f_{peak} = \sqrt{v^2 + (0+m)^2}$$
$$f_{peak} = \sqrt{v^2 + m^2} \quad (17)$$

$$f_{min} = \sqrt{v^2 + (a-m)^2}$$
$$f_{min} = \sqrt{v^2 + (0-m)^2}$$
$$f_{min} = \sqrt{v^2 + m^2} \quad (18)$$

Taking the average of Equations 17 and 18 gives Equation 19.

$$f_{avg} = \frac{f_{peak} + f_{min}}{2}$$
$$f_{avg} = \frac{\sqrt{v^2 + m^2} + \sqrt{v^2 + m^2}}{2}$$
$$f_{avg} = \sqrt{v^2 + m^2} \quad (19)$$

Because f_{peak} and f_{avg} are the same, 1.25 f_{avg} will always be larger than f_{peak}, suggesting that a ductility factor should always be applied for this type of loading.

However, consider the bracket connection shown in Figure 14. The bracket plate-to-column flange interface is subjected to shear and bending, very similar to how a chevron gusset interface is subjected to load. If we consider only the comparison of f_{peak} and 1.25f_{avg}, a ductility factor would almost always seem to be necessary. However, one should consider how the ductility factor was developed. It was developed to address proximity and distortional effects on interfaces where a uniform stress distribution is assumed. The bracket connection shown in Figure 14 certainly does

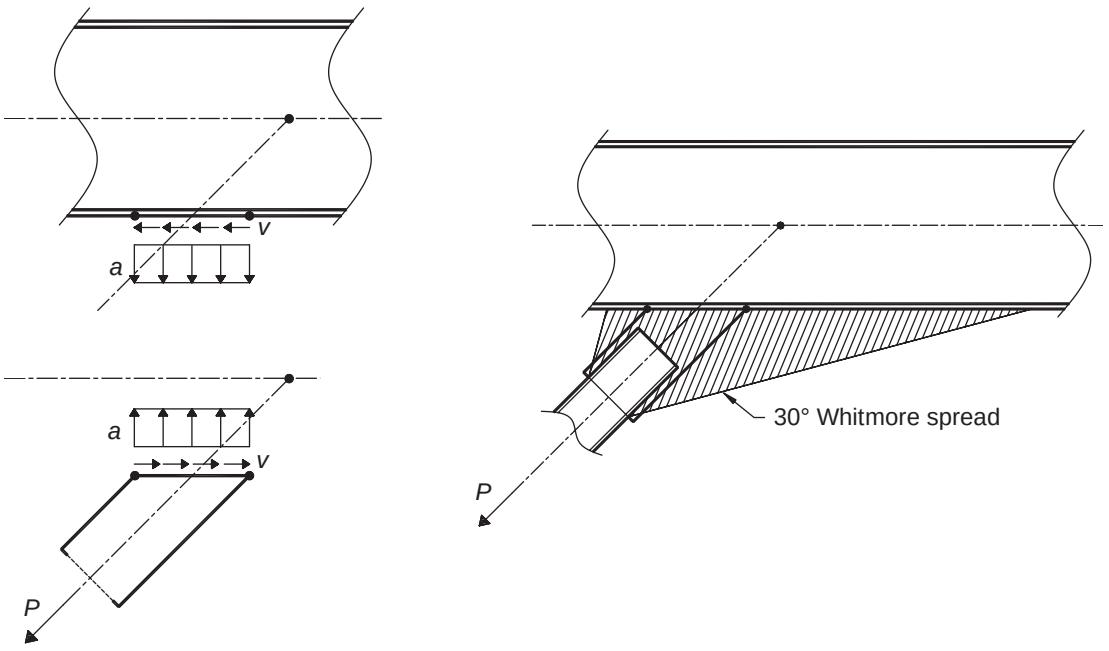

(a) flat bar – force distribution *(b) flat bar – Whitmore spread*

Fig. 12. Flat bar brace connection—shear and axial interface loads.

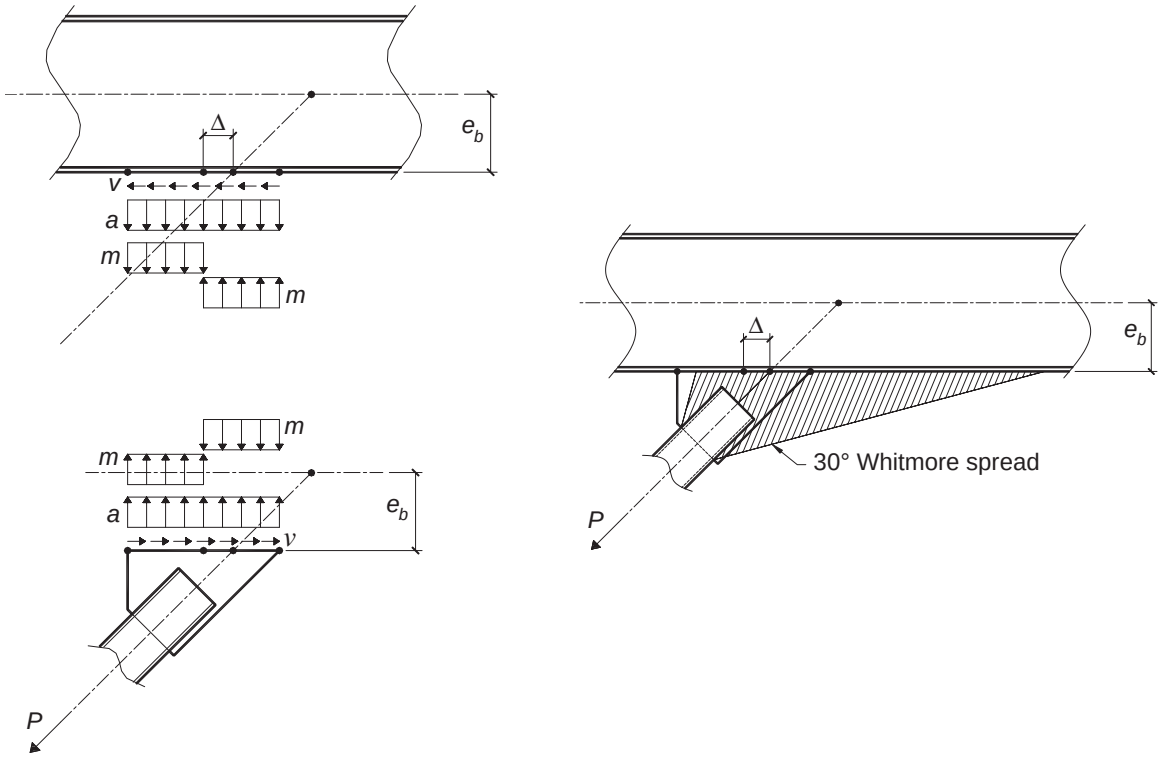

(a) shaped gusset – force distribution *(b) shaped gusset – Whitmore spread*

Fig. 13. Flat bar brace connection—shear and axial interface loads.

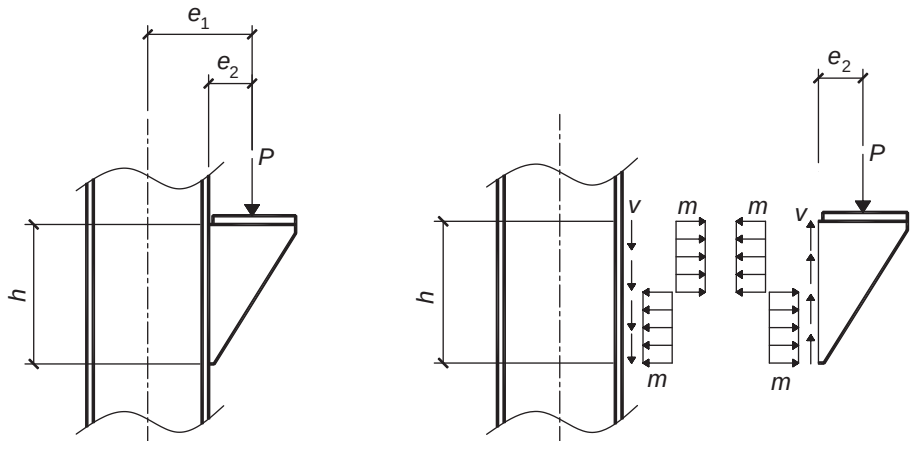

(a) shaped gusset – force distribution *(b) shaped gusset – Whitmore spread*

Fig. 14. Bracket plate connection (combined shear and bending).

not present issues related to proximity like that shown in Figure 5. In regard to distortional effects, the length ("*h*" as shown in Figure 14) of the interface for this type of connection is typically relatively short; therefore, any curvature in the column would be negligible in regard to distortional effects, so applying a ductility factor is not required. With these considerations, the authors argue that a ductility factor is not required on the interface weld for such a connection. However, if the length of the interface was to increase substantially, such curvature of the column could rationally be assumed to affect the stress distribution along the weld. Engineering judgment would be required when evaluating the interface stresses, and an alternative rational approach to analysis would be required.

Combined Shear, Axial, and Moment

Under this loading, all of the terms in Equations 8 and 9 are nonzero, giving equations for f_{peak} and f_{min} as shown in Equations 20 and 21.

$$f_{peak} = \sqrt{v^2 + (a+m)^2} \tag{20}$$

$$f_{min} = \sqrt{v^2 + (a-m)^2} \tag{21}$$

Taking the average of Equations 20 and 21 gives Equation 22.

$$f_{avg} = \frac{\sqrt{v^2 + (a+m)^2} + \sqrt{v^2 + (a-m)^2}}{2} \tag{22}$$

Because f_{peak} and f_{avg} are different, one would have to evaluate whether or not a ductility factor would be applicable.

Consider the chevron (i.e., midspan) gusset connection shown in Figure 9(c). As discussed in Fortney and Thornton (2015, 2017), the welded interface will always transfer a combination of shear and axial loads along with bending [refer to Figure 7(a)]. The shear and axial loads are typically assumed to be uniformly distributed along the interface, and the moment is assumed to be distributed as a plastic moment distribution as shown in Figure 7(b).

When a moment acts on an interface weld in this type of connection, the interface moment has traditionally been converted to an equivalent normal force and added to the calculated normal force. Figure 15(a) shows a representative sketch of a combination of shear, *V*, normal force, *A*, and bending, *M*, acting on an interface of length, *L*. The moment, *M*, is converted to a force couple, acting at *L*/4 from the centroid of the weld, representing a plastic stress distribution as shown in Figure 15(b). From here, one could size the welds on the left and right halves of the interface based on the

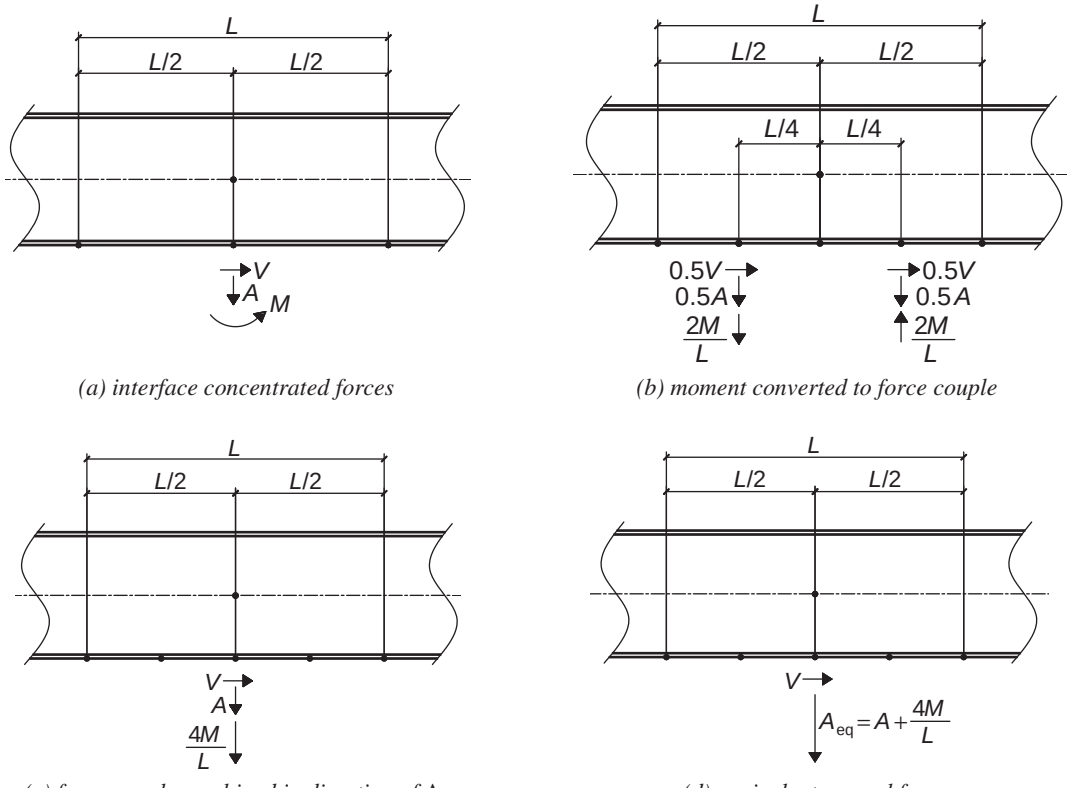

(a) interface concentrated forces

(b) moment converted to force couple

(c) force couple combined in direction of A

(d) equivalent normal force

Fig. 15. Converting interface moment into equivalent normal force.

resultant forces acting on the two halves of the interface.

The resultant force acting on the left half of the interface [see Figure 15(b)] is given in Equation 23.

$$R_{left} = \sqrt{(0.5V)^2 + \left(0.5A + \frac{2M}{L}\right)^2} \quad (23)$$

The resultant force acting on the right half of the interface [see Figure 15(b)] is given in Equation 24.

$$R_{right} = \sqrt{(0.5V)^2 + \left(0.5A - \frac{2M}{L}\right)^2} \quad (24)$$

Each of the resultant forces determined from Equations 23 and 24 would have different directional strength increase "coefficients" due to the different vector directions. One would simply provide a weld along the entire interface length equal to the larger of the two required welds; the weld size required for the left side of the interface, as shown in Figure 15(b), will typically govern the weld size. One can think of R_{left} as R_{peak} and R_{right} as R_{min}. This typically is not done, however. For further discussion on evaluating R_{peak} and R_{min}, refer to AISC Design Guide 29, *Vertical Bracing Connections—Analysis and Design*, Appendix B (Muir and Thornton, 2014), where it is shown that the maximum possible variance between R_{peak} and R_{min} (referenced as R_{plus} and R_{minus} in Design Guide 29) is 3.37%.

Typically, the force couple is converted into a total normal force and assumed to act in the same direction as the true normal force, A. These two forces would then be combined to give a total equivalent normal force, A (i.e., N_{eq}), as shown in Figures 15(c) and 15(d). The resultant force for the interface loads shown in Figure 15(d) is given in Equation 25.

$$R = \sqrt{V^2 + \left(A + \frac{4M}{L}\right)^2} \quad (25)$$

In Equation 25, the $(A + 4M/L)$ term is the equivalent normal force. This method is used in several examples in the Design Examples Companion to the AISC *Steel Construction Manual* (AISC, 2017b) as well as AISC Design Guide 29.

It may not be immediately recognizable, but Equations 23 and 25 give the same resultant vector in both magnitude and direction. Thus, using the "equivalent normal force" method is another way of calculating the peak force (or stress if put in those terms). Where confusion seems to come into play with the "equivalent normal force" method is that there is no "average" stress with this method. So, how would one evaluate the need for using the ductility factor using this method? The answer is that this method is just another way of calculating the peak force (or stress). The average force/stress is still calculated using Equation 22.

It is important to mention that in most vertical brace connection example problems (braces framing to beam-column joints) presented in AISC documents, the equivalent normal force is used to calculate the peak force, and an average force is not calculated. However, a ductility factor is used on the resultant force calculated from the square root of the sum of the squares of interface shear and the equivalent normal force (f_{peak}). Applying the 1.25 ductility factor to a resultant force determined using f_{peak} is not correct! This approach is taken simply as a conservative simplifying approach to avoid the trouble of calculating f_{avg}.

Should the ductility factor be applied to the welded interface for the connection shown in Figure 9(c)? Some would argue that it depends on how the force is spread from the start of the brace-to-gusset connection (i.e., the Whitmore spread) and through the gusset to the interface. Others argue that the ductility factor was developed for corner brace connections, and therefore, the ductility factor does not apply for this type of connection. The following discussion will demonstrate that the ductility factor is applicable for the connection shown in Figure 9(c).

Whitmore Spread

If we assume that the welded interface shown in Figure 9(c) has a uniformly distributed load as a combined effect of both braces, then Saint Venant's principle should be evaluated. The evaluation can be done in terms of the Whitmore spread. Consider the midspan connection shown in Figure 16(a). Typically, the load effect of both braces would be assumed to be distributed uniformly along the entire welded interface. However, if we assume a Whitmore spread of 30° from the start of both connections, we see in Figure 16(a) that neither of the force spreads engage the entire interface. In this case, a ductility factor would be applied due to a proximity effect. However, if the force spread of each brace engages the entire interface length, as shown in Figure 16(b), then a ductility factor need not be applied due to a proximity effect.

Interface Distortion

As discussed previously, the primary reason a ductility factor is applied to a weld at the welded interface of a corner gusset is because of frame distortion. That is, as the frame laterally displaces, the angle between the beam and column increases, thus applying a distortional tension on the gusset, or decreases, thus applying a distortional compression on the gusset. It is usually overlooked, but the gusset-to-beam interface in a midspan gusset is subjected to similar distortional forces.

Figure 17 shows a schematic of an exaggerated deflection of a braced frame beam with a midspan gusset. The beam tends to go through the textbook rotation of a simply supported beam loaded transversely. However, the load transfer among the beam, gusset and welds tends to "disturb" that typical beam rotation.

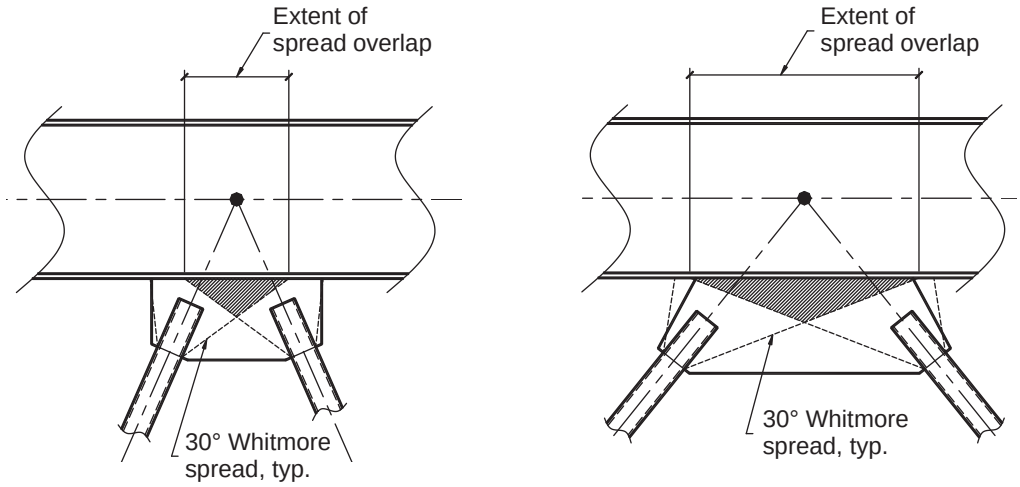

(a) small overlap *(b) complete overlap*

Fig. 16. Distribution overlap at interface.

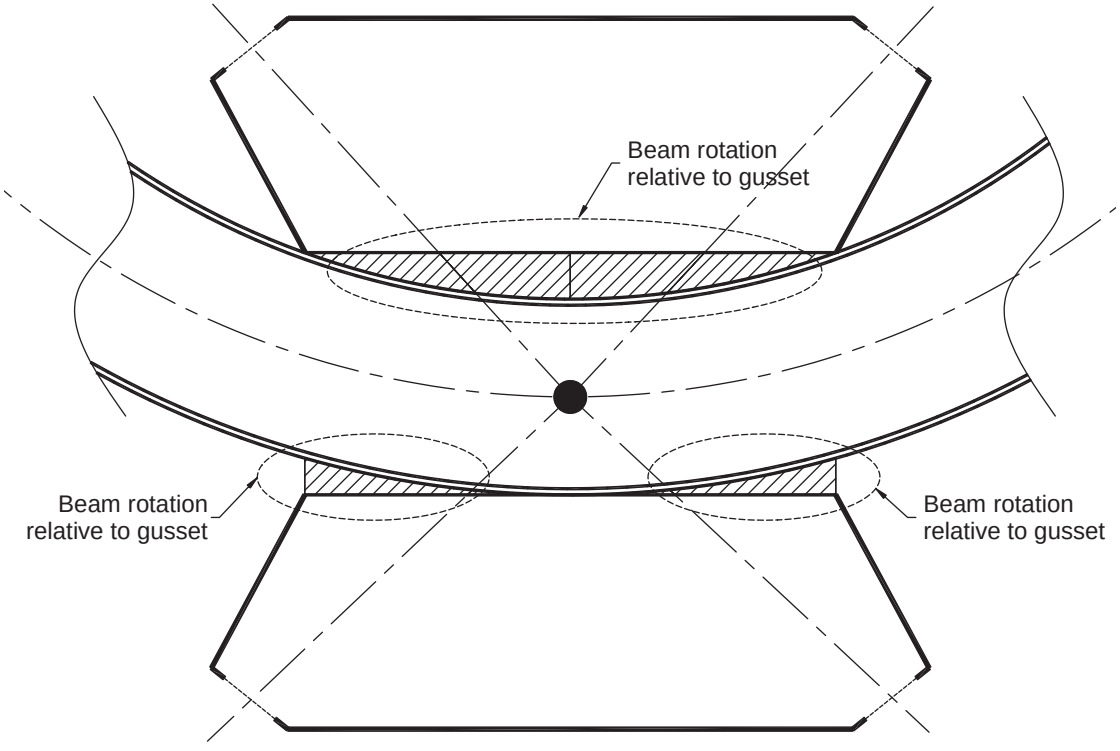

Fig.17. Beam rotation relative to gusset along interface (deformation exaggerated for illustration).

Suppose the net transverse loads acting on the beam induce downward bending as shown in Figure 17. If a gusset is installed on the top flange, the edges of the gusset will tend to compress against the beam flange while the interface tends to open up along the interface length. Conversely, if a gusset is installed on the bottom flange, the end of the gusset will tend to move away from the flange while the interface will tend to close along the length of the interface. This curvature (greatly exaggerated in the figure for visual purposes) will create distortional forces along the welded interface. Therefore, regardless of Saint Venant's principle or the Whitmore spread, a ductility factor should always be applied for the type of connection shown in Figure 9(c).

Element Capacity Welds

Some welds are designed to develop the tension, shear or flexural strength of the connecting element [e.g., single-plate shear connections, gusset-to-beam welds in corner gussets used in special concentrically braced frames (SCBF)]. When welds are sized to develop the strength of the connecting element, a ductility factor should not be applied.

Recommendations

Shear Only

A ductility factor is not applied to a weld under this type of loading.

Axial Only

For most typical connections, a ductility factor is not required. However, the spread of the load from the beginning of the load transfer point to the welded interface should be considered. If the Whitmore spread (or Saint Venant's principle) does not show that the entire interface length is engaged [e.g., Figure 11(b)], a ductility factor should be applied.

Combined Shear and Axial

The use of a ductility factor needs to be evaluated on a case-by-case basis. For flat bar–type gussets, a ductility factor is typically not required. For other types of connections, the spread of the load from the beginning of the load transfer point to the welded interface should be considered. If the Whitmore spread (or Saint Venant's principle) does not show that the entire interface length is engaged [e.g., Figure 13(b)], a ductility factor should be applied.

Combined Shear and Bending

Although a comparison of f_{peak} and $1.25f_{avg}$ without considering proximity or distortional effects will almost always suggest that a ductility factor should be applied, it would be rare for proximity or distortional effects to indicate the application of the ductility factor. For almost all cases, a ductility factor is not necessary. However, in rare cases—for example, in cases with relatively long interface lengths—one should use engineering judgment to determine if a ductility factor should be applied if distortional effects are present.

Combined Shear, Axial and Bending

For most connections, an evaluation of Equations 20 and 22 should be performed to determine whether or not Equation 20 (f_{peak}) is equal to or larger than 1.25 times Equation 22 (f_{avg}). There are permutations of combinations of v, a and m that will show that the peak force/stress is larger than 1.25 times f_{avg}. However, if the welded interface can be reasonably assumed to be subjected to distortional forces (e.g., Figure 17), a ductility factor should be applied regardless of the evaluation of f_{peak} and $1.25f_{avg}$.

Generally

It's important to note that one can simply always use a ductility factor. It will always be conservative; it just may not be necessary. However, with regard to welds designed to develop the strength of the connecting element, a weld ductility factor should not be used.

PART 3: ELEMENT CAPACITY AND (5/8)t_P WELDS

Generally, welds need only be designed to resist the loads transferred between the parts based on the structural analysis. Generally, welds need not be sized based on the available or expected strength of the joined parts. When welds are sized based on the strength of the joined parts, this is often referred to as "developing," as in "developing the plate" or "developing the strength of the beam."

One option is to provide a complete-joint-penetration (CJP) groove weld. As indicated in AISC *Specification* Table J2.5, at CJP groove welds "the strength of the joint is controlled by the base metal" not the strength of the weld. Partial-joint-penetration (PJP) groove welds with or without reinforcing fillet welds can also be used to develop steel elements. This discussion will concentrate primarily on the design of fillet welds used to develop steel elements, though CJP and PJP groove welds will be briefly addressed as well.

Typical Conditions

For a majority of conditions encountered in practice, a weld can be considered to develop the strength of the joined parts if the available strength of the weld equals or exceeds the least available strength of the parts joined.

Shear

The required weld size to develop a part subjected to shear can be determined by setting the available strength of the weld equal to the available shear yield strength of the part from AISC *Specification* Section J4.2. This is illustrated below using LRFD and Equation 6:

$$\phi 0.60F_yA_g = 1.392DL$$

Assuming a double-sided fillet weld gives Equation 26.

$$1.00(0.60)F_yt_pL_p = 1.392D(2)L_p$$
$$D = 0.216F_yt_p \quad (26)$$

A single-sided fillet weld could be used to develop the shear strength of an element. However, this is not a common practice and is typically uneconomical. Providing a double-sided fillet weld would be a much better detail.

Tension

The required weld size to develop a part subjected to tension applied transverse to the longitudinal axis of the weld can be determined by setting the available strength of the weld equal to the available tensile yield strength of the part, in accordance with AISC *Specification* Section J4.1. This is illustrated below using LRFD and Equation 6.

$$\phi F_yA_g = (1.5)1.392DL$$

Note that the 1.5 factor on the right side of the preceding equation is the directional strength factor as determined using AISC *Specification* Section J2.4.

Assuming a double-sided fillet weld gives Equation 27.

$$0.90F_yt_pL_p = (1.5)1.392D(2)L_p$$
$$D = 0.216F_yt_p \quad (27)$$

Single-sided fillet and PJP groove welds generally should not be subjected to tension applied transverse to the longitudinal axis of the weld because rotation can occur about the axis of the weld, placing increased and uncertain demand on the weld root. Where restraint prevents such rotation, the concern is less critical, and single-sided welds may be an option.

Compression

The available strength of welds relative to compression load applied transverse to the longitudinal axis of the weld is generally assumed to be equal to that relative to tension load applied transverse to the longitudinal axis of the weld. There has been little testing of such conditions. There are reasons to believe that the strength of fillet welds subjected to compression will be greater than that for welds subjected to tension. Whereas applied tension will tend to open the root of the fillet, which is a stress riser, applied compression will tend to close the root of the weld, which is not a stress riser. There may also be bearing between the parts over some portion of the joint, which is generally neglected, and it should be neglected unless the parts are fit to bear. The authors recommend that the tension and compression cases be treated identically during design while recognizing that this is conservative.

Bending

The intended meaning of "developing" the element can be less clear when related to bending. Various criteria can and are commonly used in design: elastic strength (first yield), plastic strength, and plastic strength with continued rotation. Both the elastic strength and the plastic strength conditions will be considered here. The condition of plastic strength with continued rotation will be addressed in a subsequent section.

From mechanics, the elastic strength of an element is determined from its elastic section modulus, *S*. The required weld size to develop the elastic strength of a part can be determined by setting the available strength of the weld equal to the available flexure strength of the part. This is illustrated in the following, assuming a double-sided fillet weld; using LRFD and a modified version of Equation 6 gives Equation 28.

$$\phi F_yS = (2)(1.5)1.392D\frac{l^2}{4}$$
$$0.90F_yS = (2)(1.5)1.392D\frac{l^2}{4}$$
$$D = 0.862\frac{F_yS}{l^2} \quad (28)$$

In Equation 28, l is the length of the weld.

Equation 29 can be derived for a rectangular plate bent about its strong axis.

$$D = 0.144F_yt_p \quad (29)$$

Beyond first yield, the element will begin to lose stiffness, and further increases in applied load will tend to be attracted to stiffer, nonyielded portions of the structure. For this reason, sizing the weld to develop the elastic strength may often be sufficient. In some instances, it may be desirable to develop the plastic strength of the element.

Following a procedure similar to that illustrated for the elastic strength, the weld size required to develop the plastic strength of a rectangular plate bent about its strong axis gives Equation 30.

$$D = 0.216F_yt_p \quad (30)$$

Combined Shear, Axial and/or Bending

A similar procedure as those shown earlier will also result in a weld size of $D = 0.216F_y t_p$ for combinations of applied shear, axial and/or bending.

For convenience, in practice it is useful to recognize that the weld size required to develop a plate for many of the loads considered thus far is $D = 0.216F_y t_p$. For a plate with a yield strength of 50 ksi, this can be expressed as $w = 0.675t_p$.

Special Conditions

The procedures illustrated earlier can be used for many of the conditions most commonly encountered in practice that require development of the joined elements. There are, however, some instances where those procedures will result in weld sizes that are either larger than necessary or potentially ill-suited for the demands.

Single-Plate Shear Connections

AISC *Manual* Part 10 contains recommended design procedures for single-plate shear connections. For both the conventional and extended configurations, the AISC *Manual* recommends that "…the weld between the single plate and the support should be sized as $(\frac{5}{8})t_p$, which will develop the strength of either a 36-ksi or 50-ksi plate…" The weld is sized such that the plate will yield prior to the weld fracturing, allowing the plate to act as a fuse that accommodates the beam end rotation in a ductile manner (Muir and Hewitt, 2009). It should be noted that this is only a recommendation. There is no provision in the AISC *Specification* requiring that the weld be stronger than the plate. Instead the $(\frac{5}{8})t_p$ recommendation is used as a means of satisfying AISC *Specification* Sections B3.4a and J1.2. AISC *Specification* Section B3.4a requires that "A simple connection shall have sufficient rotation capacity to accommodate the required rotation determined by the analysis of the structure." AISC *Specification* Section J1.2 requires that "Flexible beam connections shall accommodate end rotations of simple beams. Some inelastic but self-limiting deformation in the connection is permitted to accommodate the end rotation of a simple beam."

Rather than requiring engineers to determine the simple beam end rotation for every beam receiving a single-plate shear connection, the AISC *Manual* procedure is intended to accommodate rotations of about 0.03 rad, a rotation that exceeds the end rotation required of serviceable beams. In other words, the recommended $(\frac{5}{8})t_p$ weld size reflects a conservative simplification. It is important to note that this recommendation is only for single-plate simple shear connections at beam ends considered to have simple beam end boundary conditions. In other words, the recommendation, which results in a smaller weld than the more general procedure described earlier [i.e., $(\frac{5}{8})t_p$] applies only where the rotation is self-limiting and similar to a single-plate shear connection in configuration and expected behavior.

The design procedures for single-plate shear connections provided in the AISC *Manual* assume that plate yielding in some form accommodates simple beam end rotation. The conventional configuration relies on bolt plowing, or local yielding due to bearing at the plate (or potentially the beam web). The extended configuration primarily relies on flexural yielding of the plate, with bolt plowing considered in some cases. These are not the only mechanisms that can accommodate simple beam end rotation. In reality, a combination of mechanisms will be mobilized to accommodate the rotation. It may not be necessary to adhere to the $(\frac{5}{8})t_p$ weld size recommendation when other mechanisms are available or the simple beam end rotation from the analysis is small.

Large Inelastic Rotations—Seismic

In some instances, primarily related to seismic design, the weld must not only develop the flexural strength of the joined parts, but must also maintain its strength through large inelastic rotations of one of the parts joined.

One such condition involves the welds of gusset plates attaching vertical braces used in a SCBF. Per the AISC *Seismic Provisions* (AISC, 2016b), SCBF are "expected to provide significant inelastic deformation capacity primarily through brace buckling and yielding of the brace in tension." When the buckling occurs out-of-plane, large inelastic rotations occur about approximately the longitudinal axis of the weld group, which could lead to premature rupture of the weld. AISC *Seismic Provisions* Section F2.6c.4 is intended to address this concern and states, "For out-of-plane brace buckling, welds that attach a gusset plate directly to a beam flange or column flange shall have available shear strength equal to $0.6R_y F_y t_p/\alpha_s$ times the joint length." Even with the inclusion of R_y, the required weld size is still $(\frac{3}{4})t_p$.

The thickness of the gusset plate is rarely governed by the demands at the welded interfaces. Developing the weak-axis flexural strength based on the full thickness of the gusset is not often necessary. A smaller, more economical weld can sometimes be obtained by sizing the weld to develop the maximum weak-axis moment occurring in combination with the shear, compression, and strong-axis moment that result on the gusset plate edge from the brace compression force. Carter et al. (2016) developed such a method utilizing a generalized interaction equation recommended by Dowswell (2015).

Other situations where welds are required to develop the strength of the joined part while that part undergoes large inelastic rotations are the moment connections in intermediate moment frames (IMF) and special moment frames (SMF). The AISC *Seismic Provisions* require physical testing of the beam-to-column connections to confirm the strength and ductility of such connections. Either prequalified

connections provided in AISC 358, *Prequalified Connections for Special and Intermediate Steel Moment Frames for Seismic Applications* (AISC, 2016a), or connections qualified per AISC *Seismic Provisions* Section K2 can be used. In either case, the suitability of the welds, though sometimes sized by calculation, is ultimately established empirically.

Exceptions to the "Rules"

As stated in the Introduction to this paper, in some instances the authors are recommending practices based on their own knowledge, experience and judgment. Many of the recommendations are conservative. Over the decades, engineering judgment and common sense have dictated the use of certain practices or assumptions. Common engineering practice tends to, as it should, err on the side of conservatism. Apportioning of loads like "stress cops" is much maligned, though ultimately, all practical design is based on flawed assumptions. Limit states are sometimes segregated into ductile and nonductile categories. However, even though arguably the least ductile element commonly encountered in structural steel design, welds and welded joints often demonstrate ductility disproportionately greater than our common assumptions would suggest. A couple of illustrative examples will be discussed.

It is commonly assumed that the entire section must be engaged in order to develop the strength of the element. However, direct-welded, beam-to-column moment connections provide a counterexample to this common assumption. These connections are typically designed based on the assumption that the web connection carries the entire shear force and the moment is resolved into a couple with a lever arm equal to the distance between the flange centroids. There have been many tests of direct-welded, beam-to-column moment connections loaded to failure under monotonic and cyclic loading, and the specimens generally had a final failure mode of tension flange rupture with the applied moment consistently exceeding the plastic moment capacity of the beam calculated with the yield strength from tensile coupon tests (Dowswell and Muir, 2012).

The authors do not provide these examples to support more general changes to standard practice but, instead, provide them to guard against the tendency to heap ever-more-conservative and onerous requirements on conditions that are likely to perform far better than we typically assume.

Ductility Factor and Welds Sized to Develop Connected Part

As discussed previously, the ductility factor is used to enhance the ductility of the weld relative to proximity and distortional effects. When developing the joined parts, such enhancement of the weld is unnecessary because it is the yielding of the joined part(s) that provides the ductility and associated redistribution of the stress. The ductility factor should not be applied when the weld develops the joined part(s).

CONCLUSIONS

Discussion of three common connection design applications has been provided. Little background into the evolution of issues related to connecting element rupture strength at welds, the weld ductility factor, and element capacity welds is readily available in archival journals. The authors have attempted to provide insight into the backgrounds of these limit state evaluations.

The authors make recommendations on analysis and design approaches when dealing with the connection design issues discussed. These recommendations are based on the collective experience of the authors. Readers should not interpret these recommendations as the only approaches that can be used. Any rational method of analysis or rational approach can be implemented. It is the intention of the authors that the discussion and background information provided offers additional insight that can be used when considering the three issues presented in this paper.

REFERENCES

AISC (1992), *Manual of Steel Construction, Volume II: Connections*, American Institute of Steel Construction, Chicago, IL.

AISC (2016a), *Prequalified Connections for Special and Intermediate Steel Moment Frames for Seismic Applications*, ANSI/AISC 358-16, American Institute of Steel Construction, Chicago, IL.

AISC (2016b), *Seismic Provisions for Structural Steel Buildings*, ANSI/AISC 341-16, American Institute of Steel Construction, Chicago, IL.

AISC (2016c), *Specification for Structural Steel Buildings*, ANSI/AISC 360-16, American Institute of Steel Construction, Chicago, IL.

AISC (2017a), *Manual of Steel Construction*, 15th Ed., American Institute of Steel Construction, Chicago, IL.

AISC (2017b), *Design Examples*, v15.0, American Institute of Steel Construction, Chicago, IL.

Carter, C.J., Muir, L. and Dowswell, B. (2016), "Establishing and Developing the Weak-Axis Strength of Plates Subjected to Axial Loads," *Engineering Journal,* AISC, Vol. 53, No. 3, pp. 147–158.

Dowswell, B (2015), "Plastic Strength of Connecting Elements," *Engineering Journal*, AISC, Vol. 52, No. 2, pp. 47–66.

Dowswell, B. and Muir, L. (2012), "Steelwise: Developing M_p," *Modern Steel Construction*, May.

Fortney, P.J., and Thornton, W.A. (2015), "The Chevron Effect—Not an Isolated Problem," *Engineering Journal*, AISC, Vol. 52, No. 2, pp. 125–164.

Fortney, P.J. and Thornton, W.A. (2017), "The Chevron Effect and Analysis of Chevron Beams—A Paradigm Shift," *Engineering Journal*, AISC, Vol. 54, No. 4, pp. 253–296.

Hewitt, C.M. and Thornton, W.A. (2004), "Rationale Behind and Proper Application of the Ductility Factor for Bracing Connections Subjected to Shear and Transverse Loading," *Engineering Journal*, AISC, Vol. 41, No. 1, pp. 3–6.

Muir, L.S. and Thornton, W.A. (2014), *Vertical Bracing Connections—Analysis and Design*, Design Guide 29, AISC, Chicago, IL.

Muir, L.S. and Hewitt, C. (2009), "Design of Unstiffened Extended Single-Plate Shear Connections," *Engineering Journal*, AISC, Vol. 46, No. 2, pp. 67–80.

Richard, R.M. (1986), "Analysis of Large Bracing Connection Designs for Heavy Construction," *Proceedings National Engineering Conference*, Nashville, TN, June 12–14, pp. 31-1–31-44.

Williams, G.C. (1986), "Steel Connection Designs Based on Inelastic Finite Element Analysis," Dissertation, University of Arizona, Tucson, AZ.

Probabilistic Assessment of Seismic Force Demands in Biaxially Loaded Columns in Chevron-Configured Special Concentrically Braced Frames

HENRY V. BURTON, NILOFAR DOORANDISH and THOMAS SABOL

ABSTRACT

Special concentrically braced frame (SCBF) columns are designed as force-controlled elements and are intended to respond elastically during moderate-to-high return-period events. When placed at the intersection of orthogonal chevron-configured braced frames with fixed beam-column connections, SCBF columns are subjected to biaxial loading, including flexural demands developed in the beams due to unbalanced tension-compression brace forces. A probabilistic assessment of the force demands in biaxially and uniaxially loaded columns in chevron-configured SCBF is presented herein. Nonlinear response history analyses are performed on three-dimensional models of 3-, 9- and 20-story SCBF, and statistical descriptions of the results are used to investigate (1) the force demands relative to the capacity-design-based and elastic designs suggested by the American Institute of Steel Construction (AISC) *Seismic Provisions,* (2) the implications of the flexural demands transmitted to columns (via braced frame beams), and (3) the combinatorial effects of demands in biaxially loaded columns generated by orthogonal ground-motion components. At the maximum considered earthquake (MCE) hazard level, the median axial force demands in the biaxially loaded first-story columns of the three-story building are approximately at the level corresponding to the expected brace strength and exceed the design forces amplified by the overstrength factor. Axial flexure interaction is especially significant in the biaxially loaded columns of all three building cases. The results also show that the combinatorial effect of axial forces transmitted to the biaxially loaded columns via the orthogonal braces is generally lower in taller buildings and also depends on the demand level.

Keywords: special concentrically braced frames, probabilistic assessment, biaxially loaded columns, orthogonal effects, chevron braces.

INTRODUCTION

Special concentrically brace frames (SCBF) are commonly used as the seismic lateral force-resisting system (LFRS) in commercial, educational and other types of buildings. This is largely due to their cost-effectiveness in providing the strength and stiffness needed for building structures located in high seismic regions. SCBF braces are the deformation-controlled elements and are designed and detailed to sustain inelastic deformations while serving as the primary source of energy dissipation for the system. The remaining frame elements (beams, columns, and brace connections) are force-controlled and intended to respond elastically during moderate-to-high return-period events. SCBF beams, columns, and brace connection elements are therefore designed utilizing capacity design principles so that, ideally, their required strength exceeds the maximum force demands that can be delivered by the deformation-controlled elements (braces). The chevron configuration is frequently used in SCBF designs because it can provide open spaces and flexible architectural layouts However, due to the unsymmetrical cyclic axial force-deformation response of the brace in tension and compression, significant moments can be placed in the connecting beam, which are also transmitted to the columns when flexurally restrained beam-column connections are used. Improper consideration of these moments, especially in SCBF columns subjected to high axial loads, can lead to inelastic response and undesirable performance of the system.

Because of building architectural or programmatic constraints, SCBF are sometimes configured with columns located in two intersecting, orthogonal braced frames. During earthquake shaking, these columns are subjected to biaxial loading due to the simultaneous action of horizontal ground-motion components. For the case of chevron SCBF with flexurally restrained beam-column connections, the orthogonal braced frames will place axial and flexural demands in the intersecting column. As noted earlier, these columns are designed as forced-controlled components and are intended to respond elastically during moderate-to-severe earthquake shaking. Estimation of the axial and flexural demands in SCBF columns is therefore an important

Henry V. Burton, Assistant Professor, Department of Civil and Environmental Engineering, University of California, Los Angeles, CA. Email: hvburton@seas.ucla.edu (corresponding)

Nilofar Doorandish, Ph.D. Student, Department of Civil and Environmental Engineering, University of California, Los Angeles, CA. Email: niludoorandish@ucla.edu

Thomas Sabol, Adjunct Professor, Department of Civil and Environmental Engineering, University of California, Los Angeles, CA. Email: tsabol@ucla.edu

Paper No. 2018-03

part of the design process. In a real earthquake, these demands are affected by the extent and pattern of yielding in the brace elements.

Prior studies have used nonlinear response history analyses of two-dimensional structural models to investigate the seismic force demands in braced frame columns. Tremblay and Robert (2001) analyzed a set of chevron steel braced frames ranging in height from 2 to 12 stories. From the results of these analyses, the authors suggested that the brace columns be designed using a "full capacity design" approach where the axial forces are computed assuming simultaneous buckling of braces. Richards (2009) investigated the column seismic demands in SCBF with X-bracing, buckling restrained braced frames (BRBF), and eccentrically braced frames (EBF) with different heights and strength levels. The structural models were analyzed using ground motions that were scaled to be at or above the design spectra. The results showed that for low-rise SCBF, the column axial force demands exceeded the overstrength factor ($\Omega_0 = 2.0$) used to determine the upper limit on the demands for design. The author suggested using the full tensile capacity of the braces as the basis for computing column axial demands. For taller braced frames, the column axial demands in the upper stories were more than twice the design demands. However, it was also noted that this observation has limited practical implications because top-story columns are typically overdesigned. The maximum axial force demands in the base columns of taller buildings ranged from 55 to 75% of the design demands. Based on this finding, it was noted that using more realistic (less conservative) demands for braced frame column design in taller buildings could lead to significant cost savings.

To demonstrate a newly developed reliability-based methodology for establishing force demands in capacity-designed components of LFRS, Victorsson (2011) evaluated the force demands in SCBF columns. Structural models of 6- and 16-story SCBF were analyzed using incremental dynamic analyses to investigate the effect of height and number of deformation-controlled elements on brace connection and column force demands. The base column axial forces at the maximum considered earthquake (MCE) hazard level were found to be 90% and 50% of the capacity-design-based demands suggested by the 2010 AISC *Seismic Provisions* (AISC, 2010) for the 6- and 16-story frames, respectively. However, while the axial forces in the strength-controlled 6-story frame did not exceed the maximum required demands (elastic demands times the overstrength factor), this limit significantly underestimated the demands in the upper stories of the drift-controlled 16-story frame.

The objective of this study is to conduct a probabilistic assessment of biaxially and uniaxially loaded chevron SCBF columns to evaluate (1) the force demands relative to the capacity-design-based and elastic designs suggested by the 2010 AISC *Seismic Provisions*, (2) the implications of the flexural demands transmitted to columns (via braced frame beams) as a result of unbalanced tension-compression forces in chevron braces, and (3) the combinatorial effects of demands in biaxially loaded columns generated by orthogonal ground-motion components. These issues have direct implications to the design and performance of columns located in intersecting chevron-configured SCBF. Nonlinear response history analyses are conducted on three-dimensional SCBF structural models with varying heights using bi-directional loading. Force demands are described in a probabilistic manner to facilitate establishing reliability-based performance objectives for SCBF columns, which can then be linked to the prescribed design demands adopted by codes and standards.

DESCRIPTION OF BUILDING CASES

The three design cases used for the current study include 3- (SCBF-3S), 9- (SCBF-9S), and 20-story (SCBF-20S) buildings with chevron-configured SCBF. The plan dimensions, story heights, gravity loads, and framing layout of the three buildings are the same as the moment frame buildings used by Gupta and Krawinkler (1999) as shown in Figure 1. All bays are 30 ft wide and the typical story height is 13 ft. All three buildings have symmetric SCBF plan configurations and corner columns that are part of intersecting orthogonal braced frames. The braced frames in all three cases are all located on the perimeter of the building. All biaxially loaded (corner columns) are oriented with the web-direction in the z-direction (Figure 1).

The braced frames are designed in accordance with ASCE/SEI 7–10 (ASCE, 2010) and the 2010 AISC *Seismic Provisions.* (Note: All references to the AISC *Seismic Provisions* in this paper are references to the 2010 version unless noted otherwise.) The seismicity parameters ($S_S = 2.17g$ and $S_1 = 0.75g$) are based on a location in Los Angeles (–118.162, 33.996) with Site Class D. The designs are based on Risk Category II and Seismic Design Category E with a response modification factor $R = 6$, overstrength factor $\Omega_0 = 2$, drift amplification factor $C_D = 5$, and importance factor, $I = 1.0$. The seismic design loads are obtained from response spectrum analyses performed using *RAM Steel* (Bentley). SCBF beam-column connections are assumed to be flexurally rigid, and column bases are pinned. Key seismic design parameters are summarized in Table 1.

The braces are designed in accordance with AISC *Seismic Provisions* Section F2 to meet the required strength, slenderness and compactness requirements. Based on the size range of the SCBF beams and columns, the effective brace length is taken to be 3'-11" (or approximately 12%) less than that of the workpoint-to-workpoint length. The design forces in the force-controlled components (beams, columns and connections) are determined in accordance with AISC *Seismic Provisions* Section F.2.3. In all cases, the design-level

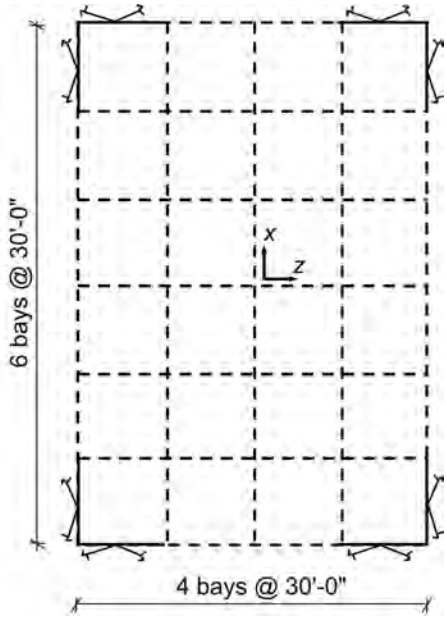

(a) SCBF-3S

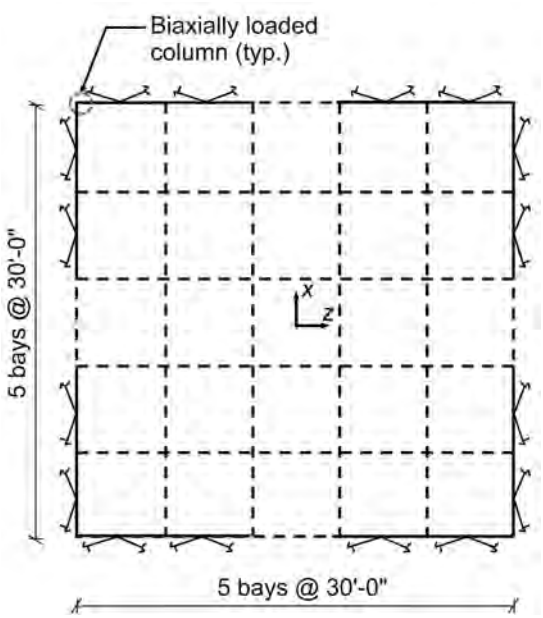

(b) SCBF-9S

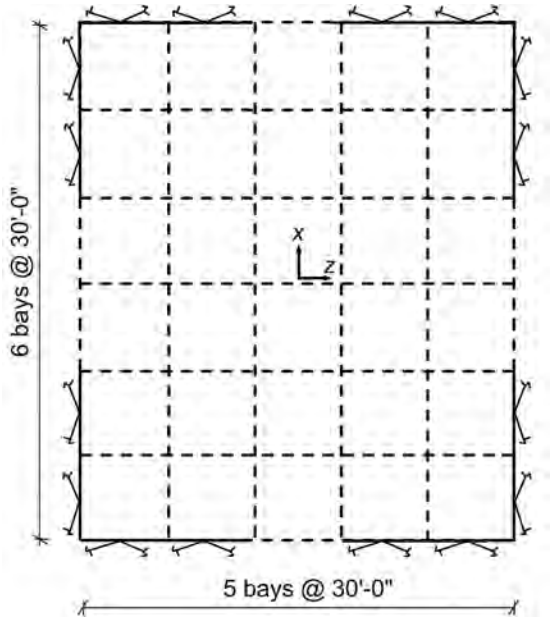

(c) SCBF-20S

Fig. 1. Floor plans showing the layout of the braced frames.

Table 1. Summary of Key Building Design Parameters						
Building	Number of Stories	Seismic Weight (kips)	Approximate Period[1], T_a(s)	Seismic Response Coefficient, C_s	Design Base Shear, V (kips)	Design Drift[2] (%)
SCBF-3S	3	5,247	0.44	0.24	1259	0.68
SCBF-9S-A	9	17,106	0.93	0.14	2395	0.70
SCBF-9S-B	9	17,106	0.93	0.14	2395	0.70
SCBF-20-S	20	47,117	1.81	0.07	3298	0.96

[1] ASCE/SEI 7-10 Equation 12.8-7
[2] Includes drift amplification factor, $C_D = 5$

demands from response spectrum analyses amplified by the overstrength factor was lower than the expected brace-capacity-based demands, therefore, the former was used in the design.

In addition to gravity, the beams are designed for the unbalanced brace compression and tension forces. The strength of the columns is determined based on gravity loads plus the seismic demands corresponding to the amplified response spectrum analysis forces for the case where the compression braces are removed as required by AISC *Seismic Provisions* Section F2.3, Exception 2. Note that there is no explicit requirement for the columns to be designed for the moments transmitted from the SCBF beams, which are generated by the unbalanced brace force (e.g., if the beam-to-column connection were fully restrained). Because some designers might choose to treat the beam boundary condition as pinned, regardless of the actual connection, the columns were designed for axial load only in this study to highlight the implications of underestimating the design loads. It is worth noting that the 2016 AISC *Seismic Provisions* (AISC, 2016) have been released, and the provision that limits the design forces in force-controlled components to elastic demands amplified by the overstrength factor has been removed. Going forward, all force-controlled components are required to be designed for the expected brace-capacity-based demand. In the current study, the demands from nonlinear response history analyses are evaluated against both the design-level demands amplified by the overstrength factor and the expected brace-capacity-based demands.

The SCBF member sizes (braces, chevron beams, and columns) and demand-to-capacity ratios are summarized in Tables 2 and 3, respectively. The demand-to-capacity ratios in the chevron beams are generally high across the three building cases, ranging from 0.82 to 0.95. The braces at the lower stories have the highest demand-to-capacity ratios for all building cases, ranging from 0.78 to 0.95. The upper-story braces are generally overdesigned and have much lower demand-to-capacity ratios (0.23 to 0.70), especially in the 9- and 20-story buildings. Like the braces, the upper-story columns are conservatively designed with the lowest demand-to-capacity ratios being less than 0.05. Because the beam-column connections are assumed flexurally rigid (welded connection), the columns are sized such that the flange width matches that of the beam. This explains why the demand-to-capacity ratios in the upper-story columns are very low (less than 0.1) compared to the other SCBF elements. The demand-to-capacity ratios in the lower-story columns range from 0.52 in the 3-story building to 0.82 in the 9- and 20-story buildings, respectively. The varying extent to which conservatism is incorporated in the SCBF columns is especially relevant to the probabilistic demand assessment presented later in the paper.

STRUCTURAL MODELING, GROUND MOTIONS, AND NONLINEAR RESPONSE HISTORY ANALYSES

Structural Modeling

Three-dimensional nonlinear structural models of the three building cases are developed in *OpenSees* (UC Berkeley) using expected gravity loads ($1.05D + 0.25L$). Only the SCBF frames are included in the structural model with a P-Δ column placed at the center-of-mass (geometric center) to account for the destabilizing effect of the gravity loads that are not explicitly considered. A schematic illustration of a single SCBF frame for the three-story building is shown in Figure 2. Beams and columns are modeled with fiber elements that incorporate the *Steel02* material model with expected strengths of R_yF_y ($R_y = 1.1$ and $F_y = 50$ ksi). For beams, the fiber element properties are used for axial force and strong-axis bending (in the vertical plane). Fiber elements in columns account for bending about both axes (i.e., P-M-M interaction). Beam-column connections are modeled as flexurally rigid. The SCBF braces are modeled using force-based nonlinear beam-column elements with the *Steel02* material (UC Berkeley) also using expected strengths ($R_y = 1.4$ and $F_y = 46$ ksi) and strain hardening of 0.3%. Initial imperfections and co-rotational transformations are used to simulate out-of-plane buckling. The discretization of

Table 2a. Summary of SCBF Brace Sizes		
Building	**Story**	**Brace Size**
SCBF-3S	1	HSS7.5×0.5
	2	HSS7.5×0.375
	3	HSS6.625×0.312
SCBF-9S	1 to 3	HSS7.5×0.5
	4 to 5	HSS7.625×0.375
	6 to 7	HSS6.625×0.5
	8 to 9	HSS6.625×0.312
SCBF-20S	1 to 10	HSS8.625×0.5
	11 to 16	HSS7.5×0.5
	17 to 18	HSS7.5×0.375
	19 to 20	HSS6.625×0.312

Table 2b. Summary of SCBF Column Sizes		
Building	**Story**	**Braced Frame Column Size**
SCBF-3S	1 to 3	W14x132
SCBF-9S	1	W14×257
	2 to 3	W14×211
	4 to 9	W14×132
SCBF-20S	1 to 2	W14×665
	3 to 4	W14×550
	5 to 6	W14×455
	7 to 8	W14×370
	9 to 10	W14×311
	11 to 12	W14×257
	13 to 14	W14×193
	15 to 20	W14×132

Table 2c. Summary of SCBF Beam Sizes		
Building	**Level**	**Chevron Beam Size**
SCBF-3S	2	W27×281
	3	W27×217
	4	W24×192
SCBF-9S	2 to 4	W30×261
	5 to 6	W27×217
	7 to 8	W27×258
	9 to 10	W24×192
SCBF-20S	2 to 11	W30×292
	12 to 17	W30×261
	18 to 19	W27×217
	20 to 21	W24×192

Table 3. Summary of Demand-to-Capacity Ratios for Braces and SCBF Beams and Columns			
	Demand-to-Capacity Ratios		
Building	Braces	Beams	Columns
SCBF-3S	0.70 to 0.86	0.82 to 0.92	0.04 to 0.52
SCBF-9S	0.23 to 0.78	0.84 to 0.89	0.04 to 0.82
SCBF-20S	0.54 to 0.95	0.85 to 0.95	0.02 to 0.82

Table 4. Modal Periods from Eigenvalue Analyses			
	Modal Periods, (s)		
Building	1st Mode	2nd Mode	3rd Mode
SCBF-3S	0.38	0.37	0.15
SCBF-9S	0.81	0.81	0.38
SCBF-20-S	2.00	2.00	0.82

the brace elements along the length, number of integration points, and number of fibers are determined based on the recommendations provided in Uriz et al. (2008). The ends of the braces are modeled as pinned, and rigid elastic elements are placed at the ends of beams, columns and braces in the region of the gusset plate. Rayleigh damping corresponding to 3% of critical damping in the first and third modes is applied. The first three modal periods for the three building cases obtained from eigenvalue analyses of the *OpenSees* models, are summarized in Table 4.

Ground Motions

Nonlinear response history analyses are conducted on the structural models of the three building cases using a single set of 26 ground motions, each with two orthogonal horizontal components. The set includes records from events with moment magnitudes ranging from 6.4 to 7.6 and rupture distances between 6.84 and 27.3 miles. The ground-motion spectra are shown in Figure 3 with the ASCE/SEI 7–10 estimated periods corresponding to the three building cases identified. The median spectral acceleration level corresponding to the code-based period for the 3-story, (T = 0.44s), 9-story (T = 0.93s), and 20-story (T = 1.83s) buildings are 0.60*g*, 0.40*g* and 0.19*g*, respectively.

Nonlinear Response History Analyses

The force demands in the biaxially loaded (corner) SCBF columns (Figure 4) is the response parameter of primary

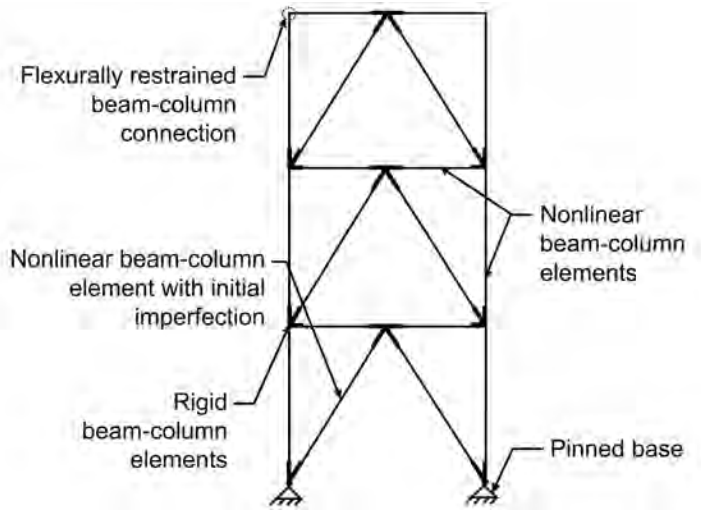

Fig. 2. Schematic illustration of OpenSees *model for a typical three-story SCBF.*

interest. However, as described later, the demands in the uniaxially loaded columns (Figure 4) are used as a benchmark to evaluate the combinatorial effect of orthogonal loading. Demands from the SCBF braces in the two principal directions of the LFRS transmit axial forces to the biaxially loaded columns. Flexural demands in the SCBF beams, which develop because of the unbalanced tension-compression response of the chevron braces, are also transmitted to these columns in the form of biaxial bending moments. Incremental dynamic analyses (IDA) are performed using bi-directional loading at ground-motion hazard levels ranging from 10 to 100% of the MCE at 10% increments. This range of ground-motion intensities is used to evaluate the effect of the extent of inelastic response on the combinatorial effects of demands from orthogonal ground motions. In the analyses, each ground-motion pair is scaled such that the geometric mean spectra matches the target intensity at the building's fundamental period.

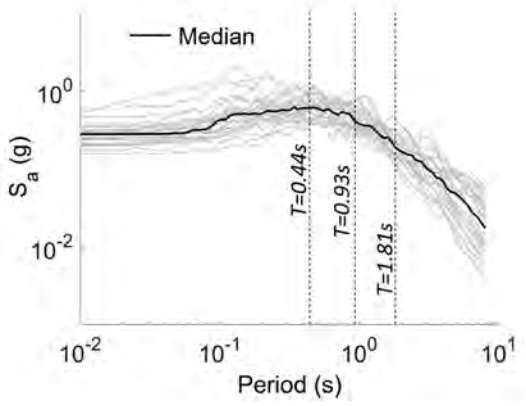

Fig. 3. Response spectra for ground motions used in nonlinear structural analysis.

PROBABILISTIC ASSESSMENT OF FORCE DEMANDS IN SCBF COLUMNS

Brace Force Demands at MCE Hazard Level

The primary goal of this section is to probabilistically assess the force demands in the SCBF columns relative to (1) the demands based on expected brace strengths, (2) the design demands obtained from response spectrum analysis (before amplifying by the overstrength factor), and (3) the nominal strengths. To facilitate interpreting those demands, median brace compressive forces at the MCE hazard level, C_{max}, in each direction, normalized by the expected brace strengths C_{exp}, are shown in Figure 5. The median C_{max}/C_{exp} ratio is approximately 0.95 for both (x and z directions) orthogonal first-story braces of all three buildings. The C_{max}/C_{exp}

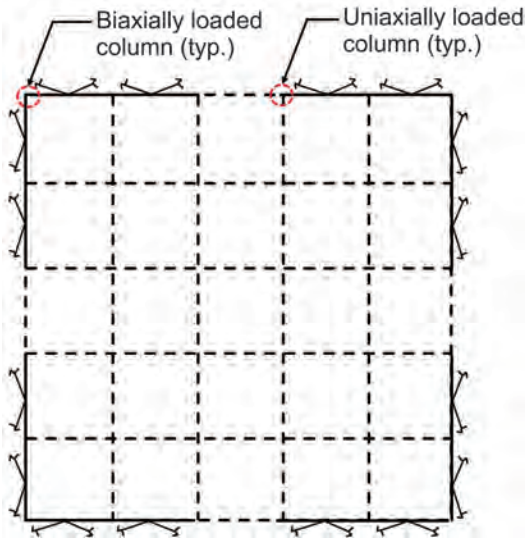

Fig. 4. Identifying biaxially and uniaxially loaded columns.

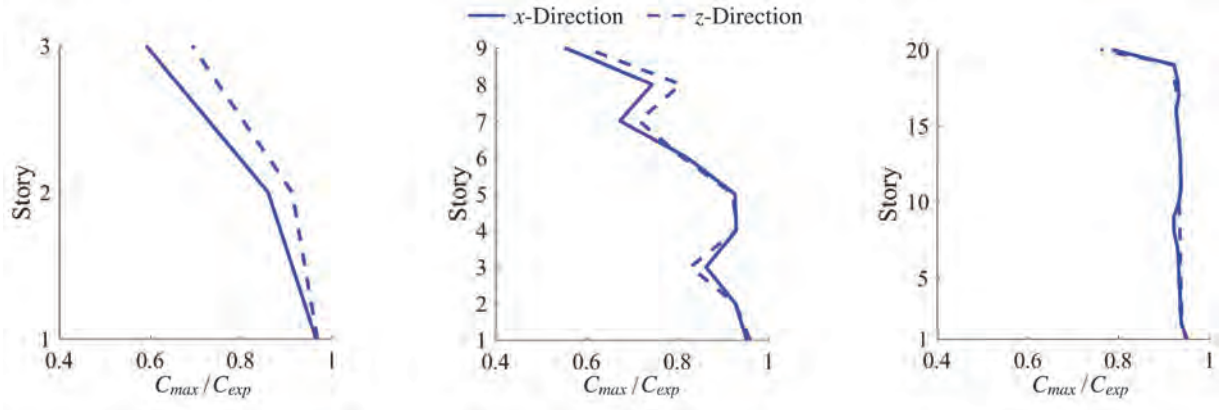

(a) SCBF-3S *(b) SCBF-9S* *(c) SCBF 20-S*

Fig. 5. Brace force demands normalized by expected strength.

ratio is generally much lower in the uppermost stories of SCBF-3S (0.6 to 0.7) and SCBF-9S (0.55 to 0.6). The C_{max}/C_{exp} profile in SCBF-20 is uniform along the height of the building between the 1st and 18th stories because the brace compressive demands for many (more than half) of the ground motions are at or near the expected strength

SCBF Column Axial Compressive Force Demands at MCE Level

Figure 6 shows the full profile of the maximum compression force in the biaxially (median, 16th and 84th percentile) and uniaxially (median) loaded columns, P_{max}, normalized by the demands based on the expected strength of the braces, P_{exp}. The median P_{max}/P_{exp} ratio for the biaxially loaded columns in the first story of SCBF-3S, SCBF-9S and SCBF-20S is 1.16, 0.61 and 0.6, respectively. The reduction in the first-story column P_{max}/P_{exp} ratio in SCBF-3S and SCBF-9S with building height is consistent with the profile trend of brace demands shown in Figures 5(a) and 5(b). Note that, for biaxially loaded columns, P_{exp} is based on 100% of expected compressive strength of the braces in one direction and 30% in the orthogonal direction—that is, the 100–30 rule is applied to obtain P_{exp}. The overall trend is that P_{max}/P_{exp} decreases up the height of the building. For example, in the uppermost story, the median P_{max}/P_{exp} ratio is between 0.06 and 0.25 for the biaxially loaded columns in all three structures. The dispersion in P_{max}/P_{exp} also decreases up the height of the building as evidenced by the reduction in the difference between the 84th and 16th percentile values, which ranges from 0.48 in the first story of SCBF-3S to 0.2 in the uppermost story. In SCBF-9S, the range is 0.18 in the first story to 0.11 in the uppermost story.

Figure 6(a) shows that P_{max}/P_{exp} in the uniaxially loaded columns is comparable to that of the biaxially loaded columns for SCBF-3S. For example, the median P_{max}/P_{exp} = 1.16 in the first story of the uniaxially loaded columns in SCBF-3S. However, for SCBF-9S and SCBF-20S, P_{max}/P_{exp} is higher for the uniaxially loaded columns (P_{max}/P_{exp} ranges from 0.69 to 0.73 in the first story). As expected, P_{max} is generally higher in the biaxially loaded columns. However, because P_{exp} for the uniaxially loaded columns is based on the compressive strength of braces in one direction, it is smaller than that of the biaxially loaded columns, which, as noted earlier, are based on 100% of compressive strength of braces in one direction and 30% in the other. The P_{max}/P_{exp} being higher for the uniaxially loaded columns in the 9- and 20-story structures but comparable to that of the biaxially loaded columns for the 3-story structure suggests that the combinatorial effects of loading from orthogonal braced frames is more significant in the latter. This finding is further explored later in the paper when a more direct approach to evaluating "orthogonal effect" is implemented.

Figure 7 shows that the median of the ratio P_{max}/P_{rsa} is 2.6, 1.7 and 1.8 in the biaxially loaded columns at the first story of SCBF-3S, SCBF-9S and SCBF-20S, respectively. Note that P_{max}/P_{rsa} is greater than the Ω_0 = 2.0 for the biaxially loaded column in SCBF-3S, which means that the median demand at the MCE level exceeds the upper limit on the design axial force set by the AISC *Seismic Provisions*. However, as noted earlier, the upper limit corresponding to the design level demands amplified by the overstrength factor has been removed in the 2016 *Provisions*. For SCBF-3S, P_{max}/P_{rsa} = 1.9 for the uniaxially loaded first-story columns, which is 37% smaller than its biaxially loaded counterpart, where P_{max}/P_{rsa} = 2.6 [Figure 7(a)]. However, P_{max}/P_{rsa} for uniaxially and biaxially loaded first-story columns are approximately equal for SCBF-9S and SCBF-20S. Again, this observation is consistent with the P_{max}/P_{exp} ratios discussed earlier and will be explored further later in the paper.

The maximum compression force in biaxially (median, 16th and 84th percentile) and uniaxially (median) loaded

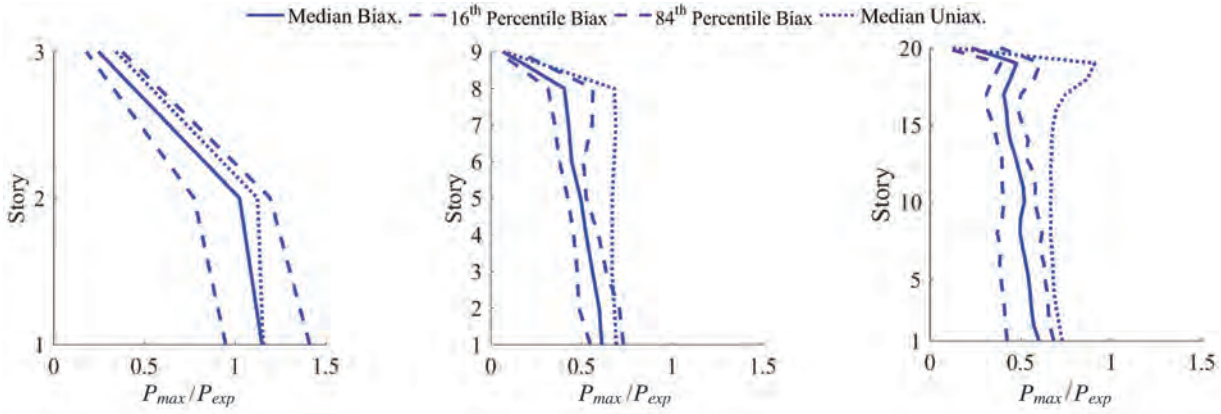

Fig. 6. Compression force demands in SCBF columns at MCE level normalized by demands based on expected strength of braces.

columns normalized by the nominal strength, P_{max}/P_n is shown in Figure 8. For SCBF-3S, the peak demand ratio occurs in the first-story columns and is about 0.5 for the biaxially loaded columns [Figure 8(a)]. For SCBF-9S and SCBF-20S, the maximum P_{max}/P_n also occurs at the first story, and the median values are 0.67 and 0.76, respectively for the biaxially loaded columns. These relative ratios are somewhat consistent with the demand-to-capacity ratios used in the design (reported in Table 3), which were 0.52, 0.82 and 0.82 in SCBF-3S, SCBF-9S and SCBF-20S, respectively. P_{max}/P_n drops off to less than 0.05 in the uppermost columns of all three buildings for the biaxially loaded columns. P_{max}/P_n in the first-story uniaxially loaded columns of SCBF-3S is approximately 20% less than its biaxially loaded counterpart. For SCBF-9S and SCBF-20S, P_{max}/P_n in the first-story uniaxially loaded columns is approximately 14% and 7% less, respectively, when compared to the biaxially loaded ones. The reduction in the difference between the demands in the uniaxially and biaxially loaded columns as the building height increases is consistent with earlier observations. The higher dispersion in the lower-story demands on the taller buildings is also consistent with earlier observations.

SCBF Column Flexural and Axial-Flexure Interaction Demands at MCE Hazard Level

Figure 9 shows that the median of the maximum flexural demands, M_{max}, in the biaxially loaded columns at the MCE hazard level are as high as approximately 100% of the nominal flexural strength, M_n, for all three buildings. The lower flexural demands in upper stories is consistent with the brace demand pattern observed in Figure 5. For all three buildings, the flexural demand ratios are comparable about the two axes. Except for the first two stories of each building, the flexural demand ratios in the uniaxially loaded columns are higher about the strong axis. The exceptions

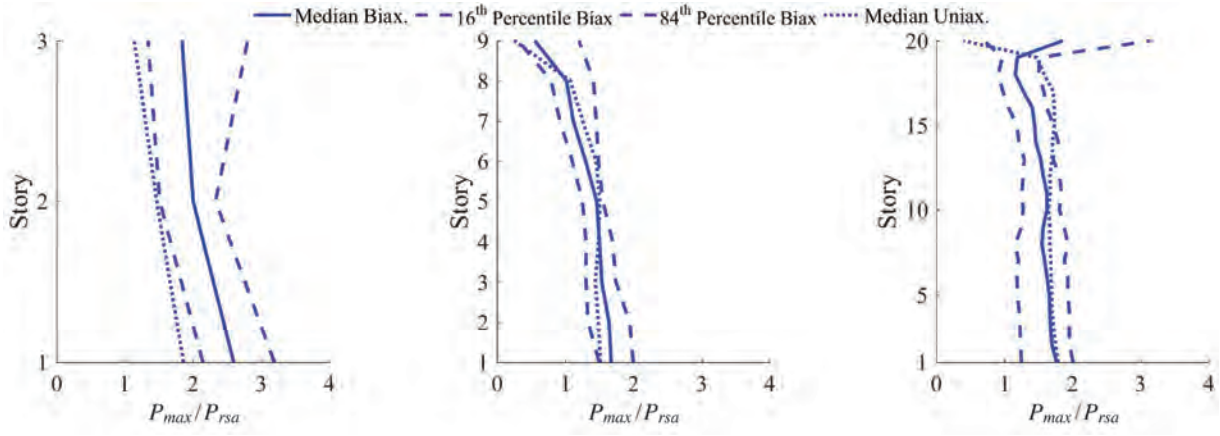

(a) SCBF-3S (b) SCBF-9S (c) SCBF 20-S

Fig. 7. Compression force demands in SCBF columns at MCE level normalized by demands from response spectrum analysis.

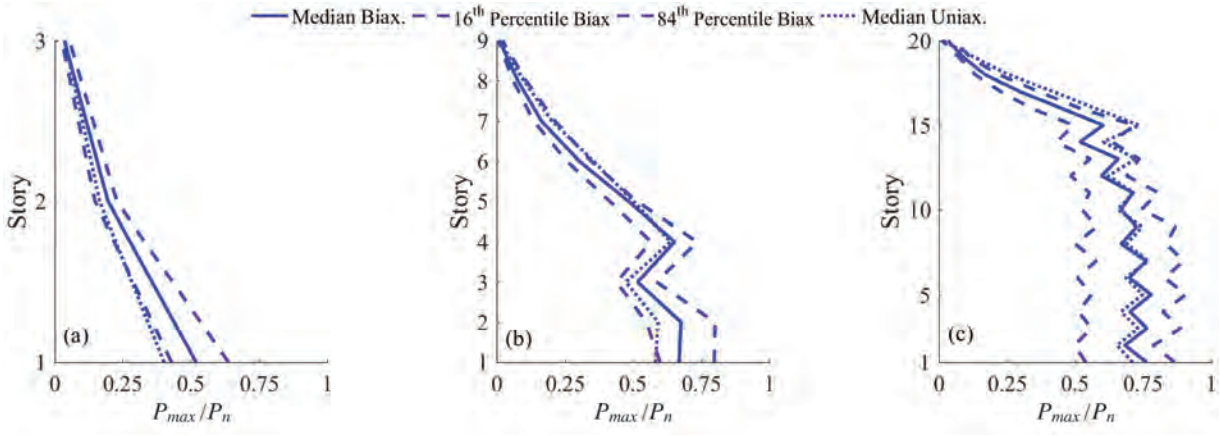

(a) SCBF-3S (b) SCBF-9S (c) SCBF 20-S

Fig. 8. Compression force demands in SCBF columns at MCE level normalized by nominal strength.

are due to high drift concentrations in the first-story weak-axis direction, which results in high flexural demands at the top of the first-story and bottom of second-story columns. Recall that these flexural demands originate from the unbalanced tension-compression response of the chevron braces, which results in significant flexural demands in the SCBF beam. If the SCBF beam column connections are flexurally restrained, as was assumed in this study, these moments are also transmitted to the columns. The AISC *Seismic Provisions* require the chevron beams to be designed for the moments caused by the brace force imbalance. However, as noted earlier, there is no explicit language requiring that the moment demands in the column be considered in the design.

It is well understood that axial force and flexural demands in beam-column elements interact to produce axial stresses. For the most part, very little attention is given to axial-flexure interaction in SCBF systems because it is generally assumed that SCBF columns are not subjected to significant moment demands. However, as presented earlier, using chevron-configured SCBF with flexurally rigid beam-column connections resulted in moment demands as high as 100% of the nominal flexural strength for the buildings considered in this study.

Figure 10 shows the profile of maximum axial-flexure interaction demands at the MCE hazard level for the biaxially and uniaxially loaded columns. The *P-M* interaction demands are described in terms of the sum of the axial and flexural demands (both axes) normalized by their respective nominal strengths ($P_{max}/P_n + M_{max,1}/M_{n,1} + M_{max,2}/M_{n,2}$). The median interaction ratio is greater than 1.0 for the biaxially loaded first- and second-story columns of SCBF-3S and the first, second, fourth and fifth stories of SCBF-9S. In SCBF-20S, the median ratio is approximately 1.17 in the first-story biaxially loaded column. The interaction ratio is generally higher for the biaxially loaded columns compared to the uniaxially loaded ones. The maximum ratio (first-story) is 5%, 8% and 14% higher for the biaxially loaded columns of SCBF-3S, SCBF-9S and SCBF-20S, respectively. The median interaction ratio drops off to approximately 40% in the uppermost biaxially loaded columns for SCBF-9S and SCBF-20S. For SCBF-3S, the median interaction ratio is approximately 65% in the uppermost story.

PROBABILISTIC EVALUATION OF COMBINATORIAL EFFECTS FOR ORTHOGONAL RESPONSE DEMANDS IN BIAXIALLY LOADED SCBF COLUMNS

When designing LFRS elements, the structure is typically analyzed independently for each horizontal translational component of earthquake loading, and the demands are combined accordingly. The rules used to combine the demands from orthogonal loads are intended to account for the simultaneous actions of ground-motion components. In ASCE/SEI 7–10, which was used to design the building cases for the current study, the 100–30 rule (Rosenblueth and Contreras, 1977) is adopted, which uses the larger of the responses obtained from combining 100% of the demand from loading in one direction with 30% of the demands associated with loading in the orthogonal direction. Other approaches to combining the demands from orthogonal earthquake loads include the 100–40 rule Newmark (1975), the square-root-sum-of-squares (SRSS) and the CQC3 rule (Smeby and Der Kiureghian, 1985). Several researchers have investigated the efficacy of these combination rules (e.g., Menun and Der Kiureghian, 1998; Heredia-Zavoni and Machiacao-Barrionuevo, 2004; Lopez et al., 2001). However, most of these studies did not consider nonlinear response in their evaluations, and none have focused on the specific issue of biaxially loaded columns in SCBF.

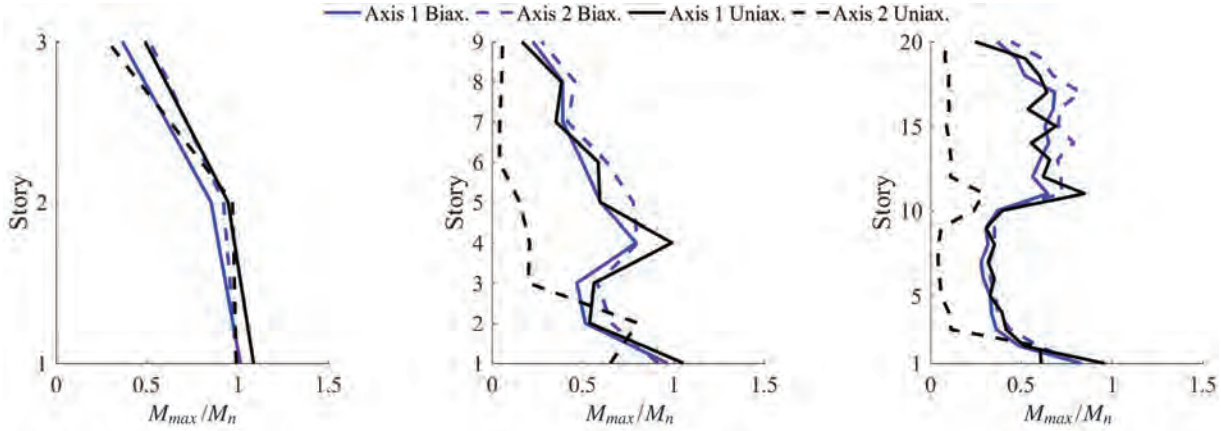

(a) SCBF-3S *(b) SCBF-9S* *(c) SCBF 20-S*

Fig. 9. Flexural demands in SCBF columns at MCE level normalized by nominal strength.

The "orthogonal effects" combination rules are used to amplify the force demands from uni-directional loading so that they are representative of the demands from bi-directional loading. As noted earlier, the corner SCBF columns are loaded biaxially by the two orthogonal ground-motion components. However, because of the symmetry of the LFRS used in the current study, the axial demands in the "non-corner" or uniaxially loaded columns are affected by a single ground-motion component. As such, the ratio of the axial compression demands in the biaxially and uniaxially loaded columns is used as the basis of evaluating the combinatorial effects of the response demands in the former. The maximum axial compressive force in the biaxially and uniaxially loaded columns are denoted as $P_{max,bi}$ and $P_{max,uni}$, respectively. For bi-directional nonlinear response history analysis performed using a single ground-motion pair, the ratio $P_{max,bi}/P_{max,uni}$ is obtained. By using a set of ground motions for each of the load cases, a full probability distribution of $P_{max,bi}/P_{max,uni}$ is determined.

Figure 11 shows the full height profile of the median, 16th and 84th percentile of $P_{max,bi}/P_{max,uni}$ corresponding to the MCE hazard level. In SCBF-3S, the median ratio is 1.3 in the first story and reduces to 1.16 in the uppermost story. It can also be observed that $P_{max,bi}/P_{max,uni}$ generally decreases as building height increases. In the first-story columns of SCBF-9S and SCBF-20S, the median $P_{max,bi}/P_{max,uni}$ is 1.17 and 1.12, respectively, which serves as further evidence that the combinatorial effects of orthogonal loading is lower for taller buildings.

Figure 12 shows the effect of ground-motion intensity on the $P_{max,bi}/P_{max,uni}$ ratios in the first-story columns. Figure 12(a) shows the median, 16th and 84th percentile ratios for SCBF-3S, which are obtained from an IDA performed at intensities ranging from 10 to 100% of the MCE hazard level. An overall increase in $P_{max,bi}/P_{max,uni}$ with the ground-motion intensity is observed. For example, the 84th percentile value ranges from 1.39 at the lowest intensity level to 1.58

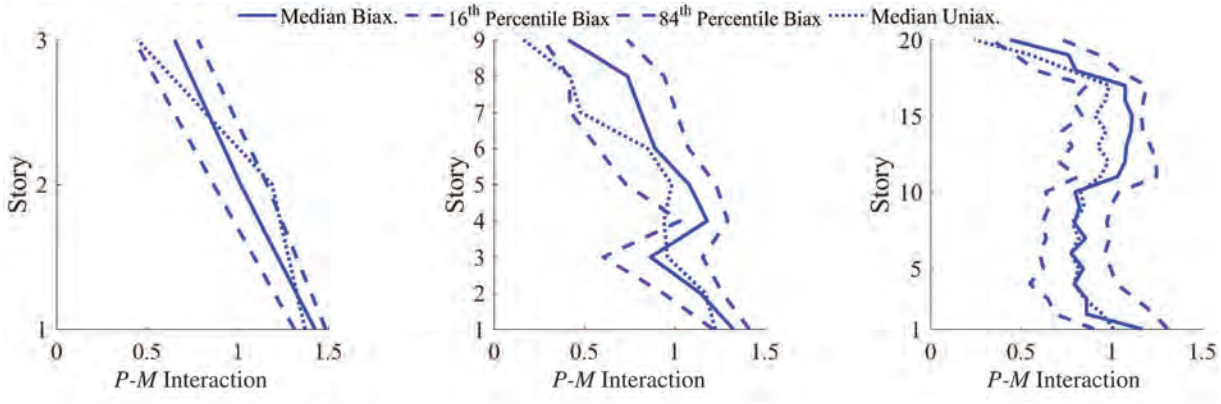

(a) SCBF-3S *(b) SCBF-9S* *(c) SCBF 20-S*

*Fig. 10. Axial-flexure (*P-M*) interaction demands ($P_{max}/P_n + M_{max,1}/M_{n,1} + M_{max,2}/M_{n,2}$) in SCBF columns at MCE level.*

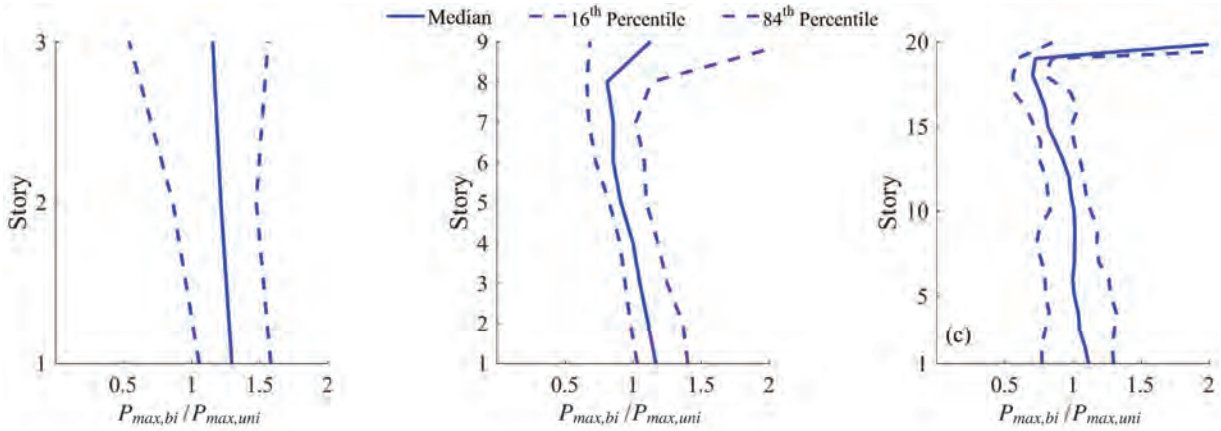

(a) SCBF-3S *(b) SCBF-9S* *(c) SCBF 20-S*

Fig. 11. Full-height profile for the ratio of compression force demands in biaxially and uniaxially loaded columns at MCE level.

at the highest intensity level. This observation highlights the need to consider both inelastic response and ground-motion intensity level when evaluating rules for combining response demands from orthogonal ground-motion components.

Figures 12(b) and 12(c) show that in addition to $P_{max,bi}/P_{max,uni}$ being generally lower, the effect of ground-motion intensity is also less significant for taller buildings. For instance, the difference between the 84th percentile $P_{max,bi}/P_{max,uni}$ at 10% and 100% of the MCE intensity level is only 0.07 in SCBF-9S compared to 0.19 in SCBF-3S. For the SCBF-20S building, the 84th percentile $P_{max,bi}/P_{max,uni}$ is approximately the same at the 10% and 100% MCE intensity levels.

The uncertainty in the values of $P_{max,bi}/P_{max,uni}$ conditioned on the ground-motion intensity level can be described by fitting a theoretical probability distribution to the empirical data-points at that intensity. The two-sample Kolmogorov-Smirnov (KS) test (Massey, 1951) is performed to determine the appropriate distribution based on the null hypothesis that the empirical values of $P_{max,bi}/P_{max,uni}$ follow that distribution. The output of the KS test is a p-value, which corresponds to the probability that there is a match between the empirical and theoretical distributions. A threshold of 5% is used as the acceptable margin of the p-value. The difference between the theoretical and empirical distributions is deemed significant if the p-value obtained from the hypothesis test falls below this threshold. The results from the KS test showed that the log-normal distribution produces a p-value that is larger than 5% across all intensity levels. Therefore, $P_{max,bi}/P_{max,uni}$ is assumed log-normal. Probability of exceedance curves for $P_{max,bi}/P_{max,uni}$ conditioned on the MCE hazard level, which are generated from the theoretical probability distributions, are shown in Figure 13. The distribution for each building is generated using the median and log-standard deviation values from the empirical data. As noted earlier, the median $P_{max,bi}/P_{max,uni}$ is generally lower for tall buildings, which results in higher overall exceedance probabilities. For example, SCBF-20S has an exceedance probability of 0.43 at $P_{max,bi}/P_{max,uni}$ = 1.0, which is almost half that of SCBF-3S. The exceedance probability corresponding to $P_{max,bi}/P_{max,uni}$ = 1.3, which ranges between 0.12 for SCBF-20S and 0.48 for SCBF-3S, can be used as the basis for evaluating the 100–30 rule.

CONCLUSIONS

A probabilistic evaluation of the force demands in the biaxially loaded columns of special concentrically braced frames (SCBF) is presented with a specific focus on (1) the maximum considered earthquake (MCE) demand levels relative to the capacity-design-based and design level forces; (2) the implications of flexural demands, which are transmitted from the chevron beams; and (3) the adequacy of the combinatorial effects of loading from orthogonal ground-motion components. Nonlinear response history analyses of three-dimensional models of 3-, 9- and 20-story SCBF are used as the basis of the evaluation.

For both the biaxially and uniaxially loaded columns, the ratio of the median MCE level axial compression demands, P_{max}, normalized by (1) the demands based on the expected brace strength, P_{exp}, (2) the demands from response spectrum analysis before amplification by the overstrength factor, P_{rsa}, and (3) the nominal compressive strength, P_n, was assessed. By comparing P_{max}/P_{exp} and P_{max}/P_{rsa} for the biaxially and uniaxially loaded columns in the three building cases, the combinatorial effect of orthogonal loads was found to decrease as the building height increased. Moreover, the three-story building case was the one where, in the first-story columns, P_{max}/P_{exp} exceeded 1.0 and P_{max}/P_{rsa} exceeded the overstrength factor for an SCBF

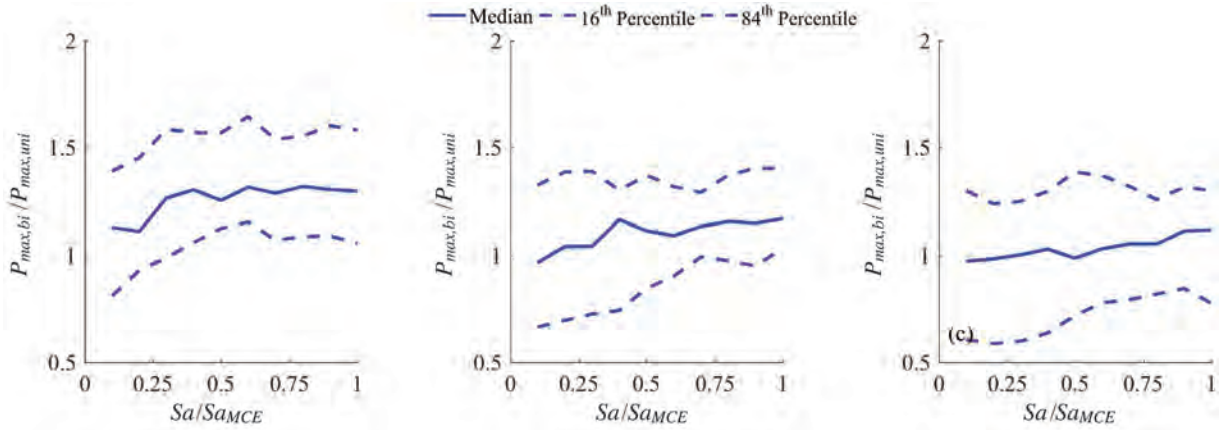

(a) SCBF-3S (b) SCBF-9S (c) SCBF 20-S

Fig. 12. Ratio of compression force demands in biaxially and uniaxially loaded first columns from IDA.

building (2.0). However, it should be noted that the latter is no longer a concern because the 2016 AISC *Seismic Provisions* (AISC, 2016) require SCBF columns to be designed for P_{exp}. The demand dispersion was found to be highest in the lower stories and generally increased with building height.

The highest P_{max}/P_n values in the biaxially loaded columns were found to be comparable with the demand-to-capacity-ratio used in design: 0.25, 0.82 and 0.82 in the 3-, 9- and 20-story building cases, respectively. For the biaxially loaded columns, the median of the maximum MCE level flexural demands was as high as 100% of the nominal strength in all three buildings. An interaction ratio was computed by summing the axial and flexural demands (both axes) normalized by their respective nominal strengths. The median of the maximum MCE level value of this ratio was found to be greater than or equal to 1 for both the uniaxially and biaxially loaded columns of all three buildings. It is worth reiterating that the goal here was to highlight the performance implications of neglecting the seismic moment generated in the SCBF columns via the chevron beams. However, it is recognized that some engineers do account for these moments in their design, and the axial-flexural interaction demand ratios presented in this study are not representative of those cases.

The combinatorial effects of orthogonal response demands in the biaxially loaded columns was evaluated by generating full probability distributions of these demands normalized by the demands in the uniaxially loaded columns ($P_{max,bi}/P_{max,uni}$). The full profile (along building height) of the median, 16th and 84th percentile of $P_{max,bi}/P_{max,uni}$ at the MCE hazard level showed that combinatorial effects are generally higher in the lower stories of the three building cases and decreased as the building height increased. Results from incremental dynamic analyses showed that while $P_{max,bi}/P_{max,uni}$ generally increased with ground-motion intensity, the effect was smaller for taller buildings.

The 100–30 combination rule was evaluated by computing the probability of $P_{max,bi}/P_{max,uni} > 1.3$. This probability was found to range from 0.12 to 0.48 for the 20- and 3-story buildings, respectively. At least for SCBF systems, this suggests that the current 100–30 rule underestimates the axial force demand in biaxially loaded columns. Note that the 2016 AISC *Seismic Provisions* implies that a 100–100 combination rule should be used to account for the simultaneous action of orthogonal ground-motion components. However, the results of this study suggest that for the considered SCBF systems, this would be overly conservative.

This study did not attempt to identify a more appropriate combination rule, principally because its focus was to assess whether the current combination rule resulted in consistently underestimating biaxial column demands in SCBF systems. It is important to note that mere exceedance of estimated demands in individual columns does not necessarily lead to poor performance (e.g., collapse). Moreover, appropriately estimating demands on biaxially loaded columns is not a material-dependent issue. Further research is needed to evaluate the performance implications of alternative combination rules. For SCBF systems, such research must consider the impact of all relevant limit states that might dominate behavior as the combination rule is varied. Similar research investigating orthogonal load effects in other seismic-force-resisting systems is also needed to assess whether the existing combination rule should be changed or alternative approaches implemented.

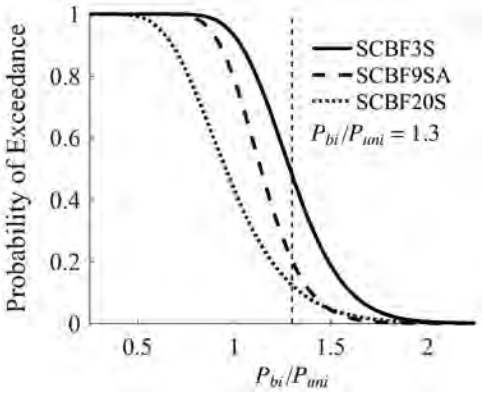

Fig. 13. Probability of exceedance curves for ratio of compression force demands in biaxially and uniaxially loaded first columns at MCE level.

ACKNOWLEDGMENTS

This research is supported by the American Institute of Steel Construction (AISC). Any opinions, findings and conclusions expressed in this paper are those of the authors and do not necessarily reflect the views of the AISC. The authors would like to thank Jim Malley, Tom Schlafly, Leigh Arbor, and Subash Goel for their valuable input on this study.

REFERENCES

AISC (2010), *Seismic Provisions for Structural Steel Buildings*, ANSI/AISC 341-10, American Institute of Steel Construction, Chicago, IL.

AISC (2016), *Seismic Provisions for Structural Steel Buildings*, ANSI/AISC 341-16, American Institute of Steel Construction, Chicago, IL.

ASCE (2010), *Minimum Design Loads for Buildings and Other Structures*. ASCE/SEI 7-10, American Society of Civil Engineers, Reston, VA.

Bentley, *RAM Steel* [Computer software], V8i, Bentley Systems Incorporated, Exton, PA.

Gupta, A. and Krawinkler, H. (1999), "Seismic Demands for Performance Evaluation of Steel Moment Resisting Frame Structures," Blume Earthquake Engineering Center, Report No. 132, Stanford University, Standford, CA.

Heredia-Zavoni, E. and Machicao-Barrionuevo, R. (2004), "Response to Orthogonal Components of Ground Motion and Assessment of Percentage Combination Rules," *Earthquake Engineering and Structural Dynamics*, Vol. 33, pp. 271–284.

Lopez O.A, Chopra A.K. and Hernandez J.J. (2001), "Evaluation of Combination Rules for Maximum Response Calculation in Multicomponent Seismic Analysis," *Earthquake Engineering and Structural Dynamics*, Vol. 30, pp. 1379–1398.

Massey Jr, F.J. (1951), "The Kolmogorov-Smirnov Test for Goodness of Fit," *Journal of the American Statistical Association*, Vol. 46, No. 253, pp. 68–78.

Menun, C. and Der Kiureghian, A. (1998), "A Replacement for the 30%, 40% and SRSS Rules for Multicomponent Seismic Analysis," *Earthquake Spectra,* Vol. 14, No. 1, pp. 153–156.

Newmark N.M. (1975), "Seismic Design Criteria for Structures and Facilities, Trans-Alaska Pipeline System," *Proceedings of the U.S. National Conference on Earthquake Engineering*, EERI, pp. 94–103.

Richards, P. (2009), "Seismic Column Demands in Ductile Braced Frames," *ASCE Journal of Structural Engineering*, Vol. 135, No. 1, pp. 33–41.

Rosenblueth E. and Contreras H. (1977), "Approximate Design for Multicomponent Earthquakes," *ASCE Journal of the Engineering Mechanics Division*, Vol. 103, pp. 881–893.

Smeby W. and Der Kiureghian, A. (1985), "Modal Combination Rules for Multicomponent Earthquake Excitation," *Earthquake Engineering and Structural Dynamics*, Vol. 13, pp. 1–12.

Tremblay, R. and Robert, N. (2001), "Seismic Performance of Low- and Medium-Rise Chevron Braced Steel Frames," *Canadian Journal of Civil Engineering*, Vol. 28, No. 4, pp. 699–714.

UC Berkely, *OpenSees* [Computer software], Version 2.5.0, University of California, Pacific Earthquake Engineering Research Center, Berkeley, CA.

Uriz P., Filippou F.C. and Mahin S.A. (2008), "Model for Cyclic Inelastic Buckling of Steel Braces," *ASCE Journal of Structural Engineering*, Vol. 134, No. 4, pp. 619–628.

Victorsson, K.V. (2011), "The Reliability of Capacity-Designed Components in Seismic Resistant Systems," Ph.D. Dissertation, Stanford University, Stanford, CA.

Steel Structures Research Update

Steel Diaphragm Innovation Initiative

JUDY LIU

INTRODUCTION

A multiyear academic-industry partnership to advance the seismic performance of steel floor and roof diaphragms in steel buildings is highlighted. Lead investigators for the Steel Diaphragm Innovation Initiative (SDII) are Samuel Easterling, Matthew Eatherton, and Cristopher Moen (Year 1), Virginia Tech; Jerome Hajjar, Northeastern University; and Rafael Sabelli, Walter P. Moore, and Benjamin Schafer, Johns Hopkins University. The team includes AISC T.R. Higgins Lectureship Award and AISC Milek Fellowship Award winners for topics ranging from developments in long-span composite slabs to buckling-restrained braced frames to continuity plate detailing for steel moment-resisting connections.

SDII has been made possible through a collaboration between the American Iron and Steel Institute (AISI) and the American Institute of Steel Construction (AISC) with contributions from the Steel Deck Institute (SDI), the Metal Building Manufacturers Association (MBMA), and the Steel Joist Institute (SJI). Additional support is provided by the National Science Foundation (NSF). SDII is managed by the Cold-Formed Steel Research Consortium (CFSRC).

The team's motivations for creating SDII stemmed from issues with respect to the knowledge base for steel diaphragm performance, codes and standards, as well as missed opportunities for advancements in seismic performance–based design. The available research on steel diaphragms was primarily focused on the strength of isolated systems; little was known about ductility or whole-building performance. Code changes were being made to increase design diaphragm forces to be commensurate with elastic load levels, despite research supporting economical design of the diaphragm considering overstrength or ductility in steel deck diaphragms (O'Brien et al., 2016). Stiffness and redundancy in steel diaphragms and their connections to the vertical system were not being utilized to their full advantage and presented opportunities for advancements and innovations in steel building systems.

Judy Liu, Ph.D., Research Editor of the AISC Engineering Journal, Professor, Oregon State University, School of Civil and Construction Engineering, Corvallis, OR, Email: judy.liu@oregonstate.edu

The team developed a five-year case and plan to "advance the seismic performance of steel floor and roof diaphragms utilized in steel buildings through better understanding of diaphragm-structure interaction, new design approaches, and new three-dimensional modeling tools that provide enhanced capabilities to designers utilizing steel diaphragms in their building systems" (SDII, 2017). The work includes providing research support for much-needed revisions to proposed seismic codes and standards for steel diaphragms. SDII is also working on innovative steel diaphragm solutions for efficient, robust and resilient steel building systems.

The Steel Diaphragm Innovation Initiative is more than halfway through its five-year effort and recently held a workshop with key stakeholders. The workshop included presentations from the research team and a brainstorming session, soliciting feedback for future research, standards development, and outreach to the engineering community (www.steeli.org). Some of the accomplishments from the third year of the initiative are highlighted here.

RESEARCH OBJECTIVES

With the overarching goal of advancing the seismic performance of steel floor and roof diaphragms utilized in steel buildings, SDII has organized its efforts into three primary thrust areas: Innovation and Practice, Experiments, and Modeling (Figure 1). Innovation and Practice tasks range from evaluation of existing design methods and technologies to seismic standards work to development and validation of new designs and technologies. The Experiments tasks include developing databases of available steel diaphragm testing and conducting new experiments to fill knowledge gaps. Modeling tasks include modeling to support the experiments as well as development of high-fidelity diaphragm models and whole-building models for exploration of various factors for diaphragm and whole-building performance. "The objective is to move the practice forward through the adoption of new design specifications for diaphragms and the creation and use of tools that allow engineers to understand and optimize in their designs of steel diaphragms for steel buildings" (SDII, 2017).

EXPERIMENTS

The team is making good progress in the Experiments thrust area. Available data on fastener tests, shear connector

pushout tests, and full-scale diaphragm tests has been collected into databases. Within the Experiments area, the data have been used to identify testing needs. In the other thrust areas, the data are being used in development of new analysis and design methods. Testing technologies, such as photogrammetry, are being explored and developed for monitoring cracking in the concrete-filled diaphragm tests and for use in other tests. Cyclic deck sidelap and structural framing connector tests have been conducted. Diaphragm-style tests are being conducted on standing seam roof panel assemblies. The team is collaborating with investigators studying chords and collectors.

Testing to Characterize Behavior across Scales

The third year saw a continuation of the coordinated testing effort to characterize the behavior from the individual fasteners to the diaphragm panel to the full composite slab and steel framing systems. The experimental investigations highlighted here are isolated fastener tests; tests to explore the sensitivity of fastener behavior to installation details; shear connector pushout tests; composite deck cantilever diaphragm tests; and full-scale, beam-style composite deck diaphragm tests. These investigations aim to fill gaps in knowledge needed for the design of bare deck for roof diaphragms and for concrete-filled floor deck diaphragms common in multistory steel building construction.

Isolated Fastener Tests

A series of 80 tests were conducted on isolated sidelap and structural framing fasteners with flat sheets of steel deck. The fasteners were tested in this manner in order to separate fastener behavior from the effects of deck geometry, such as bends, embossments, and edge distances. The sidelap fasteners tested were #10 and #12 screws. Structural framing fasteners included powder-actuated fasteners, pneumatic power-actuated fasteners, arc seam welds, and #12 screws.

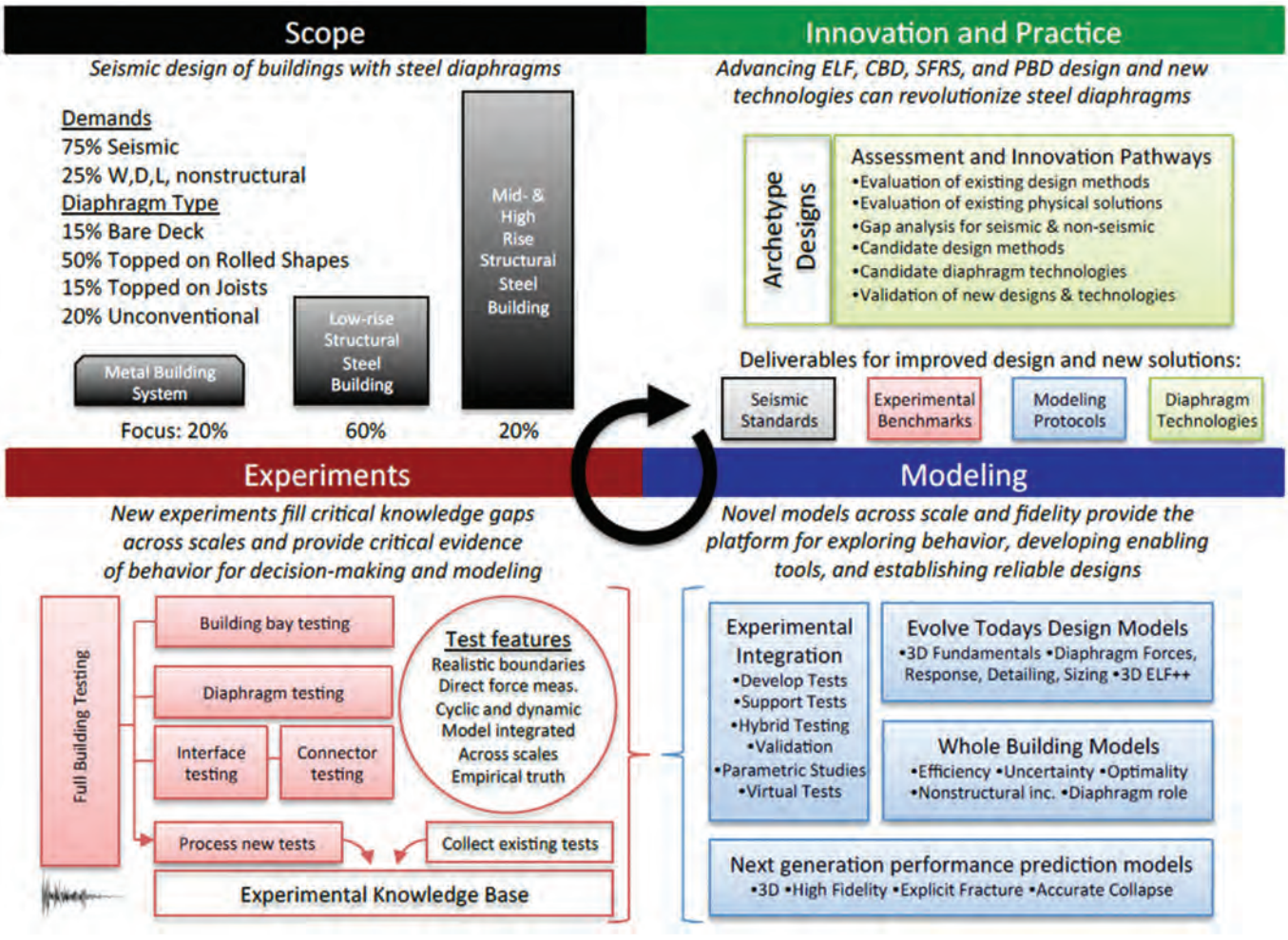

Fig. 1. SDII summary figure: Scope and three thrust areas.

Other parameters included number of deck plies for the structural fasteners (1, 2 and 4 ply to the support), deck thickness (22, 20 and 18 gage), and loading (monotonic and cyclic). For the structural framing connection tests, a 3⁄16-in.-thick plate represented the structural support steel.

Each test specimen consisted of a single fastener and overlapping sheets of steel. The test setup for the isolated fastener tests used aluminum U-shaped fixtures to keep the deck plies flat and in contact while the specimen was loaded axially [Figure 2(a)]. Load, cross-head displacement, and relative displacement between plies were measured. Observed failure modes included sidelap screw tilting and pullout, shear failure of structural screws, bearing failure at power-actuated fasteners, tearing of the sheet around the weld, and shear failure of the weld. Cyclic loading generally resulted in lower strength, with some exceptions. Arc seam welds were generally stronger than the other fasteners but also more variable in strength and failure mode. Meanwhile, comparison to companion tests showed that the presence of corrugations and realistic boundary conditions resulted in an increase in strength, 14% on average (Shi et al., 2018).

Sensitivity of Fastener Behavior to Installation Details

The sensitivity of sidelap fastener behavior to screw installation details was also investigated. This testing expanded upon the study of cyclic performance of steel deck sidelap and structural framing connections (Torabian et al., 2018a). Parameters for this study included screw edge distances (0.25, 0.375 and 0.5 in.), deck thicknesses (22, 20 and 18 gage), screw size (#10, #12), and loading (cyclic, monotonic). Note that the 0.5-in. edge distance placed the screw at a bend in the deck, and results from those tests were not available at the time of this article. In the test setup, the sidelap connected the stationary side of the deck to the moving part of the specimen, which was connected to a dynamic actuator [Figure 2(b)]. As in the other fastener tests, screw tilting and pullout was observed. For monotonic and cyclic tests, a larger edge distance resulted in a higher shear strength. The effect of edge distance on the sidelap stiffness is being analyzed (Torabian et al., 2018b).

Shear Connector Tests

Monotonic and cyclic composite shear connector tests, also referred to as "pushout" tests, are under way. The shear connector test specimens are correlated to the cyclic concrete-filled steel deck cantilever tests described later in this section. For the monotonic pushout tests, each side of the symmetric specimen has two shear studs that are welded to the flange of a WT and embedded in a 36-in. × 36-in. slab. A hydraulic jack applies load to the ends of the WTs [Figure 3(a)]. Parameters for the 41 monotonic tests include type of concrete (lightweight or normal weight), thickness of slab (4, 6.25 or 7.5 in.), and position of the stud in the rib (strong or weak). Cyclic pushout tests are conducted using a new testing rig developed for the purpose [Figure 3(b)]. Monotonic pushout tests will also be conducted with the new testing rig. The concrete portion of specimen is restrained at each side. Steel roller guides underneath the steel beam allow the steel portion of the specimen to move as load is applied in line with the top beam flange, thereby imposing realistic demands on the shear connectors. In the 16 monotonic and cyclic tests, effects of stud position, deck rib orientation, slab thickness, and lightweight or normal-weight concrete will again be investigated. Behavior for a deck oriented parallel to an edge beam will also be studied. Stud number and spacing will include 1 @ 12 in. and 2 @ 12 in. on center.

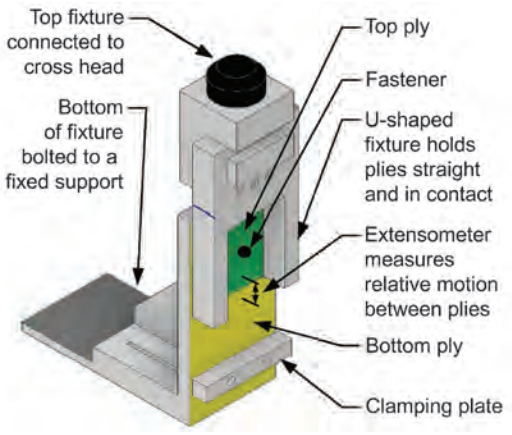

(a) isolated fastener test specimen

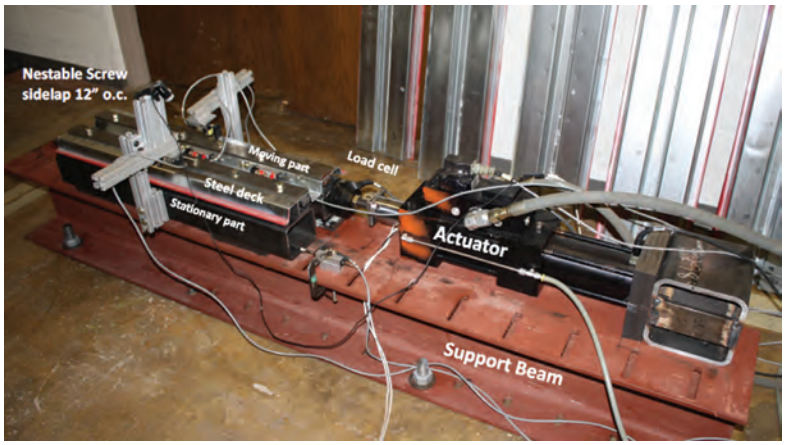

(b) deck sidelap test setup

Fig. 2. Test setup.

Cantilever Composite Deck Diaphragm Tests

Cantilever composite deck diaphragm tests are also under way [Figure 4(a)]. In these specimens, the composite deck is connected with perimeter studs to a steel frame, with the frame restrained at one side and cyclic displacements applied at the other side [Figure 4(b)]. A total of six specimens will be tested to investigate effects deck depth, slab thickness, perimeter stud configuration, and lightweight vs. normal-weight concrete. Four specimens have been designed to fail from diagonal concrete cracking; two will be limited by the strength of the perimeter shear stud anchors.

Full-Scale, Beam-Style Composite Deck Diaphragm Tests

A test program of full-scale, beam-style composite deck diaphragm tests with realistic floor framing is in development. The primary objective for these tests is to provide information on the response of the complete floor system. The test setup will be designed to follow the load path during seismic excitation of a building, from the inertia force in the concrete floor, through the shear studs into the framing system of chords and collectors, and then to the vertical lateral-force-resisting system. The test program will investigate typical floor framing as well as integration of energy dissipating fuses in the chords and collectors.

MODELING

The Modeling area has been critical for achieving objectives in the Experiments as well as the Innovation and Practice thrust areas. The team is developing and using models to support and supplement the testing programs, to assess current seismic codes and standards, and to explore potential innovations in design. Improved simplified models have been developed for conventional and new design. High-fidelity models with new capabilities (e.g., predicting fracture) are also being developed. The team is actively working on whole-building models, validated with experimental data and useful for validation of proposed designs and technologies. Some recent progress on the whole building models is highlighted.

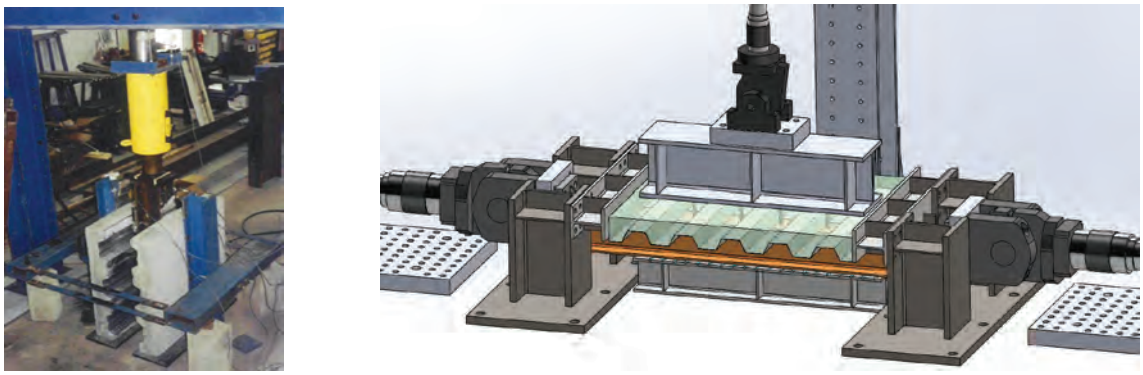

(a) test setup *(b) new testing rig for cyclic and monotonic pushout tests*

Fig. 3. Monotonic pushout test.

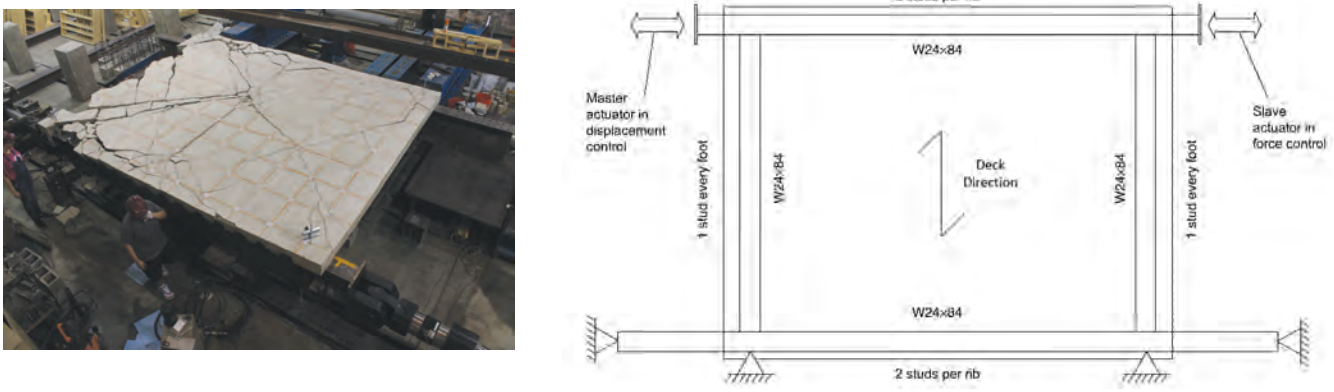

(a) cantilever composite deck specimen after testing *(b) schematic of test setup*

Fig. 4. Cantilever composite desk diaphragm testing.

Building-Scale Simulations

The whole-building models make use of the SDII archetype designs from the Innovation and Practice thrust area. The inventory of archetype buildings ranges from 1 to 12 stories in height and includes different lateral force-resisting systems such as special concentrically braced frames (SCBF), buckling restrained braced frames (BRBF), and moment frames. To date, 1-, 4-, 8- and 12-story buildings with SCBF and BRBF have been designed. The completed archetype buildings are 300 ft by 100 ft in plan with seismic-force-resisting systems designed for Seismic Design Category (SDC) D at an Irvine, California, site (Figure 5). At the floor levels, the composite slab has a 3-in. metal deck with either 7.5 in. total thickness of normal weight concrete or 6.25 in. of lightweight concrete. The roof diaphragm is assumed to be a bare 1.5-in. metal deck. The diaphragms have been designed following *Minimum Design Loads and Associated Criteria for Buildings and other Structures*, ASCE/SEI 7–16 (ASCE, 2016) standard and alternative design methods, providing opportunities for evaluation of different diaphragm design methods. Drawings, reference spreadsheets, and models can be found in Torabian et al. (2017).

Various options have been considered for reduced order modeling of the diaphragms in the building models. The options include rigid diaphragms, elastic or nonlinear shell elements, and nonlinear truss elements. These reduced-order models have been calibrated using experimental data obtained from cantilever diaphragm tests, as seen for development of the nonlinear truss element model. In the model, elastic beam-column elements were used for the perimeter steel members, and X-braces represented the deck or composite slab [Figure 6(b)]. The Pinching 4 material model in OpenSees was used in the X-braces to simulate the hysteretic behavior of the diaphragm. A comparison of the calibrated simulation and the experimental results shows that the hysteretic behavior was reasonably captured by the nonlinear truss element model of an 18-gauge deck with power-actuated fasteners and screws tested by Beck (2013) [Figure 6(a)]. Other reduced-order modeling options being explored include a hybrid shell-truss model, utilizing the shell element's ability to handle out-of-plane gravity demands.

Work continues on other aspects of the reduced-order modeling and analysis of the archetype buildings. Initial investigations of the one-story and four-story archetype building models with the diaphragm truss elements included nonlinear time history analysis at the design basis and maximum considered earthquake levels. Qayyum et al. (2017) evaluated force transfer, deformation and ductility demands, distribution of inelasticity, peak displacements, and residual displacements. Further modeling refinements included nonlinear beam-column elements with plastic hinging for the frame members and modifications to better represent fixity of the joints. Nonlinear pushover and time-history analyses have been conducted on these improved models, and the work has been extended to the other archetype buildings.

INNOVATION AND PRACTICE

The Innovation and Practice thrust area is focused on translation of SDII to industry, with improved seismic codes and standards, experimental benchmarks, modeling protocols, and new diaphragm technologies. Progress within this thrust area has included development of archetype designs, evaluation of existing design methods and technologies, performing gap analysis for seismic as well as nonseismic and nonstructural design, and exploring new design methods and technologies. Another important task is the team's efforts in codes and standards to improve the design of steel deck diaphragms. Some activities in the seismic standards work are briefly summarized.

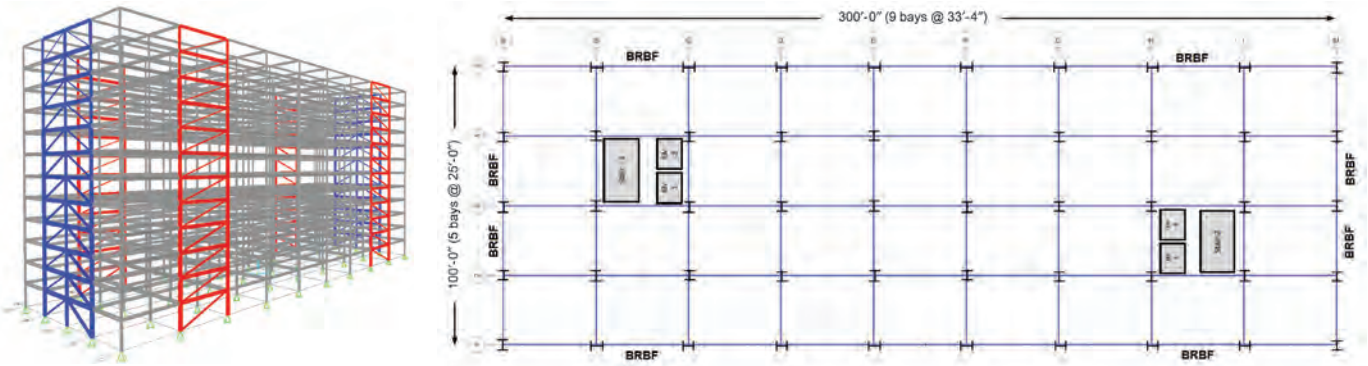

(a) isometric rendering *(b) floor plan*

Fig. 5. Building archetype.

Seismic Standards Work

SDII is already influencing standards and specifications. Contributions in the third year include technical support for the AISC *Seismic Provisions for Structural Steel Buildings* (AISC, 2016) related to horizontal truss diaphragms and the alternative diaphragm design provisions in the *Minimum Design Loads and Associated Criteria for Buildings and Other Structures*, ASCE/SEI 7–16 (ASCE, 2016). Updates to the AISC *Seismic Provisions* for concrete-filled deck diaphragms are also in progress. Research team members are making use of the SDII test database to provide modeling parameters and nonlinear acceptance criteria for steel deck systems for the new AISC standard that is currently in development, *Seismic Provisions for Evaluation and Retrofit of Structural Steel Buildings.* Team members have also proposed improvements in the AISI *North American Standard for the Design of Profiled Steel Diaphragm Panels*, AISI S310–16 (AISI, 2016), for strength predictions of steel deck diaphragms and in the AISI *North American Standard for Seismic Design of Cold-Formed Steel Structural Systems*, AISI S400–15 (AISI, 2015), for diaphragm design provisions. Through the Building Seismic Safety Council and with a peer review team from the Applied Technology Council, steel deck provisions for the alternate diaphragm design method are being prepared, and the groundwork is being laid for steel deck provisions for rigid-wall flexible diaphragm systems in ASCE/SEI 7–16.

SUMMARY AND FUTURE WORK

SDII seeks to advance the seismic performance of steel floor and roof diaphragms utilized in steel buildings and is doing so in a multi-institution effort with three coordinated thrust areas: Innovation and Practice, Experiments, and Modeling. Accomplishments in the third year of their five-year plan included experimental investigations ranging from isolated fastener tests to cantilever diaphragm tests and filling gaps in knowledge for bare deck roof diaphragms and concrete-filled floor deck diaphragms; development of models to support and supplement the testing programs, to assess current seismic codes and standards, and to explore potential innovations in design; and significant efforts in codes and standards to improve the design of steel deck diaphragms.

The research team continues to improve understanding of diaphragm-structure interaction and to develop new design approaches and three-dimensional modeling tools with enhanced capabilities. Outcomes from work by the Steel Diaphragm Innovation Initiative will include much-needed revisions to proposed seismic codes and standards for steel diaphragms and innovative steel diaphragm solutions for efficient, robust and resilient steel building systems.

ACKNOWLEDGMENTS

Special thanks to Ben Schafer for all of the materials and coordination for this article; to Matt Eatherton for his detailed review and additional content; and to Sam

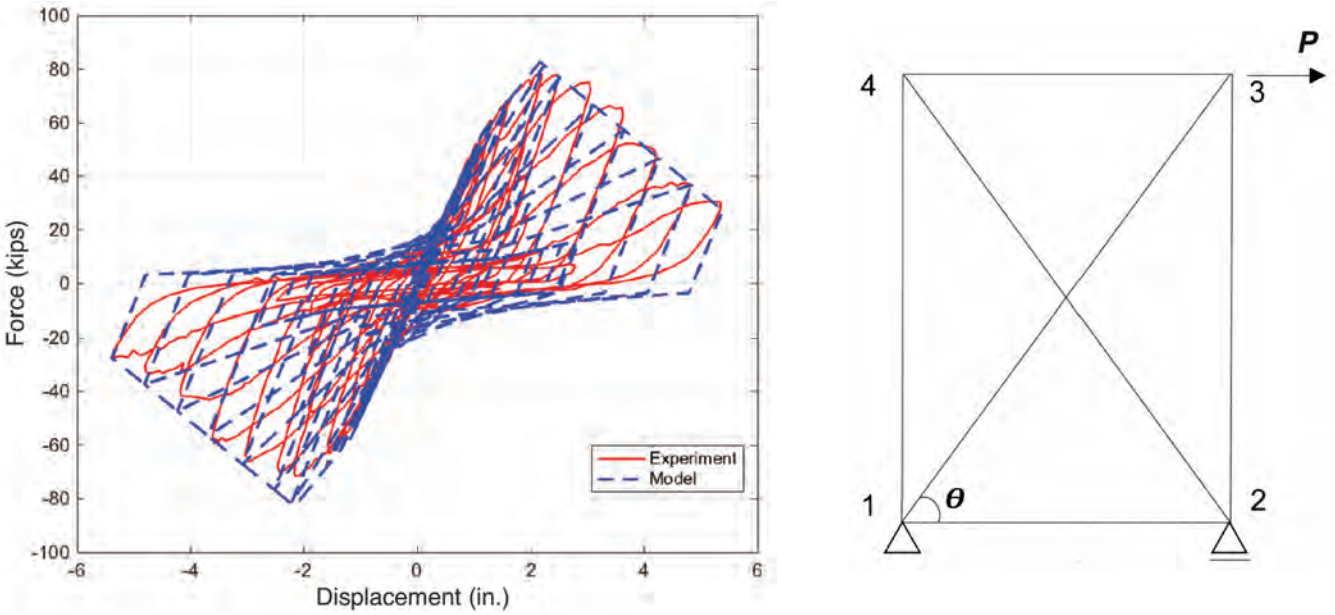

(a) comparison to experimental results *(b) schematic of the nonlinear truss element model*

Fig. 6. Reduced-order diaphragm simulation.

Easterling, Jerry Hajjar, and Rafael Sabelli for their feedback and contributions. The work of the current team of research faculty, staff, postdoctoral scholars, and graduate students is also appreciated: Shahab Torabian, Kyle Coleman, David Padilla-Llano, Nicholas Evans Briggs, Astrid Winther Fischer, Hamid Foroughi, Mithila Bhagavathi Madhavan, Raul Avellaneda Ramirez, Yifei Shi, and Gengrui Wei.

The SDII team would like to thank its sponsors: AISI, AISC, SDI, SJI, MBMA and NSF. The team would also like to thank staff and support of these organizations for their assistance with Industry Steering Group meetings, BSSC meetings, and the like. Further, several undergraduates and other students at Virginia Tech, Northeastern, and Johns Hopkins have participated in some aspects of the project—their work and efforts are also appreciated. Any findings, recommendations, or other material within are those of the researchers and do not necessarily reflect the views of the sponsors.

REFERENCES

AISC (2016), *Seismic Provisions for Structural Steel Buildings*, ANSI/AISC 341-16, American Institute of Steel Construction, Chicago, IL.

AISI (2015), *North American Standard for Seismic Design of Cold-Formed Steel Structural Systems*, AISI S400-15, American Iron and Steel Institute, Washington, DC.

AISI (2016), *North American Standard for the Design of Profiled Steel Diaphragm Panels*, AISI S310-16, American Iron and Steel Institute, Washington, DC.

ASCE (2016), *Minimum Design Loads and Associated Criteria for Buildings and Other Structures*, ASCE/SEI 7–16, American Society of Civil Engineers, Reston, VA.

Beck, H. (2013), "Inelastic Cyclic Diaphragm Tests with Hilti Powder-Actuated Fastener X-HSN 24," Report No. XE_13_162, Technical Center of Hilti Corporation, Liechtenstein.

O'Brien, P., Flori, S., Moen, C.D. and Eatherton, M.R. (2016), "Characterizing the Load Deformation Behavior of Steel Deck Diaphragms," International Specialty Conference on Cold-Formed Steel Structures, Baltimore, MD, November, 15 pp.

Qayyum, B., Eatherton, M.R. and Easterling, W.S. (2017), "Seismic Behavior of One-Story Steel Buildings with Inelastic Diaphragm,." *Proceedings 11th U.S. National Conference on Earthquake Engineering*, Los Angeles, CA, June 25–29.

SDII (July 20, 2017). "Steel Diaphragm Innovation Initiative Case and Research Plan," version 4.0, Steel Diaphragm Innovation Initiative (available on request).

Shi, Y., Torabian, S., Schafer, B.W., Easterling, W.S. and Eatherton, M.R. (2018), "Sidelap and Structural Fastener Tests for Steel Deck Diaphragms," *Proceedings Wei-Wen Yu International Specialty Conference: Cold-Formed Steel Structures*, November 7–8, St. Louis, MO.

Torabian, S., Easterling, W., Hajjar, J.F. and Schafer, B.W. (2017), "SDII Building Archetype Design v1.0," CFSRC Report R-2017–04, permanent link: jhir.library.jhu.edu/handle/1774.2/40638.

Torabian, S., Fratamico, D., Shannahan, K. and Schafer, B.W. (2018a), "Cyclic Performance and Behavior Characterization of Steel Deck Sidelap and Framing Connections," *Proceedings Wei-Wen Yu International Specialty Conference: Cold-Formed Steel Structures*, November 7–8, St. Louis, MO.

Torabian, S., Folk, H. and Schafer, B.W. (2018b), "Effect of Connection Details on the Cyclic Behavior of Nestable Screw Sidelaps," *Proceedings Wei-Wen Yu International Specialty Conference: Cold-Formed Steel Structures*, November 7–8, St. Louis, MO.

ERRATA

Clearance for Welded Joints

Bo Dowswell

Vol. 56, No. 1, 2019

In the paper ABSTRACT, the last two sentences of the paragraph are revised to:

The results of this study, which was limited to only eight specimens, validated the common practice of cutting the edge square at doubler plates less than ⅜-in. thick. For doubler plates thicker than ¼ in., a groove angle, α, of 15° to 30° may be required to ensure consistent weld quality.

Guide for Authors

Scope

Engineering Journal is dedicated to the improvement and advancement of steel construction. Its pages are open to all who wish to report on new developments or techniques in steel design, research, the design and/or construction of new projects, steel fabrication methods, or new products of significance to the uses of steel in construction. Only original papers should be submitted.

General

Papers intended for publication should be submitted by email Margaret Matthew, editor, at **matthew@aisc.org**.

The articles published in the *Engineering Journal* undergo peer review before publication for (1) originality of contribution; (2) technical value to the steel construction community; (3) proper credit to others working in the same area; (4) prior publication of the material; and (5) justification of the conclusion based on the report.

All papers within the scope outlined above will be reviewed by engineers selected from among AISC, industry, design firms, and universities. The standard review process includes outside review by an average of three reviewers, who are experts in their respective technical area, and volunteers in the program. Papers not accepted will not be returned to the author. Published papers become the property of the American Institute of Steel Construction and are protected by appropriate copyrights. No proofs will be sent to authors. Each author receives three copies of the issue in which his contribution appears.

Manuscripts

Manuscripts must be provided in Microsoft Word format. Include a PDF with your submittal so we may verify fonts, equations and figures. View our complete author guidelines at **www.aisc.org/ej**.

Smarter. Stronger. Steel.

American Institute of Steel Construction
130 E Randolph St, Ste 2000, Chicago, IL 60601
312.670.2400 | www.aisc.org/ej